UNRAVELING DEEP-OCEAN CONNECTIONS TO CLIMATE WITH DEEP-SEA CORAL RECORDS OF RADIOCARBON AND CD/CA

Thesis by

Selene Farrell Eltgroth

In Partial Fulfillment of the Requirements for the

Degree of

Doctor of Philosophy

CALIFORNIA INSTITUTE OF TECHNOLOGY

Pasadena, California

2006

(Defended December 16, 2005)

ACKNOWLEDGEMENTS

I would like to thank all the people who made this work possible. First, I give heartfelt thanks to Ben Mazin for his love and support through this process. I am grateful to my fellow graduate students too numerous to name who have provided advice and guidance along this path from beginning to end. Thanks to my lab mates over the years: Jeff Mendez, Alex Gagnon, Jessie Wang, Kim Cobb, Laura Robison, Kate McIntyre and Diego Fernandez. Thanks to my thesis advisor Jess Adkins. I am also grateful to John Southon and Michaele Kashgarian for their help. I'd also like and Ken Farley and Dimitri Papanastassiou for advising on a couple of early projects. And a final note of gratitude to Ernie for his fine lunches that fueled me through my days here.

ABSTRACT

We generated records of radiocarbon and trace metals in deep-sea corals to investigate the role of the deep ocean during episodes of rapid environmental change. Our record of radiocarbon ages measured in a modern deep-sea coral from the northeastern Atlantic shows the transfer of bomb radiocarbon from the atmosphere to the deep ocean. We detect bomb radiocarbon at the coral growth site starting in 1975–1979. Our record documents a $\Delta^{14}C$ increase from –80 ± 1‰ (average 1930–1979) to a plateau at –39 ± 2‰ (average 1994–2001). From a suite of fossil deep-sea corals, variability in North Atlantic intermediate water $\Delta^{14}C$ during the Younger Dryas (13.0–11.5 ka) supports a link between abrupt climate change and intermediate ocean circulation. We observe rapid shifts in deep-sea $\Delta^{14}C$ that require the repositioning of large $\Delta^{14}C$ gradients within the North Atlantic. The shifts are consistent with changes in the rate of North Atlantic Deep Water formation. We also observe a decadal scale event at 12.0 ka that is marked by the transient return of radiocarbon to the eastern and western basins of the North Atlantic.

To develop a nutrient proxy for use in deep-sea corals, we measured Cd/Ca in 14 modern corals. Several of these corals had anomalously high Cd/Ca that we explain with a systematic bias in Cd/Ca obscuring the signal of seawater Cd/Ca. When these high Cd/Ca corals are removed from the calibration, the best-fit coral-water partition coefficient is 1.3 ± 0.1. Examining Cd/Ca in fossil deep-sea corals, we find that our coral from the Younger Dryas (12.0 ka) resembles the high Cd/Ca corals of the modern calibration and probably does not reflect seawater Cd/Ca. The Cd/Ca record from a 15.4 ka coral resembles our low Cd/Ca calibration samples and probably reflects average seawater Cd/Ca.

TABLE OF CONTENTS

LIST OF ILLUSTRATIONS AND TABLES

Chapter 1

INTRODUCTION

Calcium carbonate-precipitating organisms in the ocean are among the most successful and reliable substrates for paleochemical oceanographic studies. Paleooceanographers take advantage of isotopic and elemental substitution into the biogenic $CaCO_3$ lattice to monitor ocean history and learn about the role of the ocean in global climate. Measurements of these isotopic ratios and trace elements became possible with the advent of sensitive mass spectrometric techniques. Planktonic and benthic foraminifera (single cellular $CaCO_3$ precipitating organisms) preserved in sediments as well as surface corals in reef environments have proven invaluable recorders of their environment. Biological processes occasionally affect these records, and the accuracy of paleochemical proxies must be demonstrated in the modern environment before they may be trusted to reconstruct past ocean parameters. The deep ocean is especially important to global climate as the primary store and transporter of heat and CO_2 in the climate system. Deep-sea corals, largely forgotten by the oceanographic community for many years, have recently returned to prominence. Deep-sea corals offer unique advantages over benthic foraminifera because they are individually datable, they offer the capacity for high-resolution records within a given coral, and they are large enough to accommodate multiple tracers in a single coral. In this work, we are particularly interested in understanding the capacity of the ocean to influence rapid climate change, a timescale particularly suited to

deep-sea corals. We approach this issue by monitoring and developing new tools to monitor deep-ocean chemistry recorded in deep-sea corals during times of rapid change.

The work presented here falls into two categories: (1) using an established tracer in deep-sea corals to draw inferences about the ocean system in the past and (2) developing a new tracer of nutrients in deep-sea corals to specifically quantify the relative mixing proportions that contribute to a given deep water parcel. Adkins et al. (2002) demonstrated that deep-sea corals are accurate recorders of the $\Delta^{14}C$ of dissolved inorganic carbon, and in chapters 2 and 3 we present two deep-sea coral records of North Atlantic $\Delta^{14}C$ from different time intervals.

In chapter 2, we measure radiocarbon in samples from a long-lived modern colonial deep-sea coral that was collected in 2001. Large quantities of ^{14}C were generated by the atmospheric detonation of nuclear weapons and subsequently incorporated into atmospheric CO_2. Our record monitors this pulse of ^{14}C-labeled CO_2 moving into the deep North Atlantic. This study illustrates the accuracy of deep-sea coral as recorders of seawater radiocarbon and is the first high-resolution record of bomb radiocarbon at a fixed location in the deep ocean. Our results impact the climate and ocean modeling community by observing the rate of CO_2 infiltration into the ocean, useful for calibrating the rate of CO_2 transfer to the deep ocean.

In chapter 3 we investigate radiocarbon in smaller solitary deep-sea corals from the Norrth Atlantic that have been U-series dated. This allows us to reconstruct deep-sea $\Delta^{14}C$ during the Younger Dryas cold interval. The atmospheric $\Delta^{14}C$ record during the Younger Dryas shows a rapid increase that cannot be accounted for by a corresponding increase in

production rate. The $\Delta^{14}C$ increase has therefore been attributed to a sudden drop in the rate of North Atlantic Deep Water (NADW) formation, the major sink for atmospheric radiocarbon. Our deep-sea coral record tests this hypothesis and illustrates the increased influence of radiocarbon depleted southern source water in the intermediate/deep North Atlantic. Our data also show a transient return to enriched radiocarbon (well-ventilated) conditions during the middle of the Younger Dryas

In chapter 4, we present measurements of Cd/Ca in a suite of modern deep-sea corals to evaluate the tracer for deep-ocean reconstructions of nutrients. We found that the relation between Cd/Ca in the coral and Cd/Ca in the water is not simple. Based on the Cd/Ca signatures, we divided the corals into 3 utility groups and applied these structures to the Cd/Ca records that were generated in 2 fossil corals from the North Atlantic. We found our Cd/Ca record from the Younger Dryas to be unreliable, but a record from 15.4 ka probably reflects the average nutrient concentration at the coral growth site.

Bibliography

Adkins, J. F., S. Griffin, M. Kashgarian, H. Cheng, E. R. M. Druffel, E. A. Boyle, R. L. Edwards, and C. C. Shen. 2002. Radiocarbon dating of deep-sea corals. *Radiocarbon* 44 (2):567-580.

Chapter 2

THE TRANSFER OF BOMB RADIOCARBON TO THE DEEP OCEAN: OBSERVATIONS FROM A NORTH ATLANTIC DEEP-SEA CORAL

Selene F. Eltgroth, Jess F. Adkins and John Southon

Abstract

Radiocarbon ages measured in a deep-sea coral from 1400 meters depth off of Bermuda show the infiltration of bomb radiocarbon into the intermediate/deep ocean. Our high-resolution time series is created from closely spaced radial cross sections, with samples taken from the center of concentric coral growth bands that we show to be the oldest portion of the section. Prebomb radiocarbon ages from the 55 cm long *Enallopsammia rostrata* demonstrate that the vertical growth rate of the coral is linear (0.80–0.95 mm/yr) and the coral lived for 580–690 years. Using this age model to reconstruct $\Delta^{14}C$, we first detect bomb radiocarbon at the coral growth site in 1975–1979, and show that $\Delta^{14}C$ increased from –80 ± 1‰ (average 1930–1979) to a plateau at –39 ± 2‰ (average 1994–2001).

Introduction

In the absence of anthropogenic influence, the ^{14}C content of the atmosphere is governed by the balance between atmospheric production by cosmic ray-generated neutrons and uptake of $^{14}CO_2$ into marine and terrestrial reservoirs, where it is ultimately lost to by radioactive decay (Broecker and Peng 1982). In the recent past, anthropogenic

perturbations to the atmospheric $^{14}C/^{12}C$ ratio by the combustion of fossil fuels and atmospheric nuclear weapons testing have come to dominate the observed $^{14}C/^{12}C$ fluctuations (Stuiver and Quay 1981; Nydal and Lovseth 1983). The largest signal in the atmospheric $\Delta^{14}C$ record of the Northern Hemisphere is a 1000‰ pulse that reaches a maximum in 1963 (Nydal and Lovseth 1983). This pulse is a byproduct of the atmospheric detonation of nuclear weapons begun in 1945 and because of its magnitude, is an unambiguous signal as it moves into the terrestrial and marine reservoirs. Monitoring the response of the surface and deep ocean reservoirs to the atmospheric bomb input is essential to understanding the rate of new deep water formation and estimating the inventory of bomb radiocarbon in the modern ocean.

The surface ocean $\Delta^{14}C$ of dissolved inorganic carbon (DIC) is naturally depleted relative to the atmosphere because of the balance between the upwelling of ^{14}C depleted deep-water and the uptake of atmospheric CO_2 into the surface ocean (Broecker and Peng 1982). Tracking the movement of bomb $\Delta^{14}C$ into the surface ocean has been accomplished with direct ^{14}C analyses of surface seawater samples (Key, Kozyr et al. 2004), and with measurements from annually banded surface corals (Druffel and Linick 1978; Druffel and Suess 1983; Druffel 1989; Guilderson, Schrag et al. 1998; Schmidt, Burr et al. 2004). The seawater measurements provide observations of the spatial distribution within the surface ocean at a given time, while the annually banded coral data provide long time series of surface records at a given location.

Deep-ocean $\Delta^{14}C$ is set by the relative proportions of source waters that have mixed into the deep sea and by the radiocarbon decay that has occurred since the time the water

was last at the surface. Reliable measurements of modern $\Delta^{14}C$ in the deep ocean are made up of direct measurements from the water column beginning in the late 1950s (Broecker, Gerard et al. 1960). $\Delta^{14}C$ profiles of the modern North Atlantic from the ocean surveys GEOSECS, TTO, and WOCE provide good spatial coverage of this deep ocean over discrete time intervals (Stuiver and Ostlund 1980; Key, Kozyr et al. 2004), but high resolution records spanning the gaps in time between the surveys do not yet exist.

Given the success of surface corals for reconstructing past surface ocean $\Delta^{14}C$ over time, deep-sea corals are a natural choice of substrate for generating high-resolution time series of ^{14}C in the deep ocean. Adkins et al. (2002) showed that, like their surface relatives, modern deep-sea corals preserve the record of $\Delta^{14}C$ of ambient dissolved inorganic carbon in their aragonite skeletons. Because deep-sea corals do not contain annual bands, however, an alternate method to determine the calendar age of the coral must be employed. Previously, deep-sea coral $\Delta^{14}C$ reconstructions have targeted the last glacial and deglacial times using U-series dating to determine the calendar age of the sample (Adkins, Cheng et al. 1998; Mangini, Lomitschka et al. 1998; Schroder-Ritzrau, Mangini et al. 2003; Frank, Paterne et al. 2004; Eltgroth, Adkins et al. 2005; Robinson, Adkins et al. 2005). Here, our objective is to create a high-resolution reconstruction of modern $\Delta^{14}C$ in the deep North Atlantic from closely spaced radiocarbon measurements on a recently collected deep-sea coral.

Samples and Methods

Our *Enallopsammia rostrata* (De Pourtalès, 1878) specimen (figure 2.1) was collected alive in September 2001 with the *DSV Alvin* from a depth of 1410m on the north slope of Bermuda (64W 32N) (figure 2.2). This coral offers advantages for time series reconstructions over smaller species like *Desmophyllum dianthus* because of its increased size (~10 times longer vertical length) and wide radial cross section. Radial sections were cut perpendicular to the direction of coral growth above and below the main branch point (positions indicated in figure 2.1). Concentric bands were identified under UV light, and sample transects were taken from the center to the edge of each section along the longest possible transect (10–16 mm). We observed that banding in the radial sections is asymmetric, with the center of the concentric bands located at a corallite remnant close to the corallite face of the coral. Sample preparation procedures for deep-sea coral sampling, cleaning, leaching, and graphitization prior to ^{14}C analysis are identical to those outlined in Eltgroth *et al.* (2005). Sample masses ranged from 11 to 44 mg and at least 24% of each sample was leached away, sufficient to remove contaminating sources of modern ^{14}C outside of the aragonite lattice (Adkins, Griffin et al. 2002). Our conventional radiocarbon ages (Stuiver and Polach 1977) were measured at the UC Irvine Keck Carbon Cycle Accelerator Mass Spectrometry Laboratory using an inorganic calcite blank to account for the background signal from the graphitization and the AMS measurement. Deep-sea $\Delta^{14}C$ was calculated from these measurements according to:

$$\Delta^{14}C = \left(\frac{e^{-\frac{^{14}C\ Age}{Libby\ Mean\ Life}}}{e^{-\frac{Calendar\ Age}{True\ Mean\ Life}}} - 1\right) \times 1000‰ \qquad \text{(equation 2.1)}$$

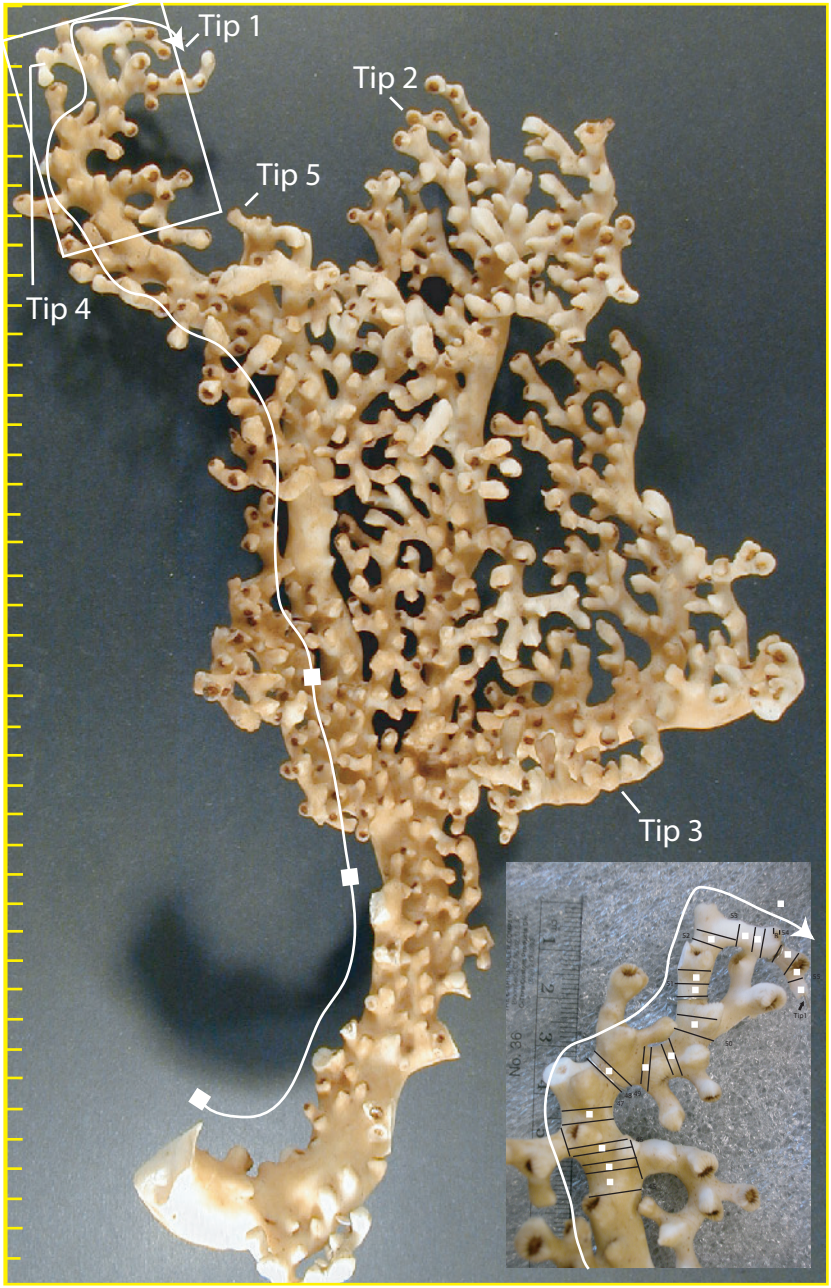

Figure 2.1. E. rostrata sample ALV-3701-8. The line traces the branch that was selected for the time series. White squares represent the position of samples that were taken for the radiocarbon time series, and arrows point to the tips that were analyzed. Scale at left shows 1cm divisions. The inset emphasizes the closely spaced samples taken for the bomb radiocarbon time series. Highly curved areas of the coral were avoided.

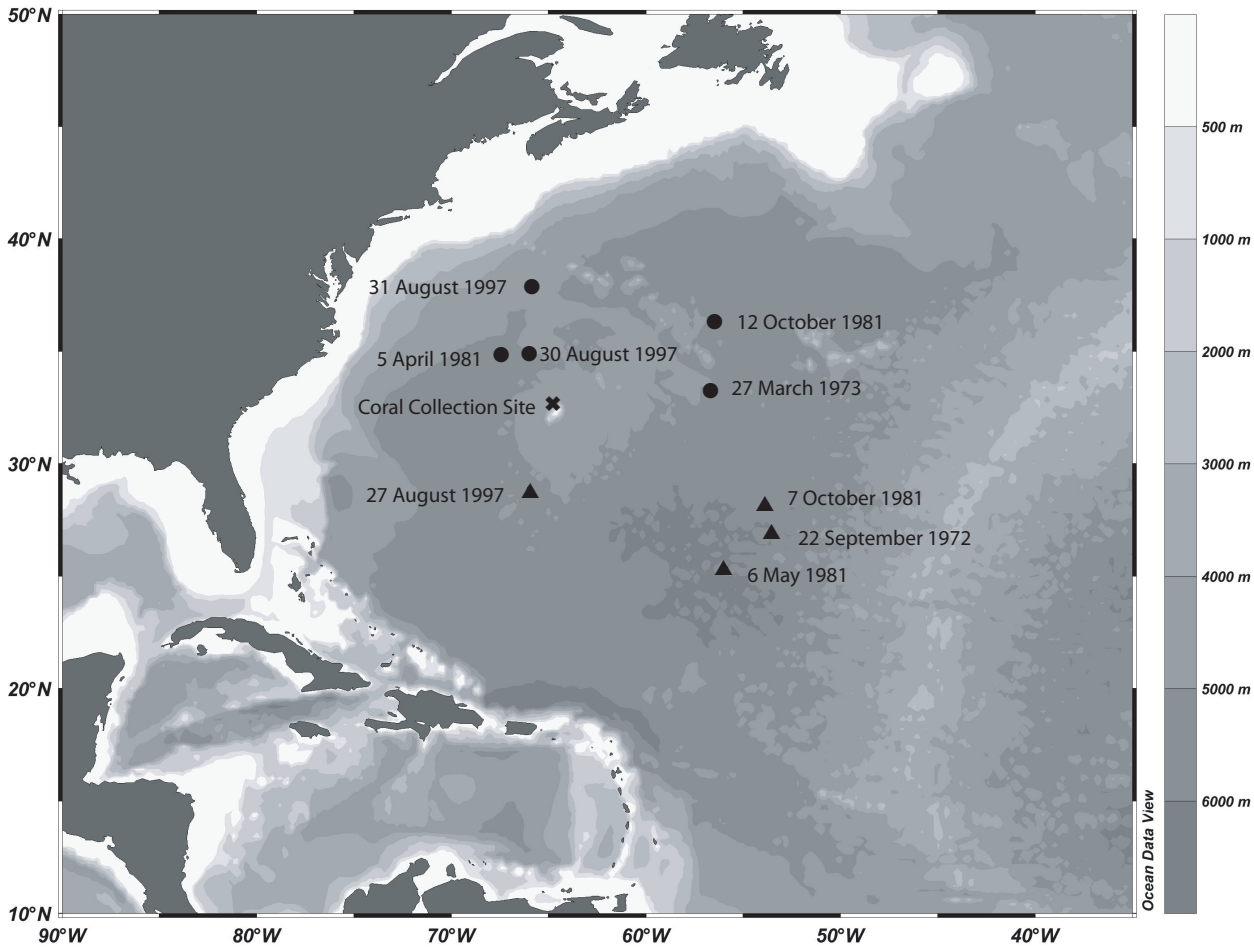

Figure 2.2. Map of the northwest Atlantic showing the locations of our coral specimen (✖) and nearby stations with $\Delta^{14}C$ profiles (● to the north of the coral collection site and ▲ to the south). The stations are labeled by the date of sample collection.

where the conventional ^{14}C age is a measure of $^{14}C/^{12}C$ of the present day sample, and the calendar age serves to correct the $^{14}C/^{12}C$ for radiocarbon decay back to the original concentration at the time of coral skeleton precipitation. The calendar age of each coral sample was determined from a coral age model derived from the preindustrial, prenuclear ^{14}C results for our coral specimen with the youngest tip of the coral fixed at the date of coral collection as discussed in the following text.

Results

We found variable ^{14}C ages for 5 corallite tips with the youngest one, Tip 1, at the apex of the largest branch (table 2.1). The excess ^{210}Pb results of Adkins *et al.* (2004) likewise showed that the corallite tips were of variable age and a tip at the end of the same branch, adjacent to Tip 1, was the most recently precipitated. Specific differences between the ^{14}C and excess ^{210}Pb methods are due to the distinct sample locations and the larger samples size required for ^{210}Pb analyses (1.5g). Based on these results, we focused our time series analysis on the branch that terminates at Tip 1 since it is most likely to contain the deep ocean interval with bomb radiocarbon infiltration.

We analyzed transects through 3 radial sections to determine the optimal place to sample the coral for the time series construction. The radial section results (figure 2.3, table 2.2) reveal that the maximum ^{14}C age is reached within 1–4 mm of the section center, and that the radial growth rate is linear (20–30 μm/yr) outside of this central area. Therefore, we sampled as close to the center as possible and always within the inner 4 mm when constructing the time series.

UCIAMS #	Sample ID	^{14}C Age (^{14}C yr before 1950)	Error (2σ)
6473	Tip 1	315	40
8634	Tip 1	260	40
6460	Tip 1	275	30
8630	Tip 2	530	30
6461	Tip 2	485	30
6478	Tip 2	595	50
6483	Tip 3	685	50
8615	Tip 3	690	30
8632	Tip 3	730	30
8631	Tip 4	560	30
8628	Tip 5	360	40

Table 2.1. Tip Radiocarbon Results

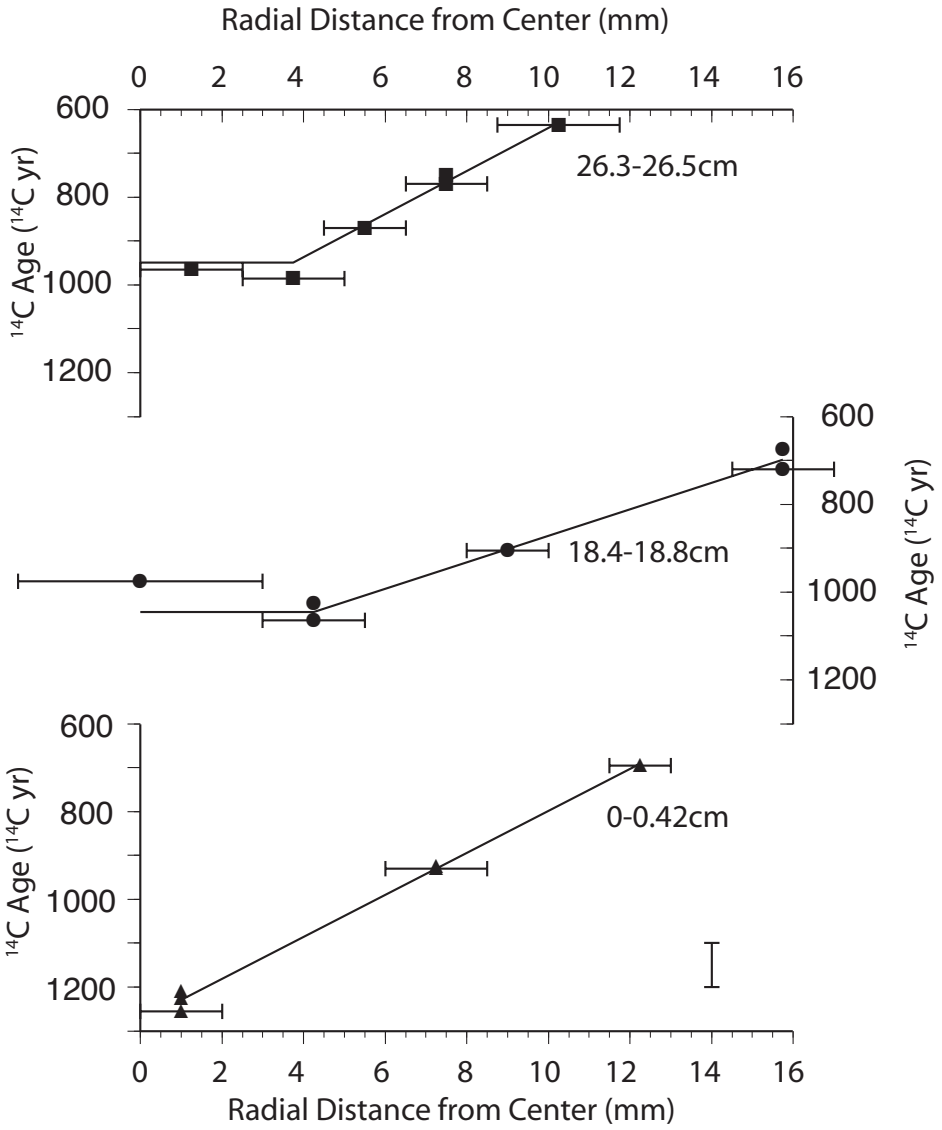

Figure 2.3. The radial section ^{14}C ages plotted with distance from the coral section center show that the oldest part of the coral is at the section center. Outside of the central region (1-4mm) the coral growth rates are linear. Each curve is labeled with its position in the coral (cm from the coral base).

UCIAMS #	Sample Position		Radial Position		^{14}C Age	Error (2σ)
	Lower	Upper	Inner	Outer	(^{14}C yr before 1950)	
	(cm from Coral Base)		(mm from center of section)			
6497	0	0.4	0	2	1255	30
6495			0	2	1210	30
6505			0	2	1225	30
8635			6	8.5	930	30
8620			6	8.5	925	30
8613			11.5	13	695	40
11202	18.4	18.8	-3	3	975	40
8629			3	5.5	1025	40
8623			3	5.5	1065	30
8616			8	10	905	30
8626			14.5	17	675	30
8618			14.5	17	720	40
11201	26.3	26.5	0	2.5	965	40
11199			2.5	5	985	40
8622			4.5	6.5	870	40
8625			6.5	8.5	750	30
8614			6.5	8.5	770	40
8617			8.75	11.75	635	50

Table 2.2. Radial Section Radiocarbon Results

Our ^{14}C time series consists of measurements from the centers of 20 radial sections and 1 corallite at the coral positions previously identified in figure 2.1 (figure 2.4, table 2.3). To minimize the possibility of inadvertent sampling errors, highly curved regions of the coral were not sampled. The results show 2 different regions of behavior: the results from the lower part of the coral (0–52.6 cm) trace a straight line, but the results from the upper part of the coral (53.1–55 cm) show a rapid decrease in ^{14}C age that is independent of the growth rate. These results are consistent with a linear growth rate that is obscured by the movement of radiocarbon-enriched water to the coral growth site at the 53.1cm mark.

These results may also be used to estimate the vertical growth rate of the coral. The lowest 3 points in figure 2.4 are the oldest ^{14}C ages from each of the previously discussed radial sections. A linear least-squares fit to these points gives a growth rate of 0.95 mm/year. When we use all of the time series data up through 52.6 cm to determine a best-fit growth rate, including more scatter in the data, the vertical growth rate is 0.80 mm/yr, which we take as the lower bound for the vertical growth rate. The scatter between data points in the interval 45.0–48.3 cm is too large to have been driven by an environmental signal, and although these sections were sampled quite close to the radial section center (<4 mm), more recent carbonate must have been included with these specific samples, possibly because the ^{14}C age minimum at the section center was narrower in this region. Because the faster growth rate (0.95 mm/yr) is based on the oldest age for each section, scatter is reduced and this is probably a better estimate of growth rate. Based on these growth rate estimates, the coral lived for 580–690 yr. Our coral growth rates fit with the observation of $^{226}Ra/^{210}Pb$ secular equilibrium in the coral, constraining the vertical growth rate to be

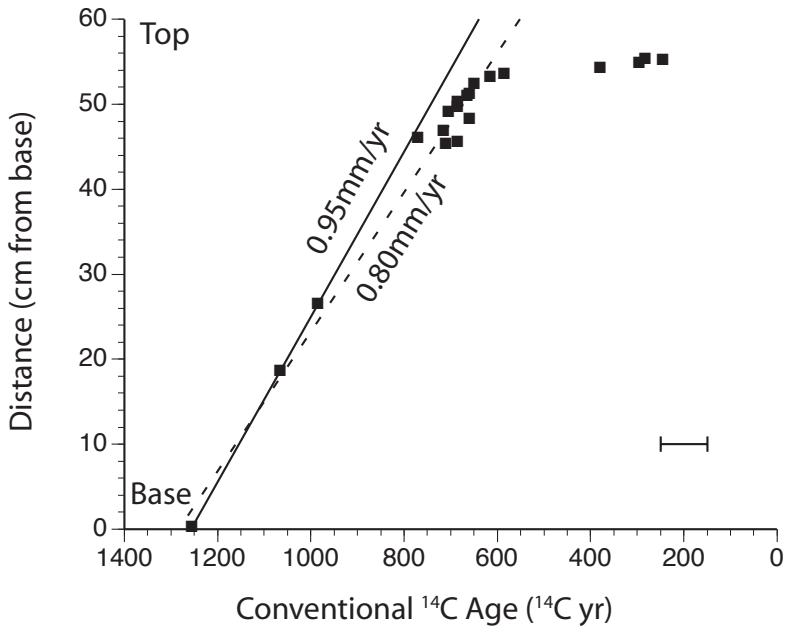

Figure 2.4. Radiocarbon age results. The x-axis is inverted so that younger ages are plotted to the right. The analytical errors in ^{14}C age (2σ) range from 30–50 ^{14}C years, and the maximum ^{14}C age error (± 50 ^{14}C yr 2σ) is shown by the error bar in the lower right of the figure. The solid line is the least-squares linear fit through the oldest ages from the 3 radial sections below 30 cm in the coral. The dashed line is the least squares linear fit through the data 0–52.6 cm. The linear region is consistent with a constant $\Delta^{14}C$ in the water and a linear growth rate. The rapid decrease in ^{14}C age at the top of the coral (53.1–55 cm) is consistent with bomb radiocarbon invading the coral growth site.

UCIAMS #	Sample Position lower (cm from Coral Base)	upper	^{14}C Age (^{14}C yr before 1950)	Error (2σ)	Age 1 0.95mm/yr (yrs AD)	$\Delta^{14}C_{Water}$ (‰)	Age 2 0.80 mm/yr (yrs AD)	$\Delta^{14}C_{Water}$ (‰)	Analytical Error (2σ) (‰)
6497	0	0.4	1255	30	1420	-88.0	1310	-75.7	3.5
8623	18.4	18.8	1065	30	1614	-87.8	1540	-79.7	3.4
11199	26.3	26.5	985	40	1697	-87.9	1639	-81.5	4.6
15087	45	45.4	710	40	1894	-78.4	1874	-76.2	4.6
15100	45.4	45.6	685	30	1898	-75.9	1878	-73.7	3.5
15084	45.9	46.1	770	40	1903	-86.2	1884	-84.2	4.6
15092	46.6	46.9	715	30	1911	-80.8	1894	-78.9	3.4
15080	48	48.3	660	40	1926	-76.2	1911	-74.5	4.6
15094	48.8	49.1	705	40	1934	-82.2	1921	-80.8	4.6
15089	49.5	49.8	685	40	1941	-80.8	1930	-79.5	4.6
15099	50	50.3	685	40	1947	-81.4	1936	-80.2	4.6
15086	50.8	51	665	40	1955	-80.0	1946	-79.0	4.6
15088	51	51.3	660	40	1957	-79.7	1949	-78.8	4.6
15097	52	52.6	650	50	1969	-79.9	1963	-79.2	5.7
15091	53.1	53.3	615	50	1979	-76.9	1975	-76.5	5.7
15095	53.3	53.7	585	40	1982	-73.8	1978	-73.4	4.6
15101	54.1	54.4	380	40	1990	-50.8	1988	-50.6	4.7
15082	54.5	55	295	30	1995	-41.3	1994	-41.2	3.6
15093	55	55.3	245	40	1999	-35.8	1999	-35.8	4.8
6473	55	55.3	315	40	1999	-44.2	1999	-44.2	4.8
8634	55	55.3	260	40	1999	-37.6	1999	-37.6	4.8
6460	55	55.3	275	30	1999	-39.4	1999	-39.4	3.6

Table 2.3. Radiocarbon Time Series Results

slower than 5 mm/yr (coral age at least 110 years) (Adkins, Henderson et al. 2004). The growth rates are also in agreement with those established for other species of deep-sea coral, which range from 0.1 to 3 mm/yr (Druffel, King et al. 1990; Cheng, Adkins et al. 2000; Risk, Heikoop et al. 2002; Adkins, Henderson et al. 2004). The position of the radial sections above and below the branch point illustrate that the vertical coral growth rate is linear across the branch point, making this coral an excellent candidate for radiocarbon and other geochemical reconstructions of the deep-sea. To use these estimates of growth rate to determine calendar ages along the coral growth axis, we set the age at the end of the branch to September, 2001, the date that the coral was collected.

Discussion

The recent $\Delta^{14}C$ history of the North Atlantic (1950–2001) at 1400m based on the calendar ages derived from the estimated growth rates is shown with the atmosphere and surface ocean records in figure 2.5. The lower bound is based on the faster growth rate (0.95 mm/yr), and the upper bound is based on the slower growth rate (0.80 mm/yr). Any one coral ^{14}C age measurement can move from the black line to the edge of the gray area along ^{14}C decay vectors (shown as black arrows for three points in figure 2.5). The reconstructed $\Delta^{14}C$ time series shows a stable $\Delta^{14}C$ in the intermediate/deep-water up to the early 1970s with a value of –80 ± 1‰. We detect the first influence of bomb radiocarbon with the slight rise in $\Delta^{14}C$ starting in 1975–1979. $\Delta^{14}C$ then increases by 41‰ to plateau at –39 ± 2‰ (1994–2001).

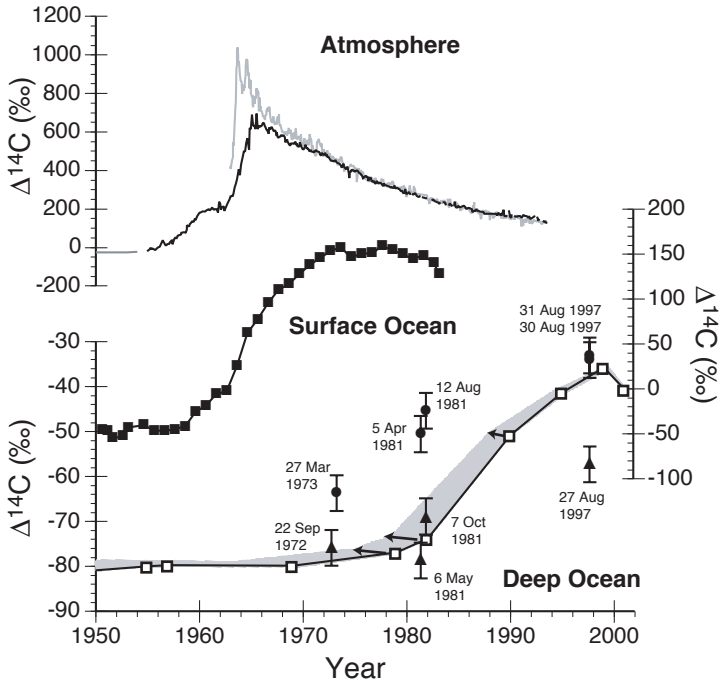

Figure 2.5. Our $\Delta^{14}C$ reconstruction for 1400 meters deep off of Bermuda from 1950-2001 with the atmospheric record (Manning and Melhuish 1994; Nydal and Lovseth 1996; Stuiver, Reimer et al. 1998) and surface ocean record (Druffel 1989). In the bottom panel, the lower curve is based on the 0.95 mm/yr vertical growth rate, the upper curve is based on the 0.80 mm/yr vertical growth rate. The arrows show the trajectory of the errors due to uncertainty in the calendar ages. The open squares are the data points with the faster growth rate. The circles and triangles are the isopycnal matched $\Delta^{14}C$ results from the survey data and correspond to the points in figure 2.2.

At first glance, the nearest isopycnal (σ_θ) matched GEOSECS, TTO, and WOCE station $\Delta^{14}C$ data appear to disagree with the coral results, but a closer look reveals that the prebomb southern stations (triangles) agree with our pre-bomb record and the more northern stations in the late 1990s (circles) agree with the end of our $\Delta^{14}C$ record. Comparing to the GEOSECS data of the North Atlantic from 1972–1973, the more southern station –76 ± 4‰ agrees with our prebomb value of –80 ± 1‰. The 4 stations from TTO in 1981 show that the bomb pool has reached the more northern stations (–45 ± 4‰, –51 ± 4‰), but $\Delta^{14}C$ in our record (–70 ± 4‰) is just beginning to rise and is in line with the $\Delta^{14}C$ observations from the more southern stations (–69 ± 4‰, –79 ± 4‰). Because the more northern WOCE stations from the late 1990s (–34 ± 4‰, –33 ± 4‰) agree with our coral result (–39‰ ± 2), we conclude that this intermediate/deep ocean site is fully engulfed in the bomb radiocarbon pool and that the $\Delta^{14}C$ of this site has begun to level off. The WOCE station that is just south of Bermuda had not yet been nearly engulfed in the bomb radiocarbon pool at the time the deep-sea coral was collected and has a value of –57 ± 4‰.

A comparison of the deep ocean $\Delta^{14}C$ record to the coral record from the surface ocean near Bermuda (Druffel 1989) and the atmospheric record (Manning and Melhuish 1994; Nydal and Lovseth 1996; Stuiver, Reimer et al. 1998) shows the movement of atmospheric $\Delta^{14}C$ to the surface and deep ocean reservoirs. The atmosphere and surface ocean begin to increase at nearly the same time (1955–1958), but the northern hemisphere atmosphere peaks at 1000‰ and the surface ocean at Bermuda plateaus at 150‰ 10 years

later in 1974. The maximum $\Delta^{14}C$ for the deep ocean just north of Bermuda is reached 35 years after the $\Delta^{14}C$ peak in the northern hemisphere atmosphere.

Conclusion

Radiocarbon dating of a modern *E. rostrata* deep-sea coral provides an age model for the coral from prebomb sections, which we use to obtain a $\Delta^{14}C$ time series for the time 1950–2001, when bomb radiocarbon moves into the intermediate/deep North Atlantic. Our results, like those from a study of excess ^{210}Pb (Adkins, Henderson et al. 2004), are consistent with simultaneous upward coral growth and trunk thickening. The radiocarbon data show that the coral grew upward with a linear growth rate of 0.80–0.95 mm/yr. The resulting $\Delta^{14}C$ timeseries reconstruction shows bomb radiocarbon first moving to the coral growth site in 1975–1979 and shows that $\Delta^{14}C$ increased from –80 ± 1‰ (1930–1979) to a plateau at –39 ± 2‰ (1994–2001).

Bibliography

Adkins, J. F., H. Cheng, E. A. Boyle, E. R. M. Druffel, and R. L. Edwards. 1998. Deep-sea coral evidence for rapid change in ventilation of the deep North Atlantic 15,400 years ago. *Science* 280 (5364):725-728.

Adkins, J. F., S. Griffin, M. Kashgarian, H. Cheng, E. R. M. Druffel, E. A. Boyle, R. L. Edwards, and C. C. Shen. 2002. Radiocarbon dating of deep-sea corals. *Radiocarbon* 44 (2):567-580.

Adkins, J. F., G. M. Henderson, S. L. Wang, S. O'Shea, and F. Mokadem. 2004. Growth rates of the deep-sea scleractinia Desmophyllum cristagalli and Enallopsammia rostrata. *Earth And Planetary Science Letters* 227 (3-4):481-490.

Broecker, W. S., R. Gerard, M. Ewing, and B. C. Heezen. 1960. Natural radiocarbon in the Atlantic Ocean. *Journal of Geophysical Research* 65 (9):2903-2931.

Broecker, W. S., and T. H. Peng. 1982. *Tracers in the Sea.* Palisades: LDEO.

Cheng, H., J. Adkins, R. L. Edwards, and E. A. Boyle. 2000. U-Th dating of deep-sea corals. *Geochimica et Cosmochimica Acta* 64 (14):2401-2416.

Druffel, E. R. M. 1989. Decade time scale variability of ventilation in the North Atlantic: High-precision measurements of bomb radiocarbon in banded corals. *Journal of Geophysical Research* 94 (C3):3271-3285.

Druffel, E. R. M., L. L. King, R. A. Belastock, and K. O. Buesseler. 1990. Growth rate of a deep-sea coral using 210Pb and other isotopes. *Geochimica et Cosmochimica Acta* 54:1493-1500.

Druffel, E.M., and T.W. Linick. 1978. Radiocarbon in annual coral rings of Florida. *Geophysical Research Letters* 5 (11):913-916.

Druffel, E.M., and H.E. Suess. 1983. On the radiocarbon record in banded corals: Exchange parameters and net transport of 14CO2 between atmosphere and surface ocean. *Journal of Geophysical Research* 88 (C2):1271-1280.

Eltgroth, S. F., J. F. Adkins, L. F. Robinson, K. Michaele, and J. Southon. 2005. A deep-sea coral record of North Atlantic radiocarbon through the Younger Dryas: Evidence for intermediate/deep-water reorganization. *Paleoceanography* submitted.

Frank, N., M. Paterne, L. Ayliffe, T. van Weering, J. P. Henriet, and D. Blamart. 2004. Eastern North Atlantic deep-sea corals: Tracing upper intermediate

water Delta C-14 during the Holocene. *Earth and Planetary Science Letters* 219 (3-4):297-309.

Guilderson, T.P., D.P. Schrag, M. Kashgarian, and J. Southon. 1998. Radiocarbon variability in the western equatorial Pacific inferred from a high-resolution coral record Nauru Island. *Journal of Geophysical Research* 103 (C11):24,641-24,650.

Key, R. M., A. Kozyr, C. L. Sabine, K. Lee, R. Wanninkhof, J. L. Bullister, R. A. Feely, F. J. Millero, C. Mordy, and T. H. Peng. 2004. A global ocean carbon climatology: Results from Global Data Analysis Project (GLODAP). *Global Biogeochemical Cycles* 18:GB4031.

Mangini, A., M. Lomitschka, R. Eichstadter, N. Frank, S. Vogler, G. Bonani, I. Hajdas, and J. Patzold. 1998. Coral provides way to age deep water. *Nature* 392 (6674):347-348.

Manning, M. R., and W. H. Melhuish. 1994. Atmospheric 14C record from Wellington. In *Trends: A Compendium of Data on Global Change*, edited by C. D. I. A. Center. Oak Ridge: Oak Ridge National Laboratory.

Nydal, R., and K. Lovseth. 1983. Tracing bomb 14C in the atmosphere 1962-1980. *Journal of Geophysical Research* 88 (C6):3621-3642.

———. 1996. Carbon-14 Measurements in atmospheric CO2 from northern and southern hemisphere sites, 1962-1993, edited by C. D. I. A. Center. Oak Ridge: Oak Ridge National Laboratory.

Risk, M.J., J.M. Heikoop, M.G. Snow, and R. Beukens. 2002. Lifespans and growth patterns of two deep-sea corals: Primnoa resedaeformis and Desmophyllum cristagalli. *Hydrobiologia* 471:125-131.

Robinson, LF, JF Adkins, LD Keigwin, J. Southon, DP Fernandez, S. L. Wang, and D Scheirer. 2005. Radiocarbon variability in the Western North Atlantic during the last deglaciation. *Science* submitted.

Schmidt, A., G.S. Burr, F.W. Taylor, J. O'Malley, and J.W. Beck. 2004. A semiannual radiocarbon record of a modern coral from the Solomon Islands. *Nuclear Instruments and Methods in Physics Research B* 223-224:420-427.

Schroder-Ritzrau, A., A. Mangini, and M. Lomitschka. 2003. Deep-sea corals evidence periodic reduced ventilation in the North Atlantic during the LGM/Holocene transition. *Earth and Planetary Science Letters* 216 (3):399-410.

Stuiver, M., and H.G. Ostlund. 1980. GEOSECS Atlantic Radiocarbon.

Radiocarbon 22 (1):1-24.

Stuiver, M., and H. A. Polach. 1977. Reporting of C-14 Data - Discussion. *Radiocarbon* 19 (3):355-363.

Stuiver, M., and P.D. Quay. 1981. Atmospheric 14C changes resulting from fossil fuel CO2 release and cosmic ray flux variability. *Earth and Planetary Science Letters* 53 (2):349-362.

Stuiver, M., P.J. Reimer, and T.F. Braziunas. 1998. High-precision radiocarbon age calibration for terrestrial and marine samples. *Radiocarbon* 40 (3):1127-1151.

Chapter 3

A Deep-Sea Coral Record OF North Atlantic Radiocarbon Through The Younger Dryas: Evidence for Intermediate/Deep Water Reorganization

Selene F. Eltgroth, Jess F. Adkins, Laura F. Robinson, John Southon,
and Michaele Kashgarian

Abstract

Our record of Younger Dryas intermediate depth seawater $\Delta^{14}C$ measured in North Atlantic deep-sea corals supports a link between abrupt climate change and intermediate ocean variability. Our data show that northern source intermediate water (~1700m) was replaced by ^{14}C depleted southern source water at the onset of the event, consistent with a reduction in the rate of North Atlantic Deep Water formation. This transition requires the existence of large, mobile gradients of $\Delta^{14}C$ in the ocean during the Younger Dryas. The $\Delta^{14}C$ water column profile from Keigwin (2004) provides direct evidence for the presence of one such gradient at the beginning of the Younger Dryas (~12.9 ka), with a 100‰ offset between shallow (<~2400m) and deep water. Our early Younger Dryas data are consistent with this profile and also show a $\Delta^{14}C$ inversion, with 35‰ more enriched water at ~2400m than at ~1700m. Over the rest of the Younger Dryas our intermediate/deep water coral $\Delta^{14}C$ data gradually increases while the atmosphere $\Delta^{14}C$ drops. For a very brief interval at ~12.0 ka and at the end of the Younger Dryas (11.5 ka), intermediate water $\Delta^{14}C$ (~1200m) approached atmospheric $\Delta^{14}C$. These enriched $\Delta^{14}C$ results suggest an enhanced initial $\Delta^{14}C$ content of the water and demonstrate the presence of large lateral $\Delta^{14}C$ gradients in the intermediate/deep ocean. The transient $\Delta^{14}C$ enrichment at ~12.0 ka occurred in the

middle of the Younger Dryas and demonstrates that there is at least one time when the intermediate/deep ocean underwent dramatic change but with much smaller effects in other paleoclimatic records.

Introduction

As recorded in the Greenland ice cores, the Younger Dryas is an ~1400 year long abrupt return to glacial-like conditions during the last deglaciation (figure 3.1A) (Dansgaard, Johnsen et al. 1993; Grootes, Stuiver et al. 1993). The Younger Dryas is unique among the many millennial scale Dansgaard-Oeshger (DO) oscillations that punctuate the glacial period because it occurred during the glacial termination. The age of this event (13.0–11.6 ka) means that it is easily datable by ^{14}C, a fact that makes ^{14}C a promising tool for studying rapid climate change during this interval.

Correlation across sedimentary records of the Younger Dryas has been difficult because of the radiocarbon "age plateau" over much of the interval. This characteristic is illustrated by the $\Delta^{14}C_{atm}$ record measured in planktonic foraminifera from the varved sediments of the Cariaco Basin (Hughen, Southon et al. 2000) (figure 3.1C). After the onset of the Younger Dryas, $\Delta^{14}C_{atm}$ drops at nearly the same rate as ^{14}C decays, leading to a range of calendar ages where the radiocarbon age is nearly constant. While not unique in the climate record, this aspect of the Younger Dryas represents the delicate balance between sources and sinks in the radiocarbon budget.

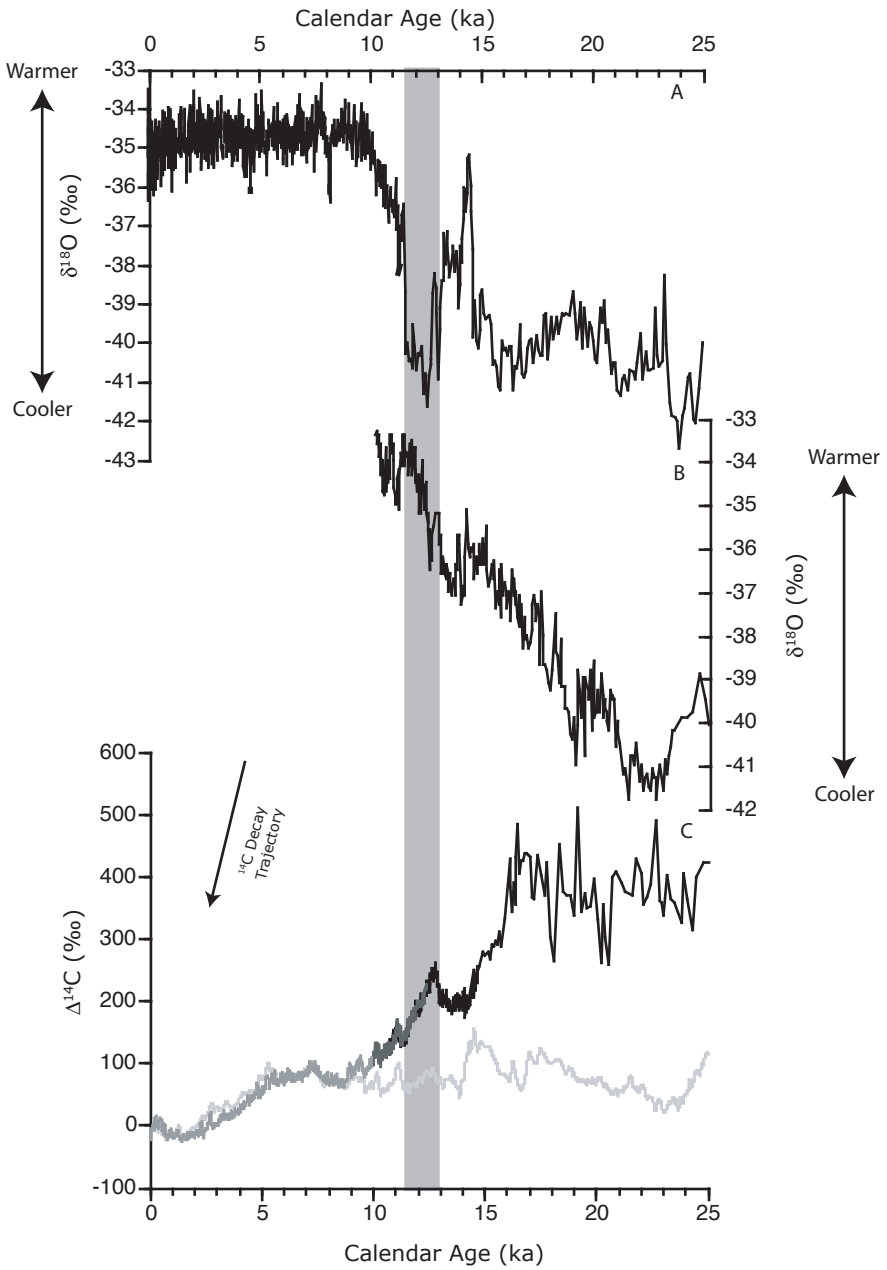

Figure 3.1. A 25 ka record of climate from (A) GISP2 $\delta^{18}O$ (Grootes, Stuiver et al. 1993) shows dramatic cooling in Greenland that is not seen in the Antarctic record of (B) Byrd $\delta^{18}O$ (Blunier and Brook 2001). A comparison between the atmospheric $\Delta^{14}C$ record (C), compiled from the tree ring record (dark gray curve) (Stuiver, Reimer et al, 1998; Friedrich, Remmele et al. 2004) and the varved sediments of the Cariaco Basin (black curve) (Hughen, Southon et al. 2000; Hughen, Lehman et al. 2004a; Hughen, Southon et al. 2004b), and the ^{10}Be based $\Delta^{14}C$ reconstruction (lower estimate) (light gray curve) (Muscheler, Beer et al. 2004) demonstrates that the atmospheric $\Delta^{14}C$ record during the Younger Dryas is larger than the production estimate of ^{14}C. Therefore the Younger Dryas peak in atmospheric $\Delta^{14}C$ was probably caused by a decrease in the ocean uptake of ^{14}C. The Younger Dryas is highlighted in the records.

The inventory of atmospheric ^{14}C is set by the balance of inputs from cosmic ray production and outputs due to both the *in situ* radioactive decay of ^{14}C and the carbon exchange with other reservoirs (equation 3.1) (Broecker and Peng 1982).

$$\frac{d^{14}C_{atm}}{dt} = Production - \lambda^{14}C_{atm} - Ocean\ Exchange \qquad \text{(equation 3.1)}$$

Over centennial and millennial timescales, this balance is dominated by two terms, the production rate and the rate of ^{14}C uptake by the oceans. Therefore, trends in the record of $\Delta^{14}C_{atm}$ can be compared with those of production and $\Delta^{14}C_{deep\ ocean}$ with one important caveat: the response time of the $^{14}C_{atm}$ system to production rate changes is much longer than that for changes in the oceanic loss term (Muscheler, Beer et al. 2004). This difference in response time arises because production rate variations alter the inventory of ^{14}C atoms in the system, but the ocean exchange term only reorganizes the existing ^{14}C atoms between reservoirs.

For $\Delta^{14}C_{atm}$ to change at the same rate as ^{14}C decays, the input from production must equal the net ocean uptake. This flux balance during the latter part of the Younger Dryas stands in contrast to its initiation where the Cariaco basin record of $\Delta^{14}C_{atm}$ shows an initial 70‰ rise over ~200 years starting at 13.0 ka (Hughen, Southon et al. 2000) (figure 3.1C). With a roughly constant radiocarbon production rate (Muscheler, Beer et al. 2004), the observed peak in Younger Dryas $\Delta^{14}C_{atm}$ is well above that expected from production alone. Since decay in the deep ocean is the largest sink for radiocarbon and North Atlantic Deep Water (NADW) formation is the primary mode of ^{14}C transport to the deep reservoir in the modern ocean (Broecker and Peng 1982), the initial sharp peak in Younger Dryas $\Delta^{14}C_{atm}$ implies a decrease in the ocean uptake, specifically a reduction in the rate of

NADW formation, that persisted for ~200 years. The subsequent decline in $\Delta^{14}C_{atm}$ is consistent with a reinvigoration of NADW formation or the activation of another ^{14}C sink that brings the ^{14}C system back toward steady state with atmospheric production.

This type of NADW variability is at the heart of the leading hypothesis to explain the mechanism behind abrupt glacial climate changes and hemispheric interconnections more generally. According to the "salt oscillator," Atlantic salinity is modulated by ice sheet formation/melting and the export of salt out of the basin with the overturning circulation (Broecker, Bond et al. 1990). When Atlantic salinity is reduced, the surface density in the high-latitude north becomes insufficient for surface water to sink, thus turning "off" NADW formation. The "bipolar seesaw", accounts for the asynchronous connection between the Arctic and Antarctic ice core records of temperature (Sowers and Bender 1995; Blunier, Chappellaz et al. 1998; Broecker 1998; Blunier and Brook 2001). In this case, the density gradient between sinking regions in the south and in the north swings back and forth with NADW "on" conditions cooling the southern hemisphere by drawing heat from the south to the north and NADW "off" conditions leading to the rapid coolings seen in the Greenland ice cores.

These theories are crucially dependent on the flux of deep water formed in the North Atlantic, yet most of our deep ocean tracers do not contain an intrinsic measure of the ventilation rate. Nutrient tracers such as $\delta^{13}C$ and Cd/Ca allow for an estimate of the relative proportions of deep source waters. A record of deep (4450m) Atlantic Cd/Ca measured in benthic foraminifera from the Bermuda Rise indicate that deep-water nutrients increased during the Younger Dryas reflecting an increased southern source influence

(Boyle and Keigwin 1987). At the same time, intermediate water (965m) nutrients from the Bahama Banks declined reflecting an increased contribution from northern source water (Marchitto, Curry et al. 1998). The evidence suggests that at the start of the Younger Dryas, NADW shoaled and was replaced by deep water from a southern source. These high resolution sediment core records indicate that deep-water is capable of rapid reorganization on time scales similar to that recorded in the Greenland ice cores. However, the volumetric reduction of northern source water at the beginning of the Younger Dryas does not necessarily mean that its flux was reduced. A second estimate of overturning rate through the Younger Dryas comes from (^{231}Pa/^{230}Th) ratios in deep-sea sediments (McManus, Francois et al. 2004). This record implies that while the overturning rate of the North Atlantic was lower during the Younger Dryas as compared to today, it was not nearly as reduced as during Heinrich 1.

In the modern ocean we estimate the ventilation age of the deep ocean by measuring the ^{14}C content of dissolved inorganic carbon (Broecker and Peng 1982; Stuiver, Quay et al. 1983). Unfortunately, for sediment studies of paleoclimate, ^{14}C is often our only chronometer, preventing it from also being a tracer of past ventilation. Two independent methods have been developed to overcome this limitation: paired benthic/planktonic ^{14}C ages and coupled U-series/^{14}C ages from deep-sea corals. In each case, the Δ^{14}C of the past deep water can be calculated directly.

Four factors determine the radiocarbon content of a water parcel. The Δ^{14}C of the atmosphere when the water was last at the surface and the surface/atmosphere offset (reservoir age) set the initial ^{14}C concentration of the water. When the water leaves the

surface ocean, mixing with other water masses and *in situ* aging will cause $\Delta^{14}C$ to evolve with time. To calculate deep ocean ventilation rates from $\Delta^{14}C$ measurements, we need to isolate this *in situ* aging component, which is directly related to the time the water has been below the surface. We have several constraints on the other three factors. Atmospheric ^{14}C content (Hughen, Southon et al. 2000; Friedrich, Remmele et al. 2004; Hughen, Lehman et al. 2004) and surface ocean reservoir ages (Bard, Arnold et al. 1994; Hughen, Overpeck et al. 1996; Siani, Paterne et al. 2001; Waelbroeck, Duplessy et al. 2001) can be estimated, and mixing ratios of deep source waters can be derived from quasi-conservative tracers such as $d^{13}C$ (Raymo, Oppo et al. 2004; Curry and Oppo 2005; Pahnke and Zahn 2005) and Cd/Ca (Boyle and Keigwin 1987; Marchitto, Curry et al. 1998). Without these corrections, reconstructed $\Delta^{14}C$ results are analogous to water column measurements made today and reflect the sum of these processes.

Comparison of benthic and planktonic foraminiferal radiocarbon ages from the same time horizon in a sediment core also provide an estimate of the ventilation age of that water (Broecker, Klas et al. 1990), with one addition to the assumptions listed above. This method is limited by the implicit assumption that the ^{14}C concentration of the surface water for planktonic foraminifera is identical to the initial surface ^{14}C concentration of the water mass in which the benthic foraminifera grew (Adkins and Boyle 1997). During periods of rapid ^{14}C fluctuation like the Younger Dryas, changing initial surface water concentrations will be incorporated in the resulting ventilation age. This point not withstanding, comparison of benthic-planktonic records in either space or time are important constraints on the past ocean ventilation rate.

Keigwin (2004) examined benthic/planktonic foraminifera pairs from a suite of North Atlantic sediment cores and demonstrated that the ^{14}C profile during the early part of the Younger Dryas consisted of ^{14}C depleted water beneath ^{14}C enriched water with a transition between the two at ~2400m. This implies that well ventilated water from the north did not penetrate below this front. Skinner and Shackleton (2004) generated a $\Delta^{14}C$ time series at 3000m in the northeast Atlantic using a correlation between their measured planktonic foraminiferal $\delta^{18}O$ record and that of Greenland ice to estimate an independent calendar age for each time horizon. The data point that falls within the Younger Dryas interval indicates that deep-water was radiocarbon depleted compared to the data point ~200 yr before. While sediment core resolution is ultimately limited by age model uncertainty due to bioturbation processes, individual deep-sea corals lack this limitation and offer improved $\Delta^{14}C$ resolution.

Modern deep-sea corals accurately record the $\Delta^{14}C$ of dissolved inorganic carbon (Adkins, Griffin et al. 2002) and have an advantage over sediment core measurements because they can be precisely dated using U-Th techniques (Cheng, Adkins et al. 2000). Two timescales of $\Delta^{14}C$ history are available in the deep-sea coral archive. A time series with resolution similar to a sediment core can be constructed by comparing results from different coral specimens. In this case, the time span of interest is bounded only by the calendar age distribution of the samples collected. In addition, finely spaced measurements within these individual corals span very brief (~100 yr) time intervals with ~10 yr resolution (see Adkins, Cheng et al. 1998; Adkins, Henderson et al. 2004). This resolution

is similar to that of ice cores and is ultimately constrained by the growth pattern of the coral.

Five previous studies have used coupled U-Th and ^{14}C ages in deep-sea corals to determine the $\Delta^{14}C$ of past seawater (Adkins, Cheng et al. 1998; Mangini, Lomitschka et al. 1998; Goldstein, Lea et al. 2001; Schroder-Ritzrau, Mangini et al. 2003; Frank, Paterne et al. 2004). Goldstein et al. (2001) found that the Heinrich 1 Southern Ocean at 1125m was more ^{14}C depleted than today with respect to the atmosphere, suggesting that the $\Delta^{14}C$ signature of the southern source water has varied in the past. Adkins et al. (1998) demonstrated that western North Atlantic intermediate/deep water $\Delta^{14}C$ decreased significantly (by ~70‰) between 13.7 and 12.9 ka. Schroder-Ritzrau et al. (2003) found a similar decrease in $\Delta^{14}C$ between 13.9 and 13.0 ka in the eastern North Atlantic, though the shallow depth (240m) and proximity to the coast suggest that these samples may have experienced atmospheric and terrestrial influences that deep, open ocean sites do not have. Their other corals from Younger Dryas intermediate water record atmosphere/ocean $\Delta^{14}C$ offsets similar to modern, with the exception of one at 11.4 ka that has a larger depletion relative to the atmosphere. Frank et al. (2004) adds one coral from 10.2 ka, toward the end of our interval of interest, which shows a $\Delta^{14}C$ offset between the atmosphere and intermediate ocean (~730m) similar to that observed in a modern coral. Here, we add to the growing body of deep-sea coral data and measure $\Delta^{14}C$ in North Atlantic samples to investigate changes in deep-water ventilation and organization over the Younger Dryas cold period.

Samples and Methods

We routinely screen new fossil deep-sea coral samples for their calendar age. Previously we have used a relatively imprecise, but high throughput, quadrupole ICP-MS technique (Adkins and Boyle 1999). With the advent of multi-collector magnetic sector ICP-MS we have switched to precisely dating every sample (Robinson, Adkins et al. 2005). We selected 7 North Atlantic *Desmophyllum dianthus* (Esper, 1794) corals with U-Th calendar ages that fall within the Younger Dryas (13.0 to 11.5 ka) from our larger sample pool. Our samples are from the Smithsonian invertebrate collection (1 sample) and from a *DSV Alvin* cruise to the New England seamounts in May-June 2003 (6 samples) (table 3.1).

Reconstructing $\Delta^{14}C$

To reconstruct $\Delta^{14}C$ in the past ocean we measure the conventional ^{14}C age of the coral and use the measured U-Th calendar age to account for closed system radioactive decay since the time of aragonite precipitation according to the expression:

$$\Delta^{14}C = \left(\frac{e^{-\frac{^{14}C\ Age}{Libby\ Mean\ Life}}}{e^{-\frac{U/Th\ Cal\ Age}{True\ Mean\ Life}}} - 1\right) \times 1000‰ \qquad \text{(equation 3.2)}$$

where the Libby Mean Life is 8033 yr and the True ^{14}C Mean Life is 8267 yr (Stuiver and Polach 1977). Conventional ^{14}C ages are $\delta^{13}C$ normalized to account for isotopic fractionation and $\Delta^{14}C$ is a measure of the relative difference between this normalized $^{14}C/^{12}C$ ratio and a standard (Stuiver and Polach 1977).

U-Th Calendar Ages

U-Th calendar ages were determined for a top portion (~1g) from each coral. Because the calendar age error is comparable to the lifetime of each coral, only one

Sample #	Coral ID	Collection Site	Latitude	Longitude	Depth (m)
YD-1	ALV-3891-1459-003-002	Gregg Seamount	38°56.9'N	61°1.6'W	1176
YD-2	ALV-3891-1758-006-003	Gregg Seamount	38°56.9'N	61°1.7'W	1222
YD-3	Smithsonian 48735.1	Azores	37°57.5'N	25°33.0'W	1069-1235
YD-4	ALV-3890-1407-003-001	Manning Seamount	38°13.6'N	60°27.6'W	1778
YD-5	ALV-3887-1549-004-012	Muir Seamount	33°45.15'N	62°35.3'W	2372
YD-6	ALV-3887-1549-004-007	Muir Seamount	33°45.15'N	62°35.3'W	2372
YD-7	ALV-3887-1549-004-009	Muir Seamount	33°45.15'N	62°35.3'W	2372

Table 3.1. *D. dianthus* sample locations and depths

calendar age measurement was necessary for each coral. Calendar ages for samples closer to the base of the coral were estimated by assuming a 1 mm/yr vertical extension rate (Cheng, Adkins et al. 2000; Adkins, Henderson et al. 2004). Smithsonian sample 48735.1 was U-Th dated by TIMS (Cheng, Adkins et al. 2000), and the New England Seamount samples were U-Th dated by MC-ICPMS (Robinson, Adkins et al. 2005).

Conventional Radiocarbon Ages

To measure a ^{14}C age, a thecal section composed of portions of a S1 septum and the adjacent smaller septa (2–3 mm thick) was cut out of each coral using a small diamond tipped saw attached to a Dremel rotary tool (figure 3.2). Visible contamination on the coral surface was mechanically abraded away with the saw, and any holes formed by endolithic deep-sea organisms were milled out with a drill bit. Each thecal section was cut transversely into pieces (14–50mg each) that were cleaned and leached (>40% mass removal in final leach just prior to graphitization) by the procedure of Adkins et al. (2002). The resulting 10mg pieces were hydrolyzed in phosphoric acid, and the evolved CO_2 was graphitzed under H_2 on an iron catalyst before ^{14}C analysis (Vogel, Southon et al. 1984). Radiocarbon ages were measured at the Lawrence Livermore National Laboratory Center for Accelerator Mass Spectrometry (sample YD-3) and at the University of California, Irvine Keck Carbon Cycle Accelerator Mass Spectrometry (UCI-KCCAMS) Laboratory (all other samples).

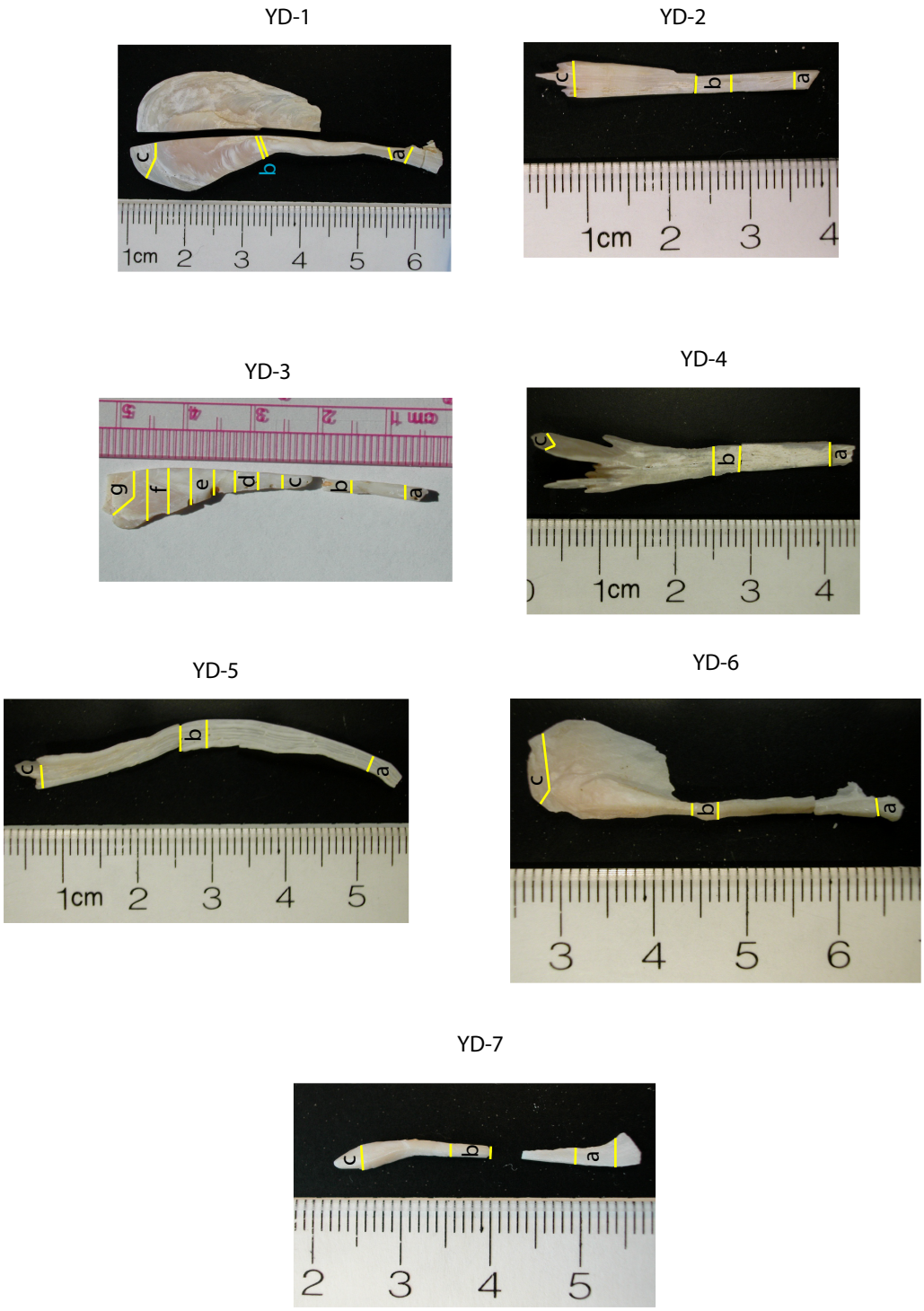

Figure 3.2. D. dianthus deep-sea coral sections sampled for ^{14}C ages. Samples are marked with their corresponding sample numbers.

Results

Our ~2000 year long $\Delta^{14}C$ time series consists of measurements from 7 individual coral skeletons with a sequence of 3 to 7 ^{14}C measurements along each coral transect. U-series and ^{14}C results are summarized in tables 3.2 and 3.3, respectively. The corals fall into two categories: those that contain large within-coral variation in their $\Delta^{14}C$ values (YD-3,4) and those with essentially constant $\Delta^{14}C$ over the entire skeletal transect (YD-1,2,5,6,7) (figure 3.3). Interpreted as a $\Delta^{14}C$ record of the seawater that bathed these corals, our data show that intermediate water (<2000m) $\Delta^{14}C$ increased by ~10–20‰ through the Younger Dryas and exhibited a transient enrichment, of magnitude ~40-50‰, in the middle of the Younger Dryas (~12 ka). Because of their uniformity in $\Delta^{14}C$, the data within each of the low-variability $\Delta^{14}C$ corals have been averaged together in the plots that follow.

Contamination with modern carbon, an issue for all corals, was especially problematic for coral YD-4 from the New England Seamounts (12.2 ka). A slight stain persisted on sample YD-4b after acid leaching and the $\Delta^{14}C$ result for this sample was elevated with respect to samples YD-4a and c (figure 3.3B, gray squares). If this contamination were composed of modern $CaCO_3$ or contained adsorbed CO_2, the contamination, and not a change in the environmental conditions, could conceivably cause the $\Delta^{14}C$ enrichment. Sample YD-4b would have to contain 1% modern $CaCO_3$ to cause the ~30‰ $\Delta^{14}C$ enrichment. The leaching experiment of Adkins et al. (2002) showed that an acid leach resulting in 5–10% sample loss was sufficient to remove any significant contaminating carbon. In the case of sample 4b, 43% of the sample mass was leached away, so it is unlikely that an exterior coating of $CaCO_3$ or adsorbed CO_2 significantly

Sample #	Coral ID	^{238}U (ppm)	Error (2σ) (ppm)	$^{230}Th/^{238}U$	Error (2σ)	^{232}Th (ppb)	Error (2σ) (ppb)	$\delta^{234}U_{Measured}$ (‰)	Error (2σ) (‰)	U/Th Raw Age (yr BP)	Error (2σ) (yr BP)	U/Th Calendar Age (yr BP)	Error (2σ) (yr BP)	$\delta^{234}U_{Initial}$ (‰)	Error (2σ) (‰)
YD-1	ALV-3891-1459-003-002	4.496	0.003	0.1141	0.0005	0.879	0.006	139.6	1.1	11,439	56	11,390	120	144.2	1.1
YD-2	ALV-3891-1758-006-003	3.665	0.003	0.1154	0.0006	0.797	0.008	140.7	1.1	11,565	63	11,500	130	145.4	1.1
YD-3	Smithsonian 48735.1	3.554	0.003	0.1205	0.0010	0.329	0.006	149.2	1.3	12,072	88	11,980	120	154.3	1.3
YD-4	ALV-3890-1407-003-001	3.361	0.002	0.1244	0.0006	1.889	0.008	144.8	1.1	12,482	67	12,230	300	149.9	1.1
YD-5	ALV-3887-1549-004-012	3.286	0.003	0.1259	0.0006	0.561	0.012	142.5	1.1	12,661	62	12,620	110	147.7	1.1
YD-6	ALV-3887-1549-004-007	4.039	0.003	0.1266	0.0006	0.584	0.008	139.6	1.1	12,776	62	12,750	100	144.7	1.1
YD-7	ALV-3887-1549-004-009	3.360	0.002	0.1266	0.0006	0.159	0.007	143.3	1.1	12,733	63	12,760	70	148.5	1.2

Table 3.2. *D. dianthus* U/Th Calendar Ages. Calendar ages are in years before the date of U-series measurement.

Sample #		Lab ID	Coral ID	Sample Span (mm from Coral Base)	^{14}C Age (^{14}C yr before 1950)	Error (2σ) (^{14}C yr before 1950)	Calendar Age (yr before 1950)	Error (2σ) (yr before 1950)	$\Delta^{14}C_{Water}$ (‰)	Propegated Error (2σ) from ^{14}C Age (‰)	Propegated Error (2σ) from Cal Age (‰)	Average $\Delta^{14}C_{Water}$ (‰)	Error ($2\sigma_{mean}$) (‰)
YD-1	a	4722	ALV-3891-1459-003-002	5.8 - 8.3	10070	70	11380	120	131	10	16	135	17
	b	4726		29.7 - 30.6	9940	60	11350	120	145	8			
	c	4709		49.7 - 54.2	10000	50	11330	120	135	8			
YD-2	a	4718	ALV-3891-1758-006-003	0.0 - 3.3	10060	70	11480	130	146	10	18	147	19
	b	4719		11.1 - 15.8	9970	60	11460	130	157	9			
	c	4711		30.5 - 35.1	10040	50	11450	130	145	7			
YD-3	a	45610	Smithsonian 48735.1	0.0 - 3.5	10780	80	11970	120	118	11	17	137	18
	b	45539		11.1 - 15.6	10420	60	11960	120	169	9			
	c	45535		17.3 - 21.6	10500	80	11950	120	156	11			
	d	45540		24.9 - 28.2	10370	60	11950	120	174	9			
	e	45541		31.3 - 33.7	10660	70	11940	120	131	10			
	f	45538		36.3 - 38.3	10750	70	11940	120	118	9			
	g	45536		41.8 - 45.6	10800	70	11930	120	110	10			
YD-4	a	4715	ALV-3890-1407-003-001	0.0 - 2.9	11010	60	12220	300	113	9	42	119	42
	b	4710		14.9 - 18.9	10780	60	12200	300	144	8			
	c	4720		39.7 - 42.6	11030	60	12180	300	106	9			
YD-5	a	4713	ALV-3887-1549-004-012	0.0 - 4.8	11380	60	12620	110	128	9	15	110	16
	b	4723		27.8 - 31.8	11410	70	12590	110	121	10			
	c	4716		50.4 - 54.4	11340	70	12570	110	127	10			
YD-6	a	4712	ALV-3887-1549-004-007	0.0 - 3.0	11500	60	12740	100	116	9	13	118	15
	b	4727		20.2 - 22.7	11370	70	12720	100	131	10			
	c	4717		39.7 - 41.9	11460	60	12700	100	116	9			
YD-7	a	4725	ALV-3887-1549-004-009	3.4 - 8.2	11470	70	12730	70	118	10	9	125	11
	b	4708		16.6 - 20.9	11340	60	12720	70	135	9			
	c	4721		31.3 - 34.2	11420	80	12700	70	123	11			

Table 3.3. *D. dianthus* Radiocarbon Ages and $\Delta^{14}C_{water}$. Calendar ages have been converted to years before 1950.

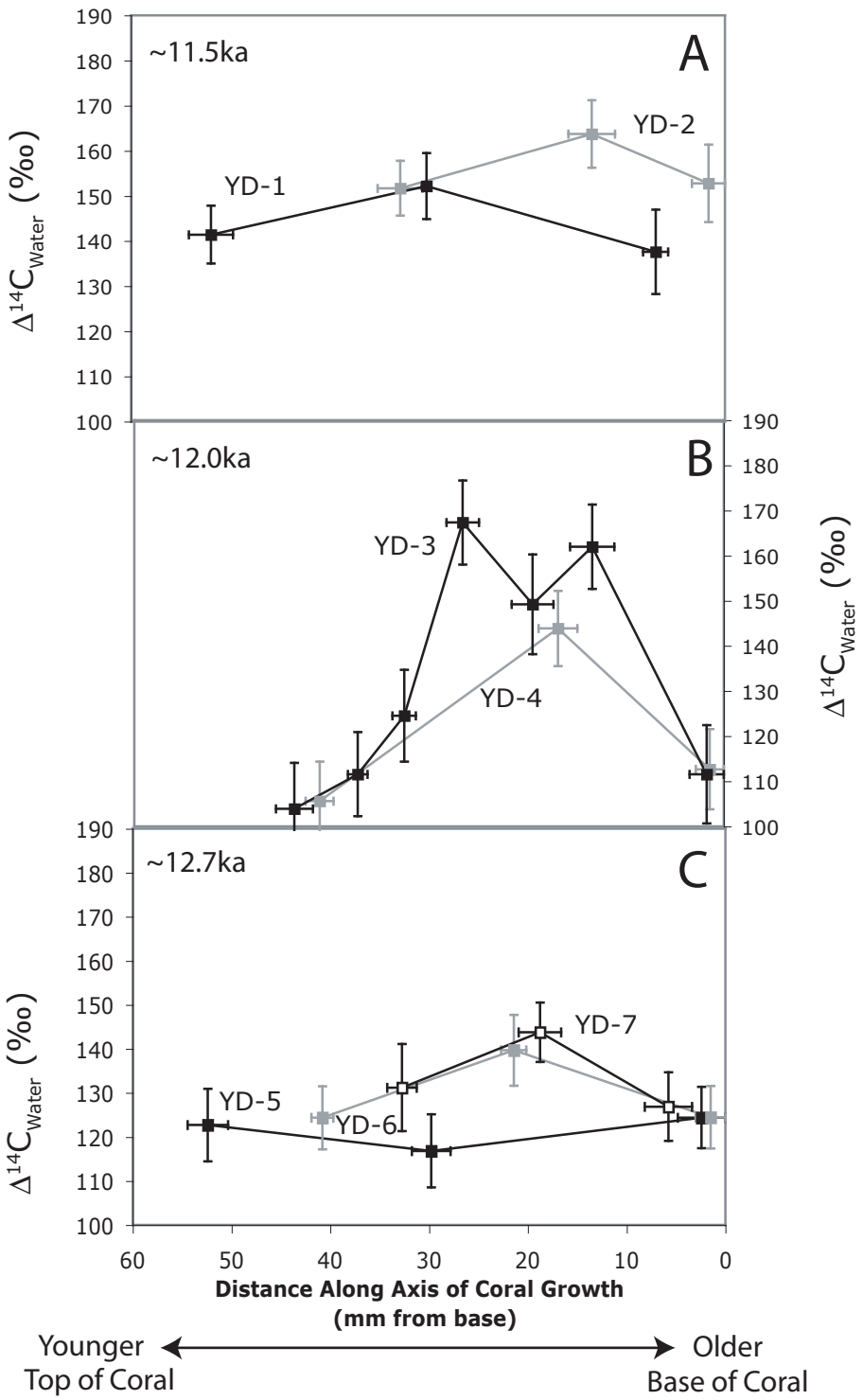

Figure 3.3. *D. dianthus* Younger Dryas $\Delta^{14}C$ results for individual coral transects. These ~100 yr long time series show significant variability only at ~12.0 ka in the middle of the Younger Dryas. The other corals at 11.5 and 12.7 ka show no significant variation over their lifetimes.

above background levels persisted. In this case, the stain comprised far less than 1% of the sample, and since the stain most likely contained organic carbon, which is not oxidized in acidic solution, it is again unlikely to be the cause of the measured ^{14}C enrichment. Furthermore, given that one other coral also shows elevated $\Delta^{14}C$ concurrently, we believe that the environmental signal in YD-4b is robust.

Calcite blanks contain less ^{14}C than samples from a radiocarbon dead (> 50 ka) deep-sea coral samples (figure 3.4). The long-term fraction modern averages (measured at UCI-KCCAMS) for our calcite blanks and a 240 ka deep-sea coral are 0.0012 ± 0.0005 and 0.0039 ± 0.0018 (2σ), respectively. For all of the data reported here, we have adjusted the measured fraction modern using the larger blank associated with the 240 ka coral and its corresponding larger uncertainty. Replacing the deep-sea coral blank with the calcite blank would give a $\Delta^{14}C$ that is ~10‰ more enriched than we report in this paper. The uncertainty in the deep-sea coral ^{14}C background defines the detection limit for our deep-sea coral ^{14}C ages (~45 ka). This uncertainty also limits the precision of our measured past $\Delta^{14}C$ values. In figure 3.5 we propagate the two blank uncertainties (calcite and coral) through the $\Delta^{14}C$ calculation over a range of calendar age errors and find that for the 10–12 ka samples in this study, our $\Delta^{14}C$ errors are primarily governed by the calendar age uncertainty (1%). For older samples, however, more precise background measurements will be needed to produce a meaningful $\Delta^{14}C$ reconstruction.

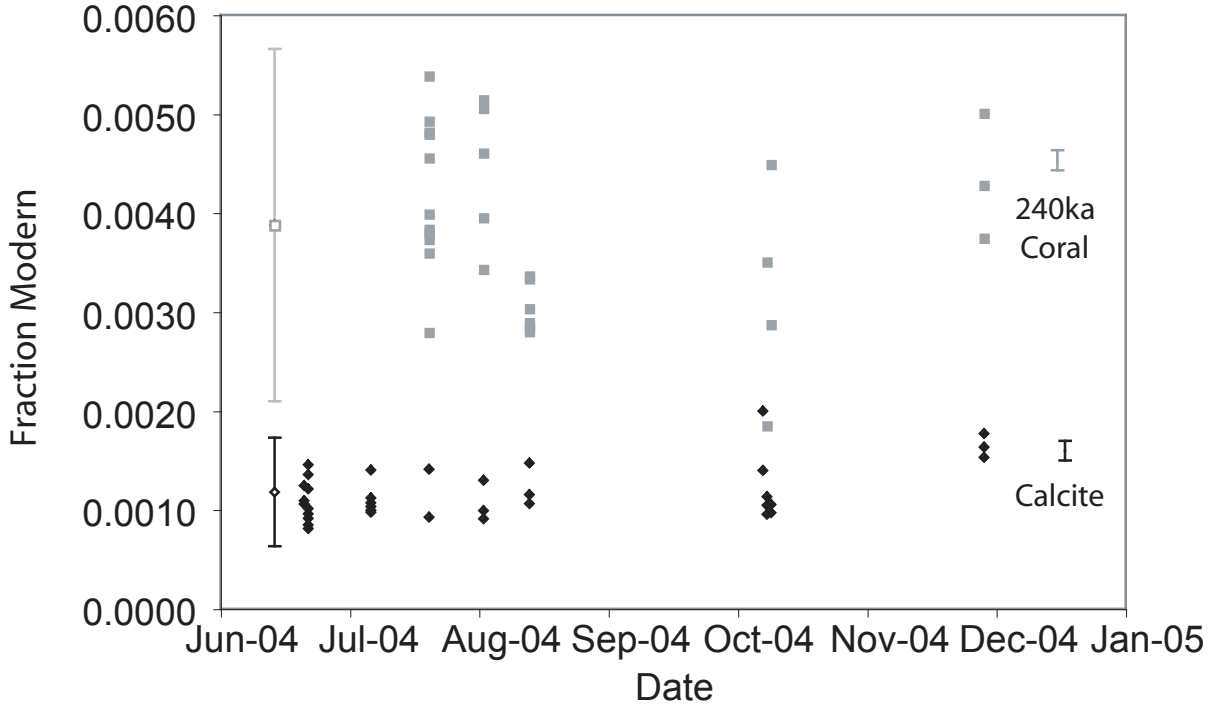

Figure 3.4. Deep-sea coral blanks (gray squares) consistently contain more ^{14}C than calcite blanks (black diamonds). These blank measurements demonstrate that our oldest coral contains some amount of refractory ^{14}C that cannot be cleaned away. The average fraction moderns (measured at UCI-KCCAMS) are 0.0012 ± 0.0005 and 0.0039 ± 0.0018 (2σ) for our calcite blanks and a 240 ka deep-sea coral, respectively (open symbols on the left). Analytical uncertainty for each measurement is given by the error bars on the right. To account for this refractory blank, the result from the 240 ka coral is used to blank correct our sample results.

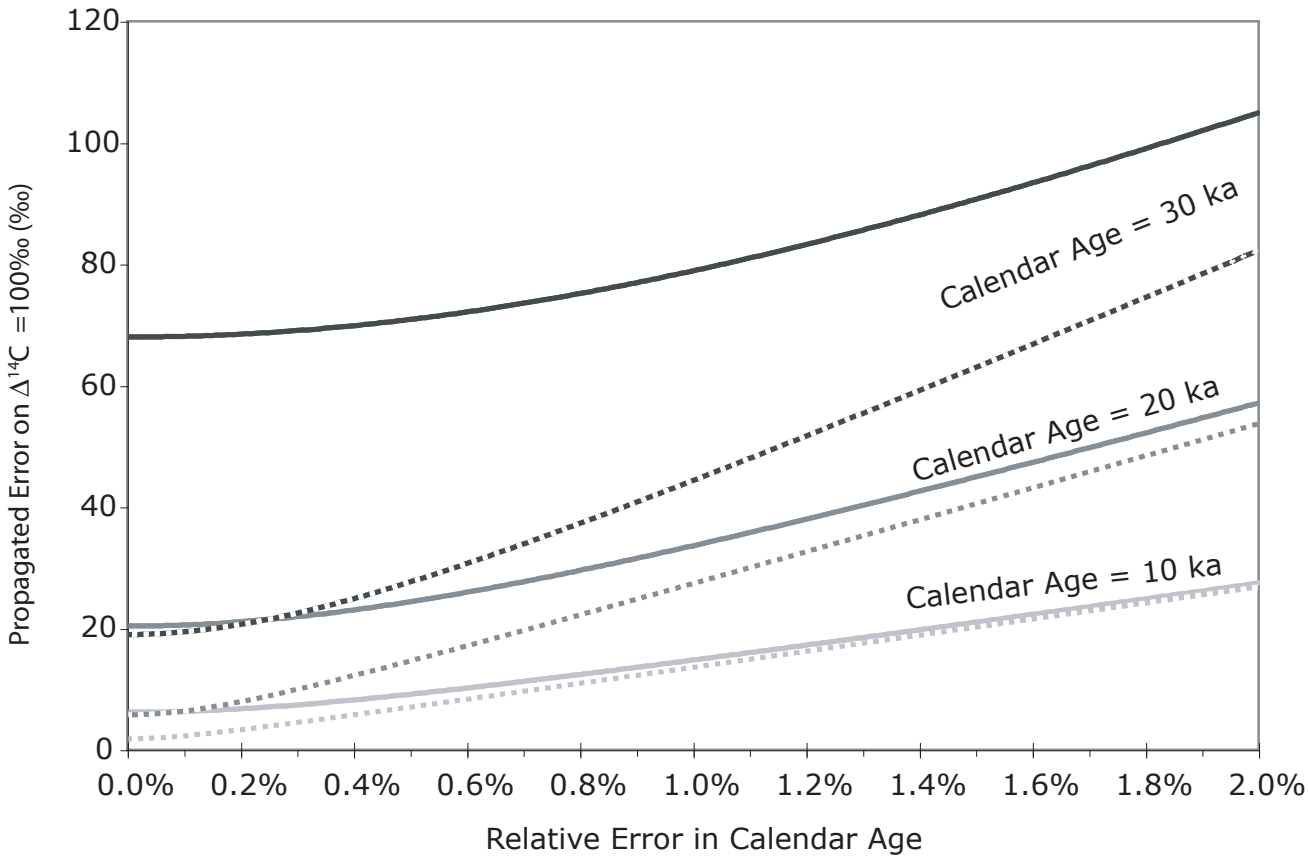

Figure 3.5. Propagated error curves for a $\Delta^{14}C_{water}$ arbitrarily picked to be 100‰ are plotted for calendar ages of 10, 20, and 30 ka. Solid lines have a radiocarbon blank uncertainty based on the measured 240 ka coral data. Dotted lines have a blank uncertainty based on the measured calcite data shown in figure 3.4. For the 10–12 ka samples in this study, our $\Delta^{14}C$ errors are primarily controlled by calendar age uncertainty. For older samples, however, more precise background measurements will be needed to reduce the propagated error.

Discussion

Our measurements of intermediate/deep-water $\Delta^{14}C$ constrain the history of North Atlantic ventilation through the Younger Dryas. Our new data is shown with 2 data points from Adkins et al. (1998), the record of atmospheric $\Delta^{14}C$ from the Cariaco Basin (Hughen, Southon et al. 2000; Hughen, Southon et al. 2004), and the GISP2 ^{10}Be based $\Delta^{14}C$ reconstruction (Muscheler, Beer et al. 2004) in figure 3.6. Over the beginning of the Younger Dryas, the ocean $\Delta^{14}C$ record at ~1700m in the North Atlantic is consistent with the inverse of the atmospheric $\Delta^{14}C$ record. From 13.0 to 12.8 ka, atmospheric $\Delta^{14}C$ rose steeply, while intermediate/deep water $\Delta^{14}C$ dropped by ~70‰ over fewer than ~800 years. If deep-ocean exchange were similar to the modern overturning circulation and continued unabated, $\Delta^{14}C$ of the deep water would follow $\Delta^{14}C_{atm}$. Instead, the observed drop in ocean $\Delta^{14}C$ is evidence that deep-ocean ^{14}C exchange was reduced, probably due to a decrease in the rate of NADW formation and subsequent invasion of ^{14}C depleted southern source water.

If the Younger Dryas was initiated by a cessation of deep-water formation at 13.0 ka, as implied by the $\Delta^{14}C_{atm}$ and the GISP2 $\delta^{18}O$ records, two possible endmember states exist for the intermediate/deep water at our site. The water may stagnate, or it may be replaced by water from another source. To distinguish between the two, we assume that the $\Delta^{14}C$ of JFA2 (160 ± 30‰ at 13.7 ka) is a value representative of pre-Younger Dryas conditions right up to the cutoff at 13.0 ka. If the intermediate water simply stagnated, it would evolve from its initial value at 13.0 ka along the $\Delta^{14}C$ decay trajectory noted in figure 3.6. Decay from 160‰ at 13.0 ka to our next data point at 12.9 ka (JFA17) would

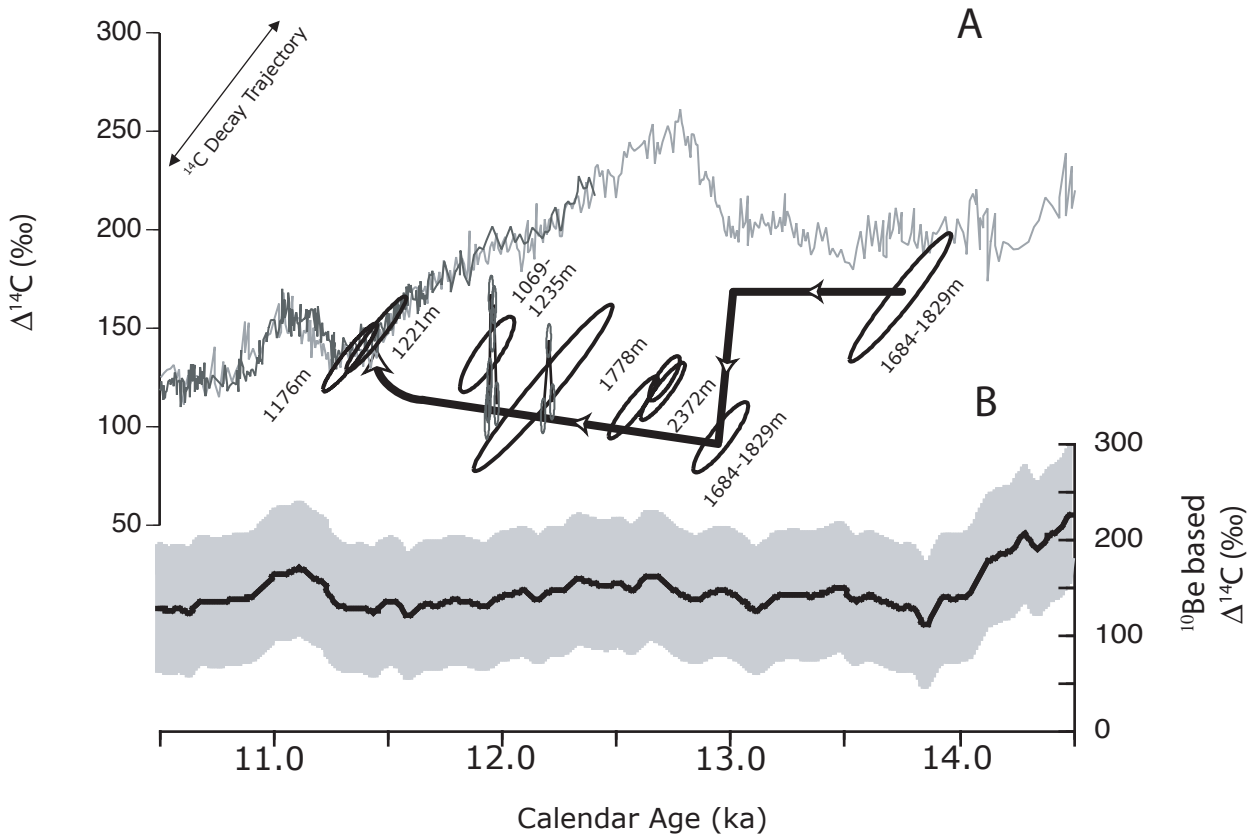

Figure 3.6. *D. dianthus* results are plotted with atmospheric $\Delta^{14}C$ (Friedrich, Remmele et al. 2004; Hughen, Southon et al. 2004b) and the ^{10}Be based $\Delta^{14}C$ reconstruction (Muscheler, Beer et al. 2004). Coral collection depths and the trajectory of projected closed system ^{14}C decay are noted on the chart. Error estimates (2σ) for the coral data are ellipses because the calculated $\Delta^{14}C$ is itself dependent on the calendar age (the x-axis). When $\Delta^{14}C$ errors are dominated by calendar age uncertainty, the major axis of the ellipse is elongated and tends toward an angle equal to the rate of ^{14}C decay. When the ^{14}C age uncertainty dominates the overall $\Delta^{14}C$ errors, the major axis tends toward the vertical. For all points, except the corals with variable $\Delta^{14}C$ at 12.0 ka, the error ellipses are based on the weighted 2σ standard errors of the triplicate ^{14}C age measurements. For the two corals at 12.0 ka the ellipses are based on the average analytical uncertainty of ± 70 years because the separate age measurements do not come from the same parent population. Two relevant points from the Adkins et al. (1998) study of North Atlantic deep-sea corals are also plotted (samples JFA2 (13.7 ka) and JFA17 (12.9 ka)). While production can account for the observed $\Delta^{14}C$ hump at 11.0 ka, production is not sufficient to account for the observed Younger Dryas peak at 12.8 ka. The line through the deep-sea coral data demonstrates how the data are consistent with behavior that is inverse to the atmosphere, which is evidence for a slowdown of North Atlantic intermediate/deep water formation.

produce only a ~13‰ depletion (to ~147‰) compared to the observed 70‰ depletion (to ~90‰). Younger Dryas deep-water formation would have had to cease completely at 13.2–13.4 ka, before any observable change in GISP2 $\delta^{18}O$ or $\Delta^{14}C_{atm}$, in order to account for the measured depletion by stagnation alone. Since stagnation can account for only a minor fraction (18%) of the observed depletion, a rearrangement of water masses, must account for at least 82% of the depletion. The movement of $\Delta^{14}C$ depleted southern source water into this region at the expense of northern source water would result in a rapid shift of the $\Delta^{14}C$ signature to a more depleted value. The magnitude and speed of the transition depend on the size of the gradient that exists in the water and the rate of the water mass reorganization. The size of this transition is large, especially when considering the entire range for the deep Atlantic today is ~85‰, and implies that large, mobile $\Delta^{14}C$ gradients existed in the Younger Dryas intermediate/deep Atlantic.

Two samples at the onset of the Younger Dryas, separated by 210 calendar years and ~600m depth, illustrate these gradients in a vertical water column profile that we compare to a modern profile from the Atlantic expedition of GEOSECS (Stuiver and Ostlund 1980) (figure 3.7). Together with the benthic/planktonic foraminiferal $\Delta^{14}C$ profile from Keigwin (2004), we see that the early Younger Dryas profile is higher in absolute value and spans a much larger $\Delta^{14}C$ range (~100‰ range from shallow to deep) than the modern profile (~15‰ range from shallow to deep). The deep-sea coral $\Delta^{14}C$ profile also highlights the water column structure above 2400m. A $\Delta^{14}C$ inversion is present with the intermediate depth water (1684–1829m) ~35‰ depleted relative to deeper water (2372m).

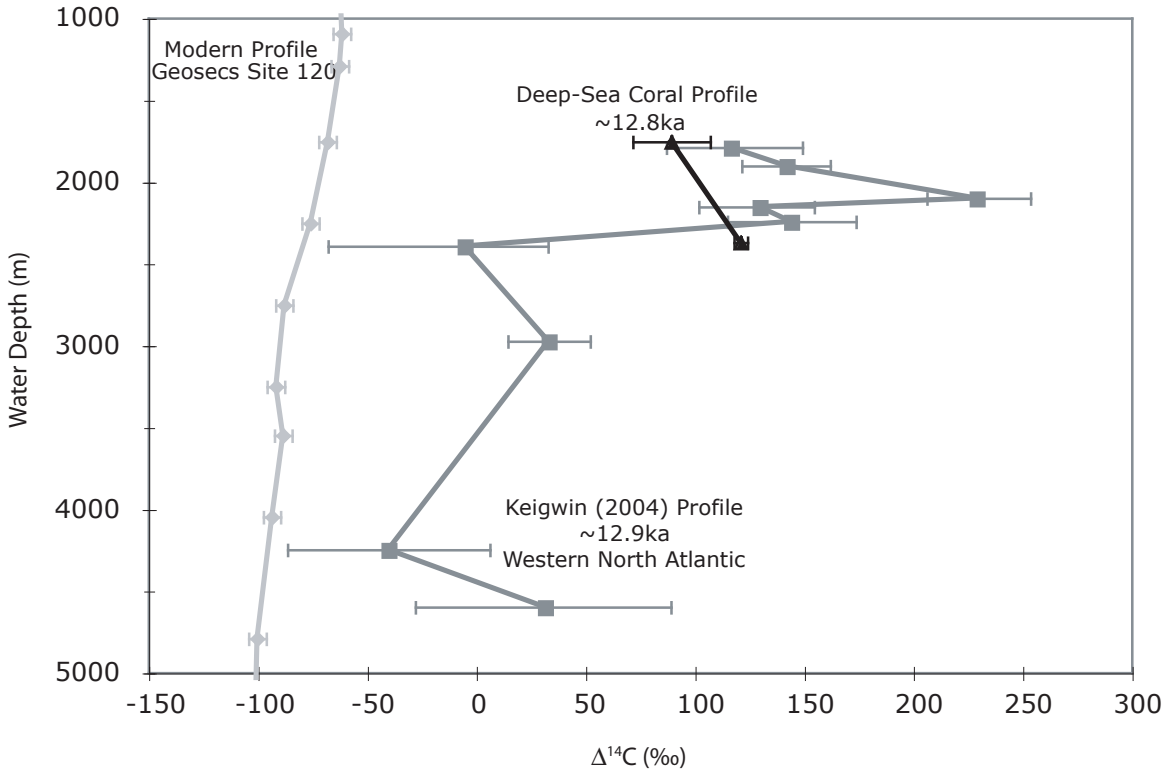

Figure 3.7. Profile of $\Delta^{14}C$ at the beginning of the Younger Dryas. Our deep-sea coral $\Delta^{14}C$ profile is consistent with Keigwin's (2004) profile. To convert Keigwin's (2004) benthic/planktonic foraminifera age differences to $\Delta^{14}C$ we converted the planktonic ^{14}C ages to calendar ages using Calib5.0, then calculated $\Delta^{14}C$ for the deep-water using the ^{14}C age of the benthic foraminifera. Comparing the modern profile from GEOSECS station 120 with the Younger Dryas profile reveals the presence of relatively enriched $\Delta^{14}C$ in the Younger Dryas ocean and the existence of a steep gradient at ~2400m.

Capitalizing on the decadal resolution possible in a single coral, we note that the variability of the within coral transect results vary depending on the timing within the Younger Dryas. As noted earlier, the three corals at the beginning and two at the end of the Younger Dryas show no significant variability in $\Delta^{14}C$ over their lifetimes (with an uncertainty of ~10‰). This consistency is in sharp contrast to the two coral records at ~12.0 ka, from opposite sides of the North Atlantic basin and separated by more than 500m depth, that both show a transient ~40‰ $\Delta^{14}C$ enrichment over their lifetimes. With their overlapping calendar age errors and similar $\Delta^{14}C$ enrichments, we interpret the $\Delta^{14}C$ record in these corals to reflect the same event on opposite sides of the North Atlantic. This pulse occurred rapidly, and the speed of the transition requires a shift in the water composition. It is likely that NADW briefly shoaled, bringing up depleted water from below, or receded, bringing in depleted water from the south.

The $\Delta^{14}C$ enriched part of the transient event approaches the $\Delta^{14}C_{atm}$, a situation that is not observed in the modern ocean, even in surface water. The trend in atmospheric $\Delta^{14}C$ (that sets the initial $\Delta^{14}C$ of the water) and the trajectory of ^{14}C decay are very similar from the $\Delta^{14}C_{atm}$ peak through the end of the Younger Dryas. Therefore, a ^{14}C enriched water mass could have formed anywhere in this time interval and evolved parallel to the atmospheric trend once isolated from the surface, or this enriched $\Delta^{14}C$ water mass could have formed because the initial $\Delta^{14}C$ of the intermediate/deep water that came to bathe the corals was simply more enriched relative to the atmosphere than in the modern ocean. Stocker and Wright (1996; 1998) used a “2.5-D” model to investigate the ocean response to a slow-down in North Atlantic overturning caused by the input of fresh water to the high-

latitude north and found that surface reservoir ages were reduced to ~200 yr (25‰) at 39˚N. This result, if applicable to the initial $\Delta^{14}C$ of intermediate/deep-water, could account for our observed $\Delta^{14}C$ within error. Given the close match of the tree ring (Friedrich, Remmele et al. 2004) and Cariaco Basin (Hughen, Southon et al. 2004) records back to 12.4 ka, it is unlikely that the atmospheric record of $\Delta^{14}C$ is underestimated through part of the Younger Dryas, but an increased reservoir age correction to the Cariaco Basin record would result in a higher peak and a steeper atmospheric decline from 12.8 ka to 12.4 ka, which would be sufficient to explain the enriched $\Delta^{14}C$ that we observe.

The 12.0 ka transient event is without an equal magnitude counterpart in any other record (figure 3.8). GISP2 $\delta^{18}O$ (Grootes, Stuiver et al. 1993) records a very small warming, and the (Pa/Th) record (McManus, Francois et al. 2004) is consistent with a small decrease in the deep North Atlantic circulation rate. The slight upward "kink" in the atmospheric $\Delta^{14}C$ record (Friedrich, Remmele et al. 2004; Hughen, Southon et al. 2004) at 12.0 ka could be interpreted as a slow-down in NADW formation (in agreement with (Pa/Th)). The surface coral reconstruction of $\Delta^{14}C_{atm}$, however, is much more variable, obscuring any "kink" in the record (Burr, Beck et al. 1998). Furthermore, we observe that Antarctic $\delta^{18}O$ from the Byrd ice core increases steeply just prior to 12.0 ka (~2‰ over ~300 yr), which suggests that this transient event may have originated in the south (figure 3.8B). However it was caused, our data from this transient event show that the intermediate water of the North Atlantic can be quite variable with little associated atmospheric effect.

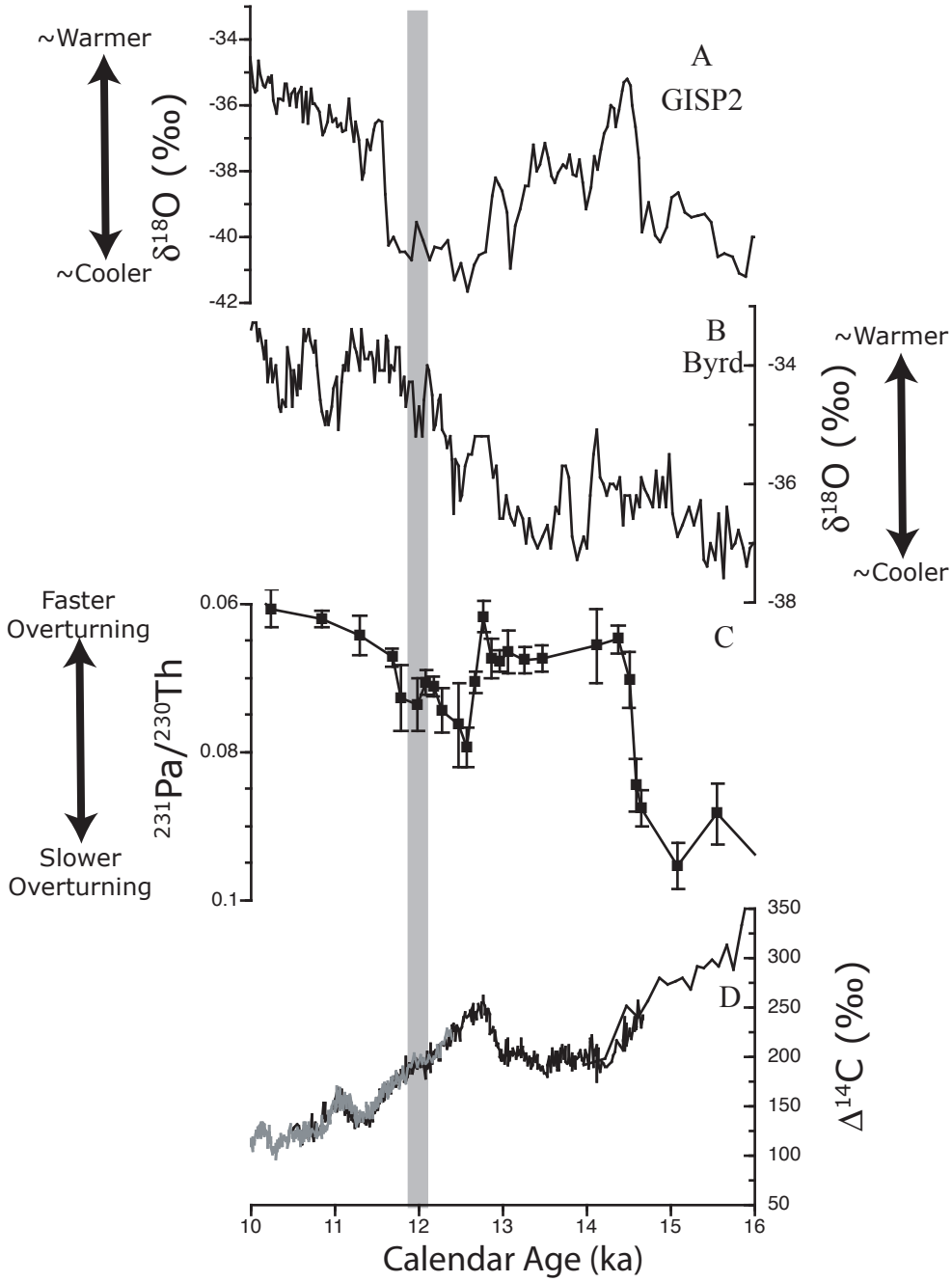

Figure 3.8. A comparison of our observed transient intermediate/deep ocean event at 12.0 ka to (A) GISP2 $\delta^{18}O$ (Grootes, Stuiver et al. 1993), (B) Byrd $\delta^{18}O$ (Blunier and Brook 2001), (C) (Pa/Th) (McManus, Francois et al. 2004), and (D) records of atmospheric $\Delta^{14}C$ (Kromer and Becker 1993; Spurk, Friedrich et al. 1998, Burr, Beck et al. 1998; Hughen, Southon et al. 2000; Hughen, Lehman et al. 2004a). The sizable intermediate/deep water event that we observe in both basins of the North Atlantic is not clearly observed in the ice-core records of northern or southern $\delta^{18}O$. The (Pa/Th) record also does not show a large shift in the strength of the meridional overturning circulation. The atmospheric $\Delta^{14}C$ record, however, does record a slight upward shift in slope that could indicate a perturbation to the carbon cycle.

After the atmospheric $\Delta^{14}C$ peak, $\Delta^{14}C_{atm}$ declines for the remainder of the Younger Dryas (12.8–11.5 ka) while the $\Delta^{14}C$ of intermediate/deep-water approaches the atmosphere. This is consistent with the reinvigoration of NADW formation bringing more ^{14}C into the deep North Atlantic from the atmosphere. At the close of the Younger Dryas, two deep-sea corals show that intermediate/deep-water $\Delta^{14}C$ (~1200m) becomes indistinguishable from atmospheric $\Delta^{14}C$. While this is a surprising result, the end of the Younger Dryas is an exceptional period. If the open ocean mode of convection were interrupted during the Younger Dryas, surface ocean water would more fully exchange with the atmosphere. A restart of the convection would then simultaneously transport the enriched $\Delta^{14}C$ to intermediate depths and cause a steep drop in $\Delta^{14}C_{atm}$. This scenario is consistent with our observed enriched corals at ~1200 meters and the steep drop in $\Delta^{14}C_{atm}$ at ~11.5 ka. After this transient, the system must return to a steady state where intermediate depths are older than the atmosphere (Frank, Paterne et al. 2004).

Conclusions

Because changes in the $\Delta^{14}C$ of the intermediate/deep ocean occur too fast to be accounted for by radioactive decay alone, we conclude that our deep-sea coral measurements of North Atlantic intermediate/deep water $\Delta^{14}C$ primarily reflect the rapid reorganization of water masses during the Younger Dryas. Our data indicate that, coincident with the rise in atmospheric $\Delta^{14}C$ and the drop in Greenland temperatures, ^{14}C depleted southern source water came to bathe our North Atlantic coral growth sites consistent with a shoaling or a reduction in NADW formation. The magnitude of the $\Delta^{14}C$

changes we observe implies that large $\Delta^{14}C$ gradients existed in the intermediate/deep ocean. One such gradient is illustrated by Keigwin's (2004) vertical profile of the water column that shows a transition to depleted $\Delta^{14}C$ at ~2400m. A transient ~40‰ enrichment in $\Delta^{14}C$ over ~100 yr at 12.0 ka on both sides of the North Atlantic basin shows that deep water is capable of rapid, transient reorganization events with a muted effect in the atmosphere. The identification of additional Younger Dryas deep-sea corals that fill in gaps between the existing data points and the development of a deep-sea coral proxy to gauge the effect of conservative mixing will further refine our understanding of this abrupt climate event.

Acknowledgements

We wish to thank Jessie Shing-Lin Wang and Diego Fernandez for help with U-Th sample preparation and analysis at Caltech. We thank the staff of the UC Irvine KCCAMS laboratory and the staff of LLNL-CAMS for help with radiocarbon sample preparation and analysis. We are grateful to Steven Cairns at the Smithsonian for providing one of the samples (YD-3) used in this study and to the crew of the *R/V Atlantis* and *DSV Alvin* pilots, whose expertise made it possible for us to collect thousands of fossil samples from the New England seamounts. This work was supported by NSF grant OCE 0096373.

Bibliography

Adkins, J. F., and E. A. Boyle. 1997. Changing atmospheric Delta C-14 and the record of deep water paleoventilation ages. *Paleoceanography* 12 (3):337-344.

Adkins, J. F., H. Cheng, E. A. Boyle, E. R. M. Druffel, and R. L. Edwards. 1998. Deep-sea coral evidence for rapid change in ventilation of the deep North Atlantic 15,400 years ago. *Science* 280 (5364):725-728.

Adkins, J. F., S. Griffin, M. Kashgarian, H. Cheng, E. R. M. Druffel, E. A. Boyle, R. L. Edwards, and C. C. Shen. 2002. Radiocarbon dating of deep-sea corals. *Radiocarbon* 44 (2):567-580.

Adkins, J. F., G. M. Henderson, S. L. Wang, S. O'Shea, and F. Mokadem. 2004. Growth rates of the deep-sea scleractinia *Desmophyllum cristagalli* and *Enallopsammia rostrata*. *Earth and Planetary Science Letters* 227 (3-4):481-490.

Bard, E., M. Arnold, J. Mangerud, M. Paterne, L. Labeyrie, J. Duprat, M. A. Melieres, E. Sonstegaard, and J. C. Duplessy. 1994. The North-Atlantic atmosphere-sea surface C-14 gradient during the Younger Dryas climatic event. *Earth and Planetary Science Letters* 126 (4):275-287.

Blunier, T., and E. J. Brook. 2001. Timing of millennial-scale climate change in Antarctica and Greenland during the last glacial period. *Science* 291 (5501):109-112.

Blunier, T., J. Chappellaz, J. Schwander, A. Dallenbach, B. Stauffer, T. F. Stocker, D. Raynaud, J. Jouzel, H. B. Clausen, C. U. Hammer, and S. J. Johnsen. 1998. Asynchrony of Antarctic and Greenland climate change during the last glacial period. *Nature* 394 (6695):739-743.

Boyle, E. A., and L. Keigwin. 1987. North-Atlantic thermohaline circulation during the past 20,000 years linked to high-latitude surface-temperature. *Nature* 330 (6143):35-40.

Broecker, W. S. 1998. Paleocean circulation during the last deglaciation: A bipolar seesaw? *Paleoceanography* 13 (2):119-121.

Broecker, W. S., Millie Klas, E. Clark, S. Trumbore, G. Bonani, W. Wölfli, and S. Ivy. 1990. Accelerator mass spectrometric radiocarbon measurements on foraminifera shells from deep-sea cores. *Radiocarbon* 32 (2):119-133.

Broecker, W. S., and T. H. Peng. 1982. *Tracers in the Sea.* Palisades: LDEO.

Broecker, Wallace S., Gerard Bond, and Millie Klas. 1990. A salt oscillator in the glacial Atlantic? 1. The concept. *Paleoceanography* 5 (4):469-477.

Burr, G. S., J. W. Beck, F. W. Taylor, J. Recy, R. L. Edwards, G. Cabioch, T. Correge, D. J. Donahue, and J. M. O'Malley. 1998. A high-resolution radiocarbon calibration between 11,700 and 12,400 calendar years BP derived from Th-230 ages of corals from Espiritu Santo Island, Vanuatu. *Radiocarbon* 40 (3):1093-1105.

Cheng, H., J. Adkins, R. L. Edwards, and E. A. Boyle. 2000. U-Th dating of deep-sea corals. *Geochimica et Cosmochimica Acta* 64 (14):2401-2416.

Curry, W. B., and D. W. Oppo. 2005. Glacial water mass geometry and the distribution of delta C-13 of Sigma CO2 in the western Atlantic Ocean. *Paleoceanography* 20 (1):PA1017.

Dansgaard, W., S. J. Johnsen, H. B. Clausen, D. Dahl-Jensen, N. S. Gundestrup, C. U. Hammer, C. S. Hvidberg, J. P. Steffensen, A. E. Sveinbjornsdottir, J. Jouzel, and G. Bond. 1993. Evidence for general instability of past climate from a 250-kyr ice-core record. *Nature* 364 (6434):218-220.

Frank, N., M. Paterne, L. Ayliffe, T. van Weering, J. P. Henriet, and D. Blamart. 2004. Eastern North Atlantic deep-sea corals: tracing upper intermediate water Delta C-14 during the Holocene. *Earth and Planetary Science Letters* 219 (3-4):297-309.

Friedrich, M., S. Remmele, B. Kromer, J. Hoffman, M. Spurk, K. F. Kaiser, C. Orcel, and M. Küppers. 2004. The 12,460-year Hohenheim oak and pine tree-ring chronology from central Europe-A unique annual record for radiocarbon calibration and paleoenvironment reconstructions. *Radiocarbon* 46 (3):1111-1122.

Goldstein, S. J., D. W. Lea, S. Chakraborty, M. Kashgarian, and M. T. Murrell. 2001. Uranium-series and radiocarbon geochronology of deep-sea corals: Implications for Southern Ocean ventilation rates and the oceanic carbon cycle. *Earth and Planetary Science Letters* 193 (1-2):167-182.

Grootes, P. M., M. Stuiver, J. W. C. White, S. Johnsen, and J. Jouzel. 1993. Comparison of oxygen-isotope records from the GISP2 and GRIP Greenland ice cores. *Nature* 366 (6455):552-554.

Hughen, K. A., J. T. Overpeck, L. C. Peterson, and S. Trumbore. 1996. Rapid climate changes in the tropical Atlantic region during the last deglaciation. *Nature* 380 (6569):51-54.

Hughen, K. A., J. R. Southon, C. J. H. Bertrand, B. Frantz, and P. Zermeño. 2004b. Cariaco basin calibration update: Revisions to calendar and 14C chronologies for core PL07-58PC. *Radiocarbon* 46 (3):1161-1187.

Hughen, K. A., J. R. Southon, S. J. Lehman, and J. T. Overpeck. 2000. Synchronous radiocarbon and climate shifts during the last deglaciation. *Science* 290 (5498):1951-1954.

Hughen, K., S. Lehman, J. Southon, J. Overpeck, O. Marchal, C. Herring, and J. Turnbull. 2004a. C-14 activity and global carbon cycle changes over the past 50,000 years. *Science* 303 (5655):202-207.

Keigwin, L. D. 2004. Radiocarbon and stable isotope constraints on Last Glacial Maximum and Younger Dryas ventilation in the western North Atlantic. *Paleoceanography* 19 (4).

Kromer, B., and B. Becker. 1993. German oak and pine C-14 calibration, 7200-9439 BC. *Radiocarbon* 35 (1):125-135.

Mangini, A., M. Lomitschka, R. Eichstadter, N. Frank, S. Vogler, G. Bonani, I. Hajdas, and J. Patzold. 1998. Coral provides way to age deep water. *Nature* 392 (6674):347-348.

Marchitto, T. M., W. B. Curry, and D. W. Oppo. 1998. Millennial-scale changes in North Atlantic circulation since the last glaciation. *Nature* 393 (6685):557-561.

McManus, J. F., R. Francois, J. M. Gherardi, L. D. Keigwin, and S. Brown-Leger. 2004. Collapse and rapid resumption of Atlantic meridional circulation linked to deglacial climate changes. *Nature* 428 (6985):834-837.

Muscheler, R., J. Beer, G. Wagner, C. Laj, C. Kissel, G.M. Raisbeck, F. Yiou, and P.W. Kubik. 2004. Changes in the carbon cycle during the last deglaciation as indicated by the comparison of Be-10 and C-14 records. *Earth and Planetary Science Letters* 219 (3-4):325-340.

Pahnke, K., and R. Zahn. 2005. Southern hemisphere water mass conversion linked with North Atlantic climate variability. *Science* 307 (5716):1741-1746.

Raymo, M. E., D. W. Oppo, B. P. Flower, D. A. Hodell, J. F. McManus, K. A. Venz, K. F. Kleiven, and K. McIntyre. 2004. Stability of North Atlantic water masses in face of pronounced climate variability during the Pleistocene. *Paleoceanography* 19 (2):PA2008.

Robinson, L. F., J. F. Adkins, L. D. Keigwin, J. Southon, D. P. Fernandez, S. L. Wang, and D. Scheirer. 2005. Radiocarbon variability in the western North Atlantic during the last deglaciation. *Science,* submitted.

Schroder-Ritzrau, A., A. Mangini, and M. Lomitschka. 2003. Deep-sea corals evidence periodic reduced ventilation in the North Atlantic during the LGM/Holocene transition. *Earth and Planetary Science Letters* 216 (3):399-410.

Siani, G., M. Paterne, E. Michel, R. Sulpizio, A. Sbrana, M. Arnold, and G. Haddad. 2001. Mediterranean Sea surface radiocarbon reservoir age changes since the last glacial maximum. *Science* 294 (5548):1917-1920.

Skinner, L. C., and N. J. Shackleton. 2004. Rapid transient changes in northeast Atlantic deep water ventilation age across Termination I. *Paleoceanography* 19 (2).

Sowers, T., and M. Bender. 1995. Climate records covering the last deglaciation. *Science* 269 (5221):210-214.

Spurk, M., M. Friedrich, J. Hofmann, S. Remmele, B. Frenzel, H. H. Leuschner, and B. Kromer. 1998. Revisions and extension of the Hohenheim oak and pine chronologies: New evidence about the timing of the Younger Dryas/Preboreal transition. *Radiocarbon* 40 (3):1107-1116.

Stocker, T.F., and D. G. Wright. 1998. The effect of a succession of ocean ventilation changes on 14C. *Radiocarbon* 40 (1):359-366.

Stocker, T. F., and D. G. Wright. 1996. Rapid changes in ocean circulation and atmospheric radiocarbon. *Paleoceanography* 11 (6):773-795.

Stuiver, M., and H. G. Ostlund. 1980. GEOSECS Atlantic radiocarbon. *Radiocarbon* 22 (1):1-24.

Stuiver, M., and H. A. Polach. 1977. Reporting of C-14 data–Discussion. *Radiocarbon* 19 (3):355-363.

Stuiver, M., P. D. Quay, and H. G. Ostlund. 1983. Abyssal water C-14 distribution and the age of the world oceans. *Science* 219 (4586):849-851.

Stuiver, M., P. J. Reimer, E. Bard, J. W. Beck, G. S. Burr, K. A. Hughen, B. Kromer, G. McCormac, J. Van der Plicht, and M. Spurk. 1998. INTCAL98 radiocarbon age calibration, 24,000-0 cal BP. *Radiocarbon* 40 (3):1041-1083.

Vogel, J. S., J. R. Southon, D. E. Nelson, and T. A. Brown. 1984. Performance of catalytically condensed carbon for use in accelerator mass spectrometry. *Nuclear instruments* 233 (2):289-293.

Waelbroeck, C., J. C. Duplessy, E. Michel, L. Labeyrie, D. Paillard, and J. Duprat. 2001. The timing of the last deglaciation in North Atlantic climate records. *Nature* 412 (6848):724-727.

Chapter 4

MEASUREMENTS OF CD/CA IN DEEP-SEA CORALS REFLECT VITAL EFFECTS AND SEAWATER CD/CA

Selene F. Eltgroth, Jess F. Adkins, and Diego P. Fernandez

Abstract

We measured Cd/Ca in a suite of modern and fossil deep-sea corals with the goal of extending the use of this nutrient proxy from benthic foraminifera to deep-sea corals. We found modern deep-sea coral Cd/Ca ranging from 0.04 to 1.5 μmol/mol, and six of these corals had anomalously high Cd/Ca with respect to the water in which they grew. Most of these high Cd/Ca corals were also marked by high Cd/Ca variability. We traced the origin of the Cd/Ca variability to a systematic trend in deep-sea corals with increasing Cd/Ca along the upward direction of coral growth. This probable vital effect is especially pronounced in the anomalously high Cd/Ca corals. We conclude that, in the case of these high Cd/Ca corals, the systematic trend in Cd/Ca has effectively obscured the signal of seawater Cd/Ca. When these high Cd/Ca corals are removed from the calibration, a correlation between Cd/Ca_{coral} and Cd/Ca_{water} is observed for the remaining 8 deep-sea corals with a best fit coral-water partition coefficient of 1.3 ± 0.1. We compared two records of Cd/Ca generated from fossil deep-sea corals recovered from the North Atlantic to our modern calibration dataset. We observed that one coral (from 15.4 ka) has low average Cd/Ca and may reflect average environmental Cd/Ca. Because Cd/Ca increases systematically toward the top of this coral, however, the within coral record cannot be

conclusively linked with nutrient composition changes. The other coral (from 12.0 ka) clearly resembles the high Cd/Ca corals of the modern calibration, so its Cd/Ca record is not credible.

Introduction

Phosphate concentrations in the deep North Atlantic serve as a volumetric tracer of deep-water circulation. With a reliable estimate of a conservative or quasi-conservative tracer like phosphate to remove the effect of source water mixing in the Atlantic, an additional radioactive tracer like $\Delta^{14}C$, may be used to determine the ventilation rate of the deep-water. This ventilation rate is essential to understanding the function of the meridional overturning circulation in the regulation of the climate system. With this in mind, our goal is to follow up the deep-sea coral Cd/Ca work of Adkins (1998) to develop this phosphate proxy for use in deep-sea corals.

Relationship Between Cadmium and Phosphate in Seawater

Cadmium profiles in the ocean are similar to profiles of PO_4 (Boyle, Sclater et al. 1976). Although the biological processes governing the seawater Cd distribution remain unidentified, the relationship between Cd and PO_4 below the ocean mixed layer has been described empirically and approximated with a simple box model. The empirical fit to the global data set has two linear portions that meet at a $[PO_4^{3-}]$ of 1.3 μmol/kg (Boyle 1988). This “kink” at 1.3 μmol/kg is thought to be caused by the input of low Cd/PO_4 water from the Subantarctic (40–55S) to intermediate water (Frew and Hunter 1992). The relationship between $[PO_4^{3-}]$ and [Cd] has since been expressed as a curve generated by a two-box

model fit that accounts for the exchange between surface and deep ocean water and the transport of particles containing Cd and PO_4 to the deep ocean where the chemical species are remineralized. The best fit of the model to the data is achieved when Cd is removed to the deep ocean box by particle transport twice as fast as for PO_4 (Elderfield and Rickaby 2000). The result of the model fit is slightly different from the two-line fit. Regardless of the fit that is chosen, the large scatter in the ocean data around the trend (~20%) is such that either fit is adequate to relate $[PO_4^{3-}]_{seawater}$ to $[Cd]_{seawater}$.

Cd/Ca in Foraminiferal Tests

Cd/Ca is an established phosphate proxy in epibenthic foraminiferal tests preserved in ocean sediments (Boyle 1981; Hester and Boyle 1982; Boyle 1988; Boyle 1992) (figure 4.1). The relationship for the partition coefficient ($D_{Cd/Ca}$) that relates Cd/Ca in the foraminiferal carbonate and Cd/Ca in the seawater is:

$$D_{Cd/Ca} = \frac{\left(\frac{Cd}{Ca}\right)_{CaCO_3}}{\left(\frac{Cd}{Ca}\right)_{Water}}. \qquad \text{(equation 4.1)}$$

The coretop calibration for calcitic foraminifera showed that $(D_{Cd/Ca})_{foram}$ described by this equation is dependent on the water depth, with a $D_{Cd/Ca}$ of 1.3 at depths shallower than 1150m that increases linearly to 2.9 at 3000 m and is constant below 3000 m (Boyle 1992). The reason for this depth dependence is not known. Using foraminiferal data from the Ontong Java Plateau in the western equatorial Pacific, McCorkle et al. (1995) found that $D_{Cd/Ca}$ decreases below 3000 m, in disagreement with previous core top results. They demonstrated that $D_{Cd/Ca}$ decreases when the calcite saturation state of the water (ΔCO_3^{2-}) drops below 0–10 μmol/kg. In contrast, the core top calibration for aragonitic foraminifera,

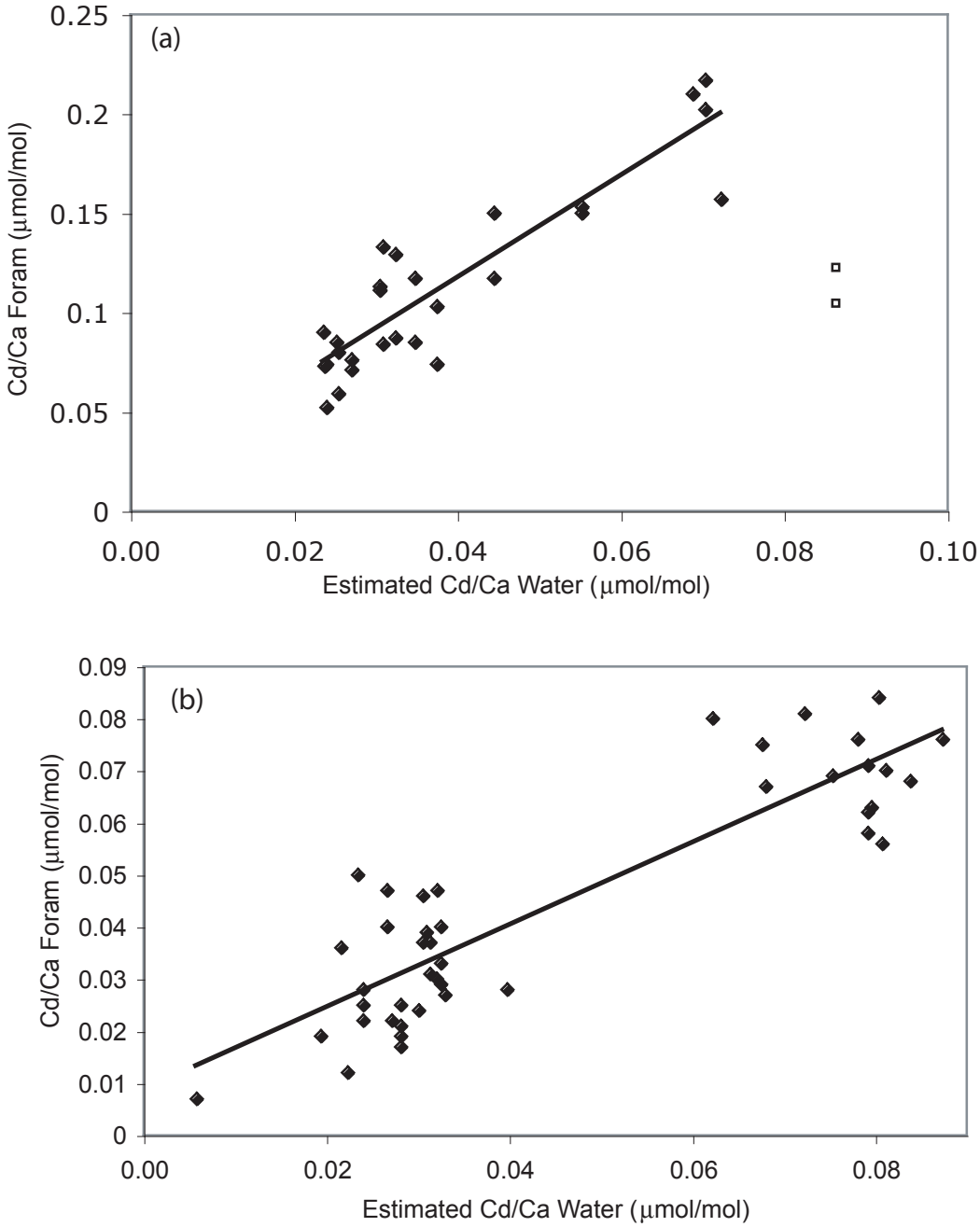

Figure 4.1. Core top Cd/Ca calibrations for (a) calcitic epibenthic forams and (b) aragonitic epibenthic forams. (a) The calcitic foram calibration plot includes foraminifera results from cores deeper than 3000m to avoid variability due to the depth dependence of the Cd/Ca partition coefficient. Each core top also contained at least 15cm of documented Holocene sediment. The data consist of Cd/Ca measurements on the foraminiferal species *Cibicidoides kullenbergi* and *Cibicidoides wuellerstorfi* by Boyle (1988, 1992). The small open squares are questionable data not included in the partition coefficient determination. The best fit partition coefficient through these calcite foraminifera results is 2.56 ± 0.01 (b) The aragonitic foram calibration includes measurements of foraminifieral species *Hoeglundina sp.* by Boyle et al. (1995). The best fit partition coefficient for the aragonitic forams is 0.79 ± 0.02. In both panels, Cd/Ca of the water was estimated from phosphate concentrations from nearby water sampling stations as described in the text.

the same $CaCO_3$ polymorph as stony corals, showed that $D_{Cd/Ca}$ is very near 1.0 with no significant depth dependence (Boyle, Lobeyrie et al. 1995). Corals have three advantages over foraminiferal climate reconstructions because they are not subject to sediment bioturbation, they can be individually dated by U-series techniques, and they are sufficiently massive to accommodate high-resolution records for multiple proxies within the same coral.

Cd/Ca in Surface and Deep-sea Corals

Annually-banded surface coral Cd/Ca has been shown to be a tracer of upwelling in the case of a surface coral from the Galapagos Islands and to track industrial emissions in a coral from Bermuda (Shen, Boyle et al. 1987). These records of surface coral Cd/Ca imply a $D_{Cd/Ca}$ of 1 (Shen, Boyle et al. 1987; Shen and Boyle 1988). Results from a Cariaco Basin coral show a transition in Cd/Ca in 1950 that is interpreted as a change in the upwelling state of the region (Reuer, Boyle et al. 2003). The results from several other surface corals from the Galapagos Islands show a lack of seasonality in Cd/Ca near the western island of Isabela and strong seasonal upwelling near the eastern islands of San Cristobal and Hood (Linn, Delaney et al. 1990; Delaney, Linn et al. 1993). Delaney et al. (1993) note potential uncertainty about reconstructing the concentrations of surface $[PO_4^{3-}]$ from Cd/Ca_{Coral} since different surface coral records from the same location (the Island of Isabela) have disparate Cd/Ca_{Coral} values. The other corals from the eastern Galapagos Islands, however, show unmistakable signals of seasonal upwelling and El Nino/Southern Oscillation events.

Based on the foraminifera and surface coral results, deep-sea corals are a promising new tool for reconstructing past $[PO_4^{3-}]$. A North Atlantic deep-sea coral Cd/Ca record at 15.4 ka showed an increase in Cd/Ca over the coral lifetime that may be interpreted as an

increase in the relative supply of nutrient rich southern source water to the coral growth site (Adkins, Cheng et al. 1998). In this study, we evaluate the accuracy of deep-sea coral Cd/Ca as a true signal of the environment using modern deep-sea corals to calibrate Cd/Ca in deep-sea coral against the Cd/Ca of the ambient seawater. We then compare our calibration result with the deep-sea coral record from 15.4 ka and a new record from the Younger Dryas at 12.0 ka.

Samples and Methods

Our suite of 14 modern *Desmophyllum dianthus* deep-sea corals were collected from the Atlantic, Pacific, and Southern Oceans from depths ranging from 421–2145 m (figure 4.2, table 4.1). We acquired these corals from the Smithsonian collection and other American and French dredge collections. We do not know how or if the samples were chemically treated after collection and prior to our analysis. The corresponding PO_4 concentrations, averaged from the nearest water profile stations compiled in the Joe Reid database, vary from 1.1 to 3.0 μmol/kg.

Deep-water carbonates contain refractory Cd that must be cleaned away before the lattice bound Cd can be precisely measured (Boyle 1981). Our cleaning procedure is designed to clean away non-lattice bound Cd in deep-sea corals, including remnant polyp material in interstitial spaces and secondary Cd precipitates on exposed coral surfaces (typically in the form of black, metal-rich crusts), without re-adsorption of previously liberated Cd from the aragonite lattice during the cleaning process. Our Cd/Ca samples were cut from thecal sections of each coral using a Dremel Tool with a diamond saw

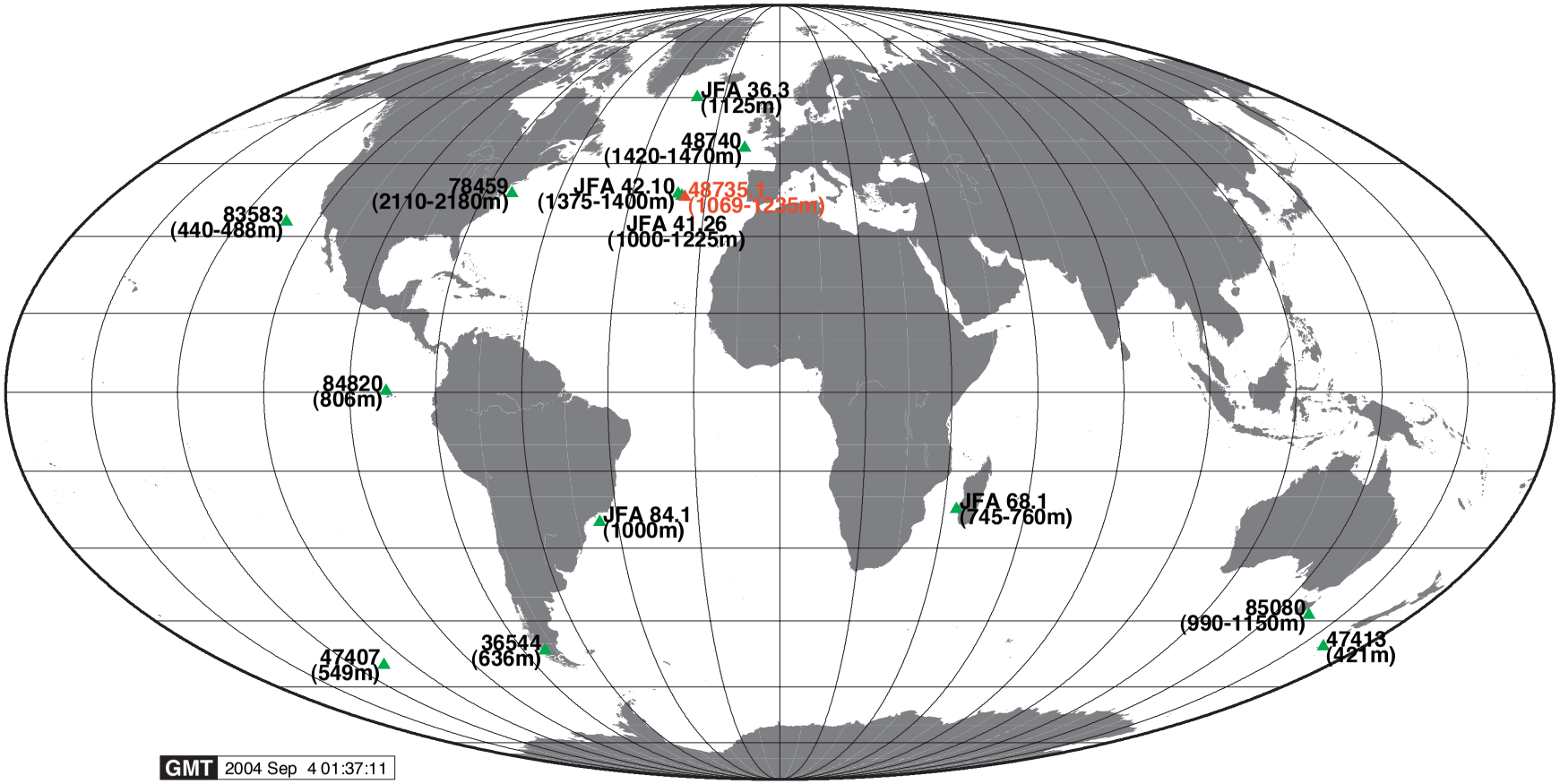

Figure 4.2. Sample map shows the positions and depths of the deep-sea corals analysed in this study.

Coral ID	Depth (m)	Latitude	Longitude	[PO4] (mmol/kg)	Water [Cd] (nmol/kg)	Water Cd/Ca (mmol/mol)
36544	636	51°31'S	73°25'W	1.76	0.455	0.044
47407	549	54°49'S	129°48'W	1.65	0.412	0.040
47413	421	50°38'S	167°38'E	1.61	0.395	0.038
48740	1420-1470	48.4°'N	10.54°'W	1.18	0.248	0.024
78459	2110-2180	38°45'N	72°39'W	1.19	0.249	0.024
83583	488-440	32°54'N	127°47'W	2.92	0.918	0.089
84820	806	0°14'N	91°36'W	2.98	0.943	0.092
85080	990-1150	43°47'S	150°29'E	1.95	0.530	0.051
JFA36.3	1125	60°2.5'N	29°40'W	1.06	0.222	0.022
JFA41.26	1000-1225	38°12.3'N	26°26.1'W	1.08	0.226	0.022
JFA42.10	1375-1400	38°41.4'N	27°33.2'W	1.38	0.301	0.029
JFA68.1	745-760	22°18.9'S	43°1.1'E	1.84	0.485	0.047
JFA84.1	1000	24°54.4'S	44°26'W	2.15	0.610	0.059

Equations:

[PO4]<1.3mmol/kg Cd=.21*[PO4]

[PO4]>1.3mmol/kg Cd=.40*[PO4]-0.25nmol/kg

Table 4.1. Coral Collection Site Data

attachment. The modern corals were observed to be largely free of the dark, metal-rich precipitates that tend to form over time on the exterior surfaces of older deep-sea carbonates, but the outer layer of carbonate was mechanically abraded away as the first step in the cleaning process as a precaution. The rigorous chemical cleaning steps we used were developed to treat foraminifera and have been adapted for use with corals (Boyle 1981; Boyle and Keigwin 1985/86; Shen and Boyle 1988; Boyle 1995; Boyle and Rosenthal 1996). The cleaning method has been described in detail with respect to deep-sea corals by Adkins (1998) and appears in the appendix following this chapter. The key procedures in the chemical cleaning process are ultrasonication to disaggregate fine particles from the coral aragonite, oxidation to oxidize organic matter, reduction to reduce and dissolve metal oxides, and several nitric acid leaches to strip away any metals adsorbed on the aragonite surface (Boyle and Rosenthal 1996). The initially large ivory colored pieces (10–100 mg) were precleaned. The resulting large pieces were crushed and sieved for 250–710 μm size fraction, small enough to allow rigorous cleaning but large enough to reduce the surface area available for Cd adsorption during the cleaning process. Approximately 0.50 mg (1–3 crushed pieces) were measured out for the rigorous trace metal cleaning in 0.5 mL centrifuge tubes. The pieces were chemically cleaned and acid leached then transferred to clean centrifuge tubes. The samples were acid leached one final time before dissolution in 250 μL 2% HNO_3. We also cleaned one surface coral blank (*Porites sp.* acquired from Dr. G. Shen) with each set of ~10 samples to ensure that the coral cleaning process did not add any extra Cd to the samples.

Cd/Ca analytical tools include atomic absorption spectrometry (AAS) (Boyle 1981; Boyle and Keigwin 1985/86; Boyle 1995), thermal ionization mass spectrometry (Rickaby, Greaves et al. 2000) and inductively coupled plasma mass spectrometry (ICP-MS) (Lea and Martin 1996; Rosenthal, Field et al. 1999). Our sample analysis was performed by isotope dilution on a Finnegan ELEMENT ICP-MS equipped with a Scott Type Spray Chamber and ESI Teflon nebulizer. We perform our Cd and Ca analyses separately.

For Cd, ^{110}Cd is our spike isotope, and ^{114}Cd is our natural isotope. Our spike is 93.63 ± 0.07% ^{110}Cd and 1.21 ± 0.02% ^{114}Cd (^{110}Cd/^{114}Cd$_{spike}$ = 77.4 ± 1.3). The spike solution was diluted to a total cadmium concentration of 3.193x10^{-12} mol/g. The natural abundances are 12.49% and 28.73% for ^{110}Cd and ^{114}Cd, respectively (^{110}Cd/^{114}Cd$_{sample}$ = 0.4347). We corrected for the Sn interference at mass 114 by measuring ^{120}Sn and multiplying this measured intensity by the natural abundance ratio (0.65%/32.59%). We mix 100 μL of our dissolved sample solution with 100 μL of our Cd spike solution to create our analytical solutions. We monitor accuracy with a spiked gravimetric standard (SGS) of known isotopic ratio. The measured SGS ratio is corrected back to ^{110}Cd/^{114}Cd = 1.605, and this correction factor is applied to each analysis to account for changing instrument fractionation.

We used two separate mass spectrometric methods to measure Ca. We measured Ca alone in our early samples (run ID α–αρ) and later developed a mixed spike for the simultaneous measurement of Mg, Ca, and Sr (run ID ασ–βε). For Ca in our early samples, we measured ^{43}Ca as our spike isotope and ^{48}Ca as our natural isotope. Our original Ca

spike solution had ^{43}Ca of 83.93% and ^{48}Ca of 0.09% ($^{43}Ca/^{48}Ca$ = 933). The total calcium concentration of this original solution was 1.578×10^{-8} mol/g. A 50 μL aliquot of the sample primary solution was diluted by adding 500 μL 5% nitric acid. Analytical solutions were made up of 100 μL of this sample secondary solution mixed with 100 μL of the spike solution. For the samples mixed with the multispike, the interference caused by $^{86}Sr^{++}$ at mass 43 is corrected by measuring the intensities at masses 43.5, 86, and 87 and the intensity of the interference is calculated using the doubly to singly ionized ratio for ^{87}Sr and multiplying this ratio by the intensity at ^{86}Sr. The properties of our mixed Mg, Ca, Sr spike are: $^{25}Mg/^{24}Mg$ = 91.01, $^{43}Ca/^{48}Ca$ = 932.6, $^{87}Sr/^{88}Sr$ = 11.03. Spike concentrations are [^{24}Mg] = 0.2447 nmol/g, [^{43}Ca]=0.1503 nmol/g, and [^{88}Sr] = 5.315 nmol/g. The natural abundances of Ca are 0.135% and 0.187% for ^{43}Ca and ^{48}Ca, respectively ($^{43}Ca/^{48}Ca$ = 0.722). Our analytical solutions were made up of 40 μL of the mixed spike, 20 μL of the sample primary, and 1 mL 5% HNO_3.

Our ICP-MS sample sequence order is listed in table 4.2. We increased the frequency with which SGSs were run to account for changes in instrument fractionation over time. For the ICP-MS analysis, we ran 70 passes for each Ca analysis and 75 passes for each Cd analysis. The Ca run is slightly shorter to account for a longer take up time needed for Ca. The analytical blank (5% nitric acid) was used to correct for instrument background. Interspersed with samples are measurements of the SGS to monitor and correct sample ratios for instrument fractionation (figure 4.3). Our SGS results show a high degree of variability for run IDs αψ and αω. The measured intensities show irregular fluctuations that are the reason for the observed variability, but the peak shapes look

Early Samples (α–αμ)	**Later Samples (αν–βε)**
Blank	Blank
SGS	SGS
Blank	Blank
6 Samples	3 Samples
2 CS	3 CS
Blank	
6 Samples	* We repeat this basic
2 CS	structure up to 10
Blank	times until all samples
6 Samples	are measured
2 CS	
Blank	
6 Samples	
2 CS	
Blank	
6 Samples	
2 CS	
Blank	
SGS	

Table 4.2. ICP-MS Sequence Structure

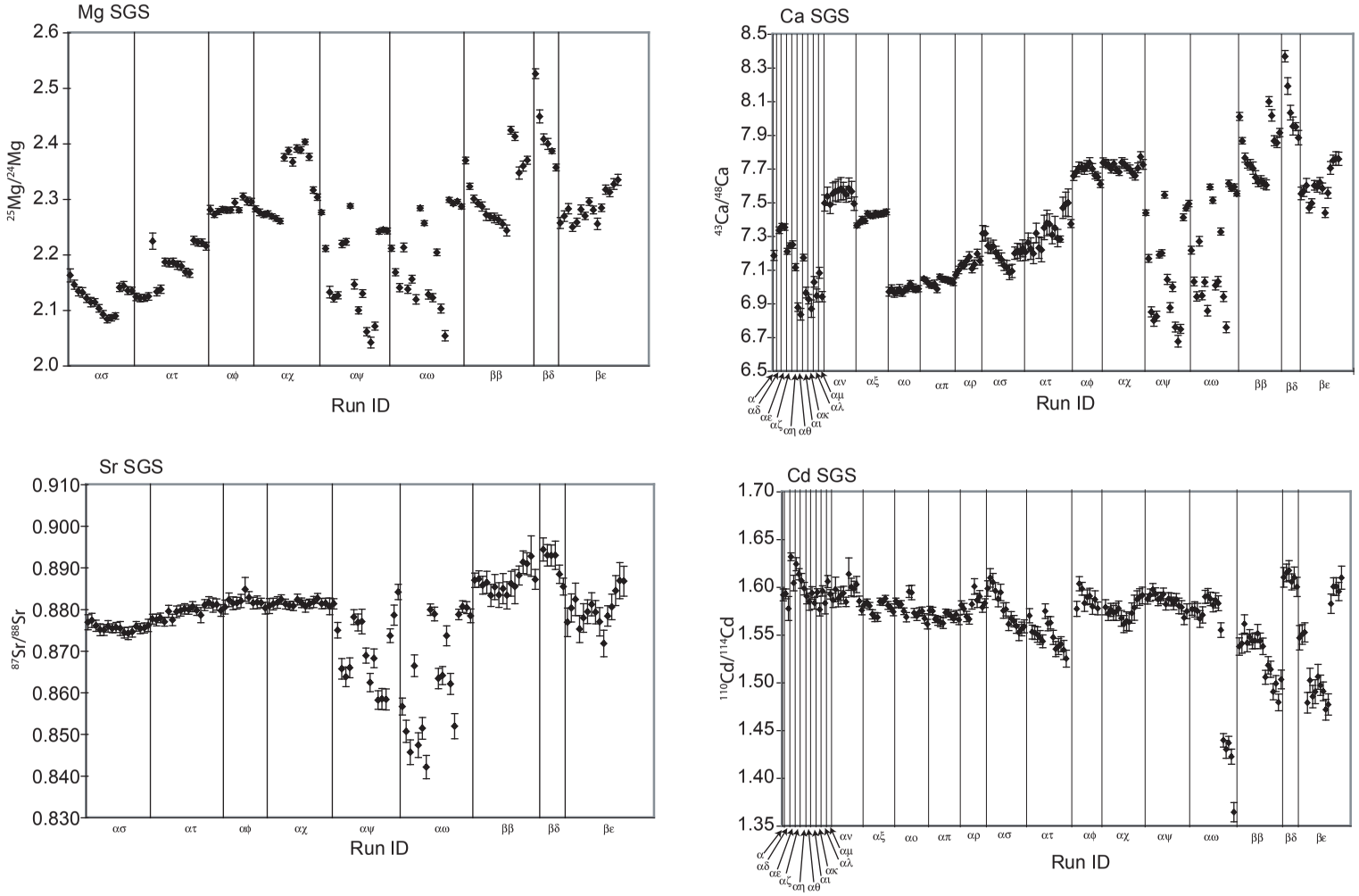

Figure 4.3. Spiked gravimetric standards (SGSs) used to correct our sample ratios for analytical effects are plotted by run ID. Error bars reflect 2σ standard errors based on multiple scans of each sample. Early measurements (α to αμ) used only 2 SGS analyses per run, which were not sufficient to account for instumental drift over the sample analyses. SGS ratio "jumps" are due to changes in the instrumental tuning parameters and recentering of peaks. Large drift in the SGS ratios is generally due to changes in peak position over time. Ca and Cd SGSs were measured over all runs (α to βε). Mg and Sr were added to the analytical method when the Mg, Ca, Sr mixed spike replaced the Ca only spike. Therefore, the Mg and Sr data are limited to runs ασ through βε.

normal. We are unsure of the reason for the instrument unpredictability. To evaluate the precision of our measurements we also repeatedly analyzed two consistency standards (figure 4.4). We observe a shift in the measured [Ca] after run αξ. At that time, we noticed that the Ca spike solution had been evaporating from its storage container. We replaced the container with another and stored the solution in a more humid environment and the [Ca] precision improved. Precision for the consistency standard was 6% (all runs) and 4% for runs αο to βε (2σ standard deviation), after we fixed the Ca spike issue. We verified our ICP-MS results by analyzing our consistency standards by AAS. Furthermore, our deep-sea coral results agree with those of Adkins (1998), who analyzed the same deep-sea samples from the Smithsonian collection using an AAS technique.

Results and Discussion

We studied 14 modern deep-sea corals for Cd/Ca and analyzed 8–39 discrete samples from each (figure 4.5). The Cd/Ca_{water} corresponding to our deep-sea coral sample sites was calculated by applying the Boyle 2-line relation to the PO_4^{3-} seawater data to determine [Cd] and dividing by [Ca]=10.3 mmol/mol. The resulting Cd/Ca_{water} varies from 0.02 to 0.10 μmol/mol (table 4.1). Our Cd/Ca_{coral} results range from 0.04–1.5 μmol/mol, a much larger span than Cd/Ca_{water} (tables 4.3 and 4.4). No clear $D_{Cd/Ca}$ can be determined from all of the data. We observe that six of the samples have elevated Cd/Ca_{coral} (average value 0.2–1.2 μmol/mol) and most of these corals additionally have substantial variability. In contrast, eight samples have significantly smaller Cd/Ca_{coral} (0.04–0.16 μmol/mol) and generally smaller variability. If we focus in on the set of corals with smaller Cd/Ca_{coral}, we estimate that the partition coefficient ($D_{Cd/Ca}$) is 1.3 ± 0.1. We illustrate this in figure 4.5b

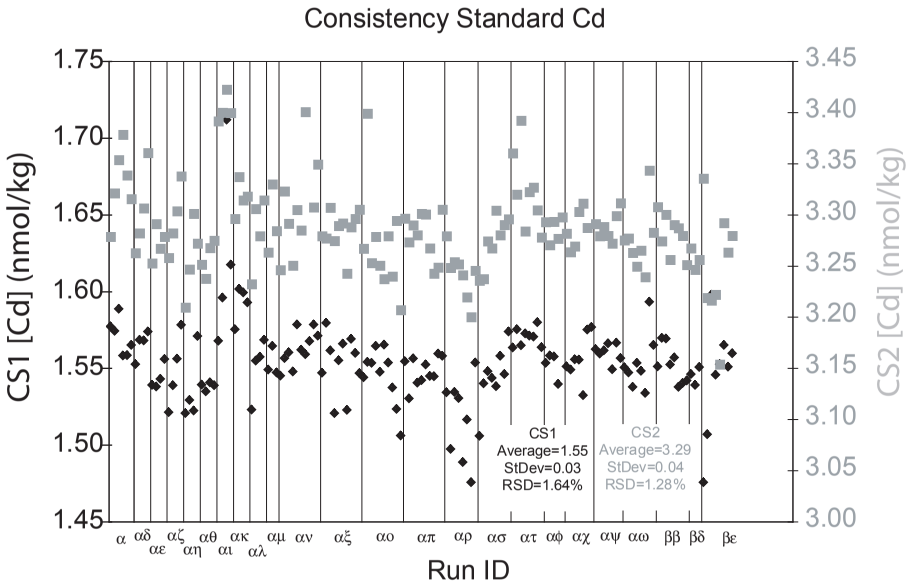

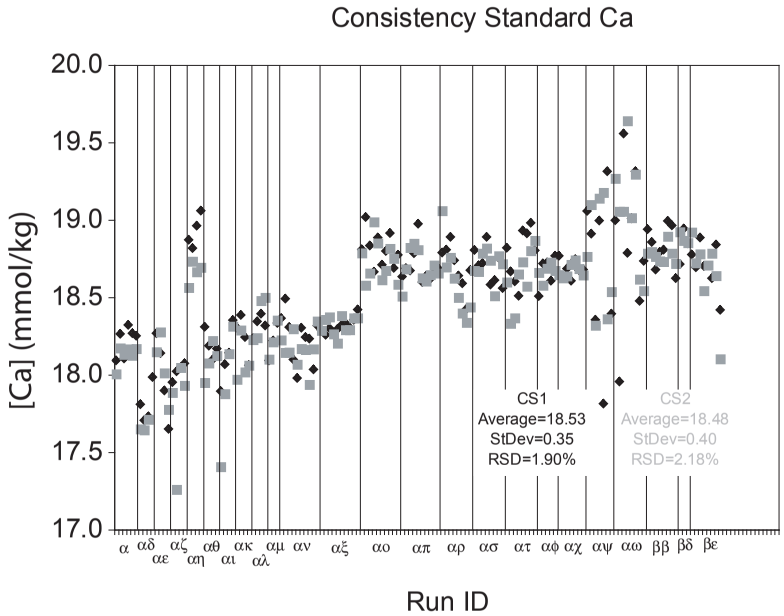

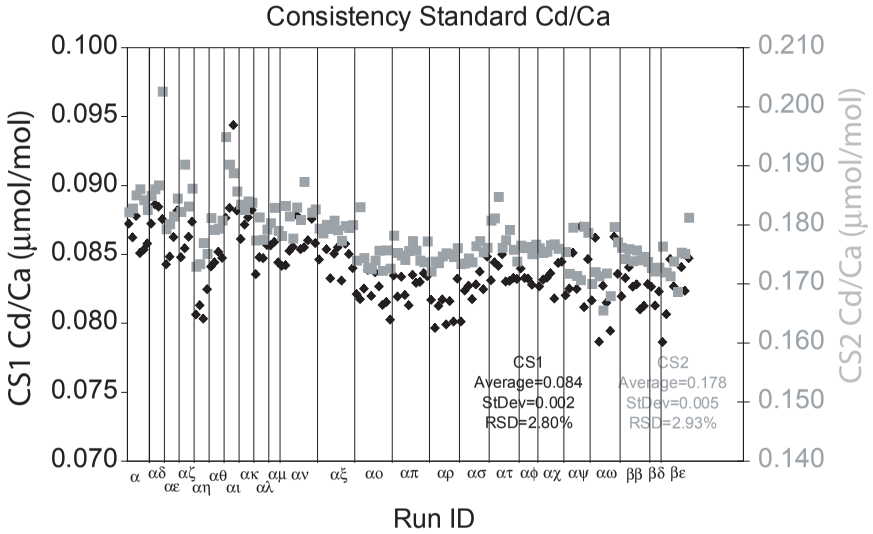

Figure 4.4. Two consistency standards run with each batch of samples give an overall Cd/Ca measurement precision of 6% (2σ standard deviation). Most of the variability is driven by changes in [Ca]. When we consider only standards run αο to βε, the precision drops to 4% (2σ standard deviation). Note that consistency standard [Ca] does not change when the spike is changed from Ca only to the Mg,Ca,Sr mixed spike starting with run ID ασ, indicating that our Ca only and mixed spike concentrations are consistent with one another.

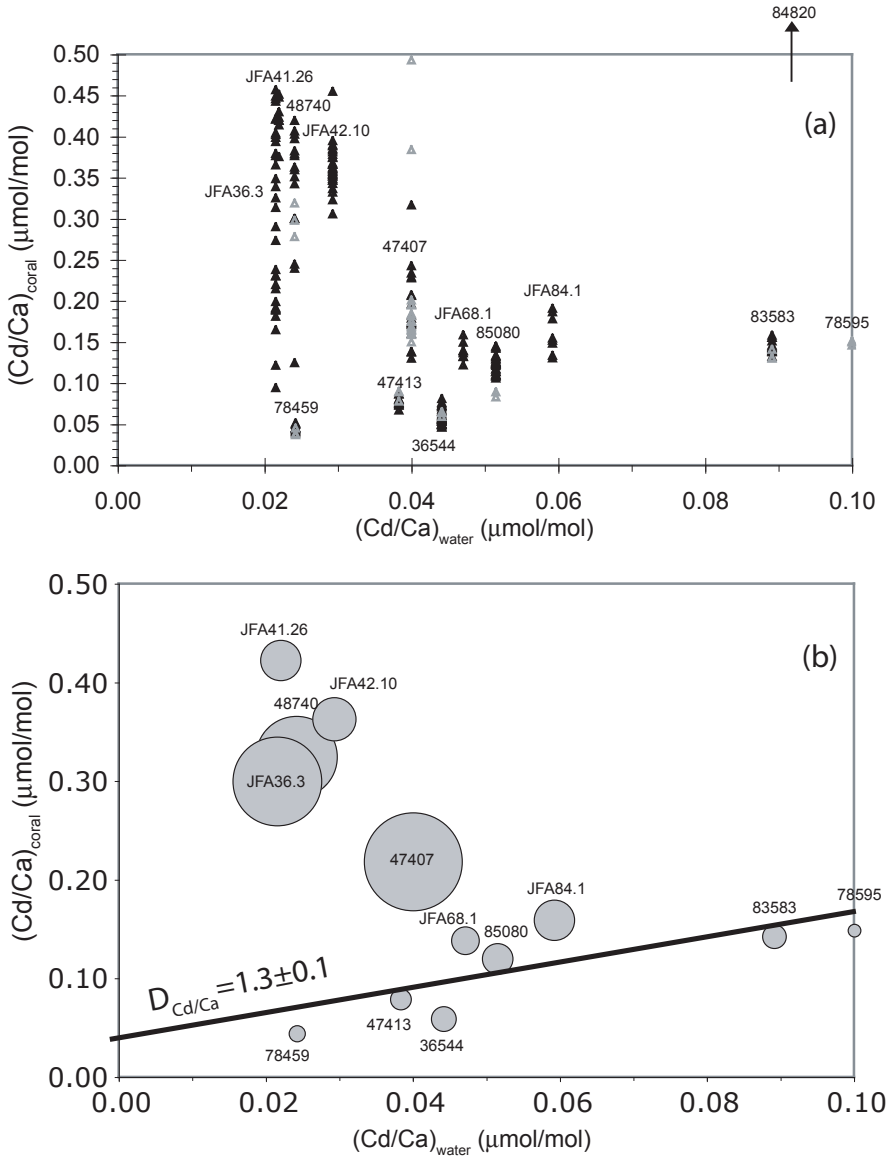

Figure 4.5. Cd/Ca deep-sea coral calibration results. (a) The results from coral 84820 (indicated by the arrow) plot off scale and range from 0.5 to 1.5 µmol/mol). The ICP-MS results from this study are marked by solid black triangles while the AAS results by Adkins (1998) are marked by gray triangles. (b) The same data plotted to emphasize differences in average Cd/Ca and within-coral variation. Each coral is plotted with the size of each data point scaled by the 2σ standard deviation. Based on these results, we divide the corals into 2 groups. High Cd/Ca, high variability corals include JFA36.3, JFA41.26, JFA42.10, 48740, 47407, and 84820. Low Cd/Ca corals with low Cd/Ca variability include 78459, 47413, 36544, JFA68.1, 85080, JFA84.1, 83583, and 78595. We use these low Cd/Ca corals to construct our best guess at the deep-sea coral Cd/Ca partition coefficient. The best fit partition coefficient is $D_{Cd/Ca} = 1.3 \pm 0.1$.

Run ID	Coral ID / Description
α	Consistency standards only
αδ	36544 samples: stepped cleaning >710mm size fraction
αε	36544
αζ	36544
αη	36544
αθ	81408
αι	47407 81408 85080
ακ	36544 stepped cleaning
αλ	47413 48740 83583
αμ	81408 84820
αν	78459 JFA42.10 JFA68.1
αξ	JFA41.26 JFA36.3 JFA84.1
αο	47413 stepped cleaning
απ	JFA42.10 stepped cleaning
αρ	85080 JFA41.26 36544 47407 JFA36.3 JFA84.1
ασ	47407 48740 85080 83583 47413 36544 78459 84820
ατ	78459 47413 85080 36544 47407 84820 83583 48740 47407
αφ	85080 horizontal cross-section
αχ	JFA42.10 horizontal cross-section
αψ	JFA36.3 vertical thecal section
αω	36544 vertical thecal section
ββ	JFA36.3 vertical septal section
βδ	36544 10-40μm standard
βε	48735.1 (Younger Dryas) vertical thecal section

Table 4.3. ICP-MS Run Description

Coral ID	Run ID	$(Mg/Ca)_{coral}$ (mmol/mol)	$(Sr/Ca)_{coral}$ (mmol/mol)	$(Cd/Ca)_{coral}$ (μmol/mol)	Average $(Cd/Ca)_{coral}$ (μmol/mol)	2σ
47407	αι	-	-	0.234	0.192	0.070
		-	-	0.160		
		-	-	0.172		
		-	-	0.173		
		-	-	0.171		
		-	-	0.138		
		-	-	0.243		
		-	-	0.228		
		-	-	0.206		
85080	αι	-	-	0.126	0.123	0.021
		-	-	0.132		
		-	-	0.142		
		-	-	0.134		
		-	-	0.130		
		-	-	0.132		
		-	-	0.121		
		-	-	0.129		
		-	-	0.144		
		-	-	0.145		
	ασ	1.12	9.00	0.125		
		1.28	10.28	0.125		
	ατ	1.35	10.19	0.108		
		1.16	10.19	0.124		
		1.45	10.41	0.123		
	αϕ	1.77	9.98	0.114		
		1.71	10.50	0.110		
		1.48	10.20	0.117		
		0.96	10.19	0.124		
		1.34	10.30	0.124		
		1.60	10.59	0.106		
		1.29	10.20	0.117		
		1.56	10.57	0.109		
		1.70	10.32	0.109		
		1.28	10.20	0.123		
		1.82	9.97	0.110		
		1.46	10.01	0.114		
		1.36	10.17	0.123		
		1.62	10.17	0.114		

Table 4.4. *D. dianthus* Trace Metal Results

Coral ID	Run ID	$(Mg/Ca)_{coral}$ (mmol/mol)	$(Sr/Ca)_{coral}$ (mmol/mol)	$(Cd/Ca)_{coral}$ (μmol/mol)	Average $(Cd/Ca)_{coral}$ (μmol/mol)	2σ
36544	ακ	-	-	0.053	0.059	0.018
		-	-	0.058		
		-	-	0.061		
		-	-	0.055		
		-	-	0.057		
		-	-	0.054		
		-	-	0.054		
	ασ	1.42	9.93	0.056		
		1.21	9.80	0.050		
		1.29	10.12	0.055		
	ατ	1.29	10.01	0.050		
		1.51	10.05	0.057		
		1.34	10.12	0.056		
	αω	1.45	9.98	0.051		
		1.64	10.02	0.046		
		1.27	9.82	0.049		
		0.79	10.21	0.073		
		0.80	10.27	0.060		
		1.07	10.20	0.068		
		0.88	10.18	0.065		
		1.21	9.46	0.072		
		1.30	9.77	0.049		
		1.56	9.89	0.049		
		1.12	10.30	0.056		
		0.94	10.02	0.056		
		0.79	10.26	0.071		
		0.79	10.29	0.073		
		0.83	10.11	0.075		
		0.77	10.10	0.076		
		1.61	9.81	0.047		
		1.03	10.05	0.053		
		1.52	9.95	0.049		
		1.04	10.08	0.066		
		0.70	10.43	0.058		
		0.87	10.17	0.062		
		1.01	9.99	0.081		

Table 4.4. *D. dianthus* Trace Metal Results (continued)

Coral ID	Run ID	$(Mg/Ca)_{coral}$ (mmol/mol)	$(Sr/Ca)_{coral}$ (mmol/mol)	$(Cd/Ca)_{coral}$ (μmol/mol)	Average $(Cd/Ca)_{coral}$ (μmol/mol)	2σ
47413	αλ	-	-	0.075	0.077	0.011
		-	-	0.079		
		-	-	0.073		
		-	-	0.075		
		-	-	0.087		
		-	-	0.087		
	ασ	1.73	10.20	0.081		
		1.58	10.07	0.076		
		1.63	10.28	0.077		
	ατ	1.63	10.21	0.080		
		1.51	10.04	0.067		
		1.70	10.03	0.074		
83583	αλ	-	-	0.155	0.145	0.015
		-	-	0.146		
		-	-	0.143		
		-	-	0.151		
		-	-	0.139		
		-	-	0.145		
		-	-	0.158		
		-	-	0.142		
	ασ	1.16	10.20	0.155		
		0.88	10.32	0.138		
		0.85	10.26	0.138		
	ατ	0.88	10.37	0.140		
		0.86	10.12	0.132		
		0.98	10.30	0.143		
48740	αλ	-	-	0.420	0.325	0.176
		-	-	0.406		
		-	-	0.379		
		-	-	0.383		
		-	-	0.360		
		-	-	0.397		
		-	-	0.351		
		-	-	0.377		
	ασ	0.95	8.87	0.245		
		1.03	10.27	0.300		
		1.10	10.30	0.363		
		1.09	8.99	0.342		
		1.15	10.08	0.300		
		0.98	10.22	0.240		
	ατ	1.15	10.66	0.403		
		1.21	10.24	0.125		
		1.30	10.21	0.132		

Table 4.4. *D. dianthus* Trace Metal Results (continued)

Coral ID	Run ID	$(Mg/Ca)_{coral}$ (mmol/mol)	$(Sr/Ca)_{coral}$ (mmol/mol)	$(Cd/Ca)_{coral}$ (μmol/mol)	Average $(Cd/Ca)_{coral}$ (μmol/mol)	2σ
84820	αμ	-	-	1.323	1.258	0.385
		-	-	1.525		
		-	-	1.419		
		-	-	0.941		
		-	-	1.106		
		-	-	0.869		
		-	-	1.461		
	ασ	1.21	10.35	1.315		
		0.90	10.67	1.154		
		1.24	10.52	1.179		
	ατ	1.37	10.62	1.442		
		1.31	10.49	1.363		
		1.29	10.52	1.253		
JFA68.1	αν	-	-	0.159	0.139	0.021
		-	-	0.149		
		-	-	0.137		
		-	-	0.132		
		-	-	0.122		
		-	-	0.139		
		-	-	0.140		
		-	-	0.133		
JFA84.1	αξ	-	-	0.152	0.159	0.043
		-	-	0.155		
		-	-	0.134		
		-	-	0.148		
		-	-	0.187		
		-	-	0.178		
		-	-	0.191		
		-	-	0.130		
JFA41.26	αξ	-	-	0.375	0.423	0.044
		-	-	0.448		
		-	-	0.430		
		-	-	0.451		
		-	-	0.414		
		-	-	0.419		
		-	-	0.420		
		-	-	0.423		

Table 4.4. *D. dianthus* Trace Metal Results (continued)

Coral ID	Run ID	$(Mg/Ca)_{coral}$ (mmol/mol)	$(Sr/Ca)_{coral}$ (mmol/mol)	$(Cd/Ca)_{coral}$ (μmol/mol)	Average $(Cd/Ca)_{coral}$ (μmol/mol)	2σ
JFA42.10	αν	-	-	0.363	0.363	0.052
		-	-	0.352		
		-	-	0.352		
		-	-	0.337		
		-	-	0.332		
		-	-	0.347		
		-	-	0.374		
		-	-	0.375		
	αχ	1.03	10.08	0.366		
		1.06	10.60	0.360		
		1.18	10.17	0.384		
		1.30	9.78	0.356		
		1.34	10.10	0.385		
		1.11	10.22	0.395		
		1.39	10.10	0.368		
		0.97	9.99	0.354		
		1.26	9.75	0.306		
		1.50	10.06	0.358		
		1.27	9.95	0.366		
		1.38	10.06	0.346		
		1.14	10.06	0.349		
		1.15	9.99	0.361		
		1.18	10.01	0.343		
		0.75	10.15	0.389		
		0.85	10.00	0.378		
		1.32	10.44	0.455		
		0.71	11.19	0.358		
		0.84	9.82	0.390		
		1.35	9.89	0.381		
		1.23	9.92	0.323		
		0.77	10.34	0.355		
78459	αν	-	-	0.044	0.045	0.007
		-	-	0.041		
		-	-	0.045		
		-	-	0.044		
		-	-	0.051		
		-	-	0.045		
		-	-	0.046		
	ασ	1.18	10.19	0.044		
		1.06	10.12	0.042		
		1.13	10.18	0.049		
	ατ	1.24	10.31	0.051		
		1.14	10.32	0.046		
		1.26	10.12	0.039		

Table 4.4. *D. dianthus* Trace Metal Results (continued)

Coral ID	Run ID	$(Mg/Ca)_{coral}$ (mmol/mol)	$(Sr/Ca)_{coral}$ (mmol/mol)	$(Cd/Ca)_{coral}$ (μmol/mol)	Average $(Cd/Ca)_{coral}$ (μmol/mol)	2σ
JFA36.3	αξ	-	-	0.404	0.300	0.212
		-	-	0.325		
		-	-	0.446		
		-	-	0.399		
		-	-	0.394		
		-	-	0.348		
		-	-	0.449		
		-	-	0.402		
	αψ	1.29	10.39	0.094		
		1.39	10.70	0.214		
		1.40	10.66	0.273		
		1.44	10.57	0.165		
		1.34	11.09	0.230		
		1.02	9.87	0.290		
		0.95	10.23	0.421		
		1.22	10.50	0.421		
		1.38	10.53	0.379		
		1.46	10.55	0.220		
		1.43	10.63	0.199		
		1.46	10.51	0.121		
		1.32	10.81	0.190		
		1.33	10.17	0.189		
		1.35	10.73	0.339		
		1.25	10.50	0.443		
		1.28	10.61	0.377		
		1.39	10.84	0.238		
		1.40	10.29	0.190		
		1.44	10.73	0.192		
		1.30	10.96	0.181		
		1.28	10.31	0.230		
		1.25	10.83	0.313		
		1.10	10.30	0.365		
		1.31	10.39	0.457		

Table 4.4. *D. dianthus* Trace Metal Results (continued)

where the size of each data point is scaled by the 2σ replicate error. Discarding data without an independent rationale is unreasonable, and we seek to understand the origin of elevated Cd/Ca in deep-sea corals.

To evaluate the source of the elevated Cd/Ca_{coral}, we consider three possible controls on Cd incorporation the coral aragonite sample. (1) Chemical processing in the laboratory could cause an elevation in Cd/Ca_{coral} by introducing a new source of Cd to the sample via cleaning solutions, by concentrating existing Cd in the coral, or by failing to remove extraneous Cd. (2) Coral vital effects could modulate Cd incorporation via biological control over the skeletal precipitation process. (3) Environmental factors at the coral growth site could influence Cd/Ca_{water} or Cd/Ca_{coral}. We shall consider each process in turn.

Our deep-sea coral cleaning procedure was designed purposely to avoid sample contamination with Cd. Each cleaning solution was tested for the presence of Cd and Sn prior to sample analysis. The 30% hydrogen peroxide solution that we initially intended to use contained Sn as a stabilizer and this solution was replaced with unstabilized 30% hydrogen peroxide that was stored in a cold, dark refrigerator to maintain effectiveness. The cleaning solutions used to treat the samples were found to contain no detectable Cd or Sn, ruling out the cleaning treatments steps as a source of new Cd. The results from the surface coral blanks reinforce this observation. The surface coral blanks contained only trace amounts of Cd after the cleaning process, indicating that significant Cd was not gained or concentrated via the cleaning process (figure 4.6).

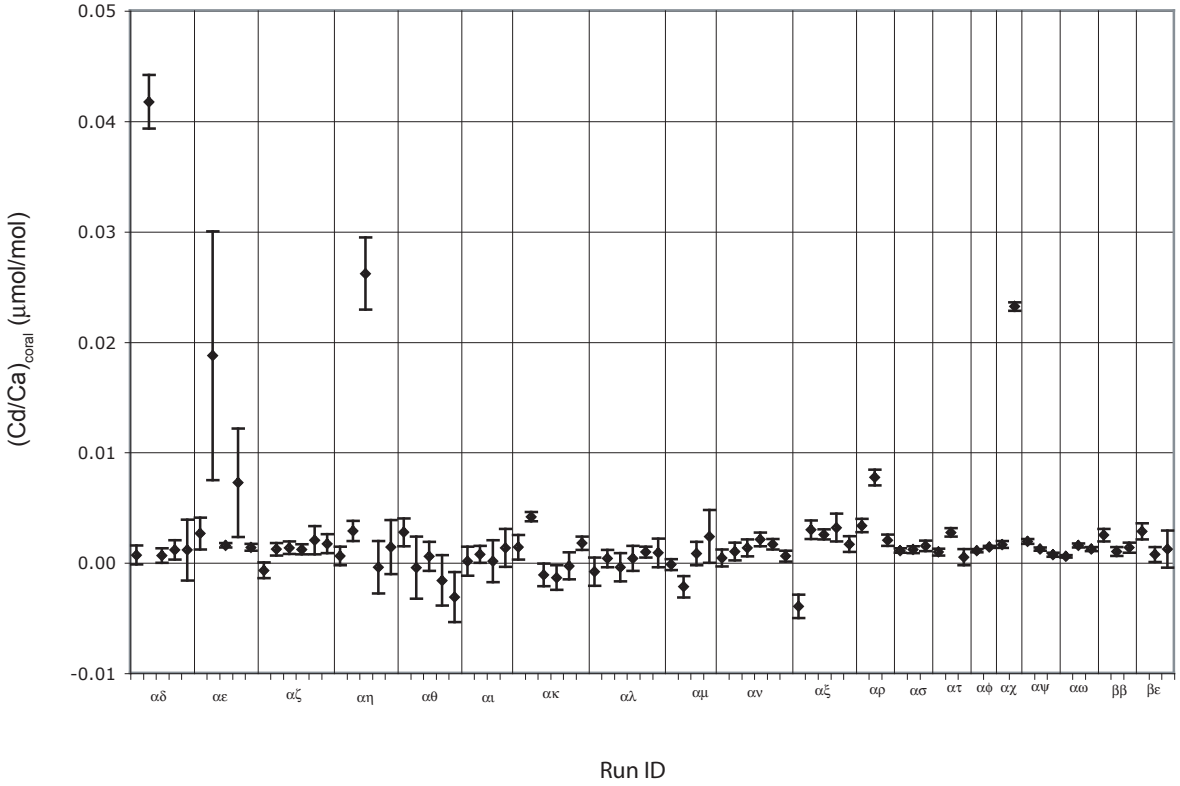

Figure 4.6. Surface coral blank results. We observe the occasional high Cd/Ca, but not of a sufficient magnitude to cause the high Cd/Ca found in the anamalously high Cd/Ca deep-sea corals. Average Cd/Ca in this surface coral is 0.00 ± 0.01 (2σ standard deviation).

We also performed a stepped cleaning test on 3 modern samples, measuring Cd/Ca after each step of the rigorous cleaning procedure and found no increase in Cd/Ca as a result of any cleaning step, indicating that existing Cd was not adsorbed to the aragonite surface and that Ca was not dissolved preferentially to Cd during the leaching steps (figure 4.7). The stepped cleaning did show that the uncleaned samples gave the most precise results, suggesting that the cleaning process may be introducing variability to the samples. Interestingly, the stepped cleaning results also show no decrease in Cd/Ca as the cleaning progresses. Unfortunately, this lack of cleaning progression means that we cannot determine whether the cleaning procedure is effective at removing non-lattice bound Cd. The nonporous structure could possibly isolate the non-lattice bound Cd in the interior of the pieces from the coral cleaning solutions (Shen and Boyle 1988). We believe this result occurs because the non-lattice bound Cd is concentrated in the outer crust of the coral that, in these pristine modern corals, was cleaned away by the mechanical abrasion of the outer surface and precleaning process before the rigorous cleaning. This results applies only to modern sample since fossil samples may have acquired additional Cd contamination over time on the sea floor.

Vital effects in *D. dianthus* have been observed for the stable isotopes $\delta^{13}C$ and $\delta^{18}O$ and the isotopic signal strongly correlates with the coral banding pattern (Adkins, Boyle et al. 2003). Likewise, Mg is concentrated in the optically dense bands in the coral, while Sr is relatively constant throughout a coral (Adkins, Robinson and Fernandez, unpublished data). We first examined Cd/Ca in relation to the coral banding (figure 4.8) and found that Cd/Ca_{coral} does not correlate with coral banding and furthermore, does not

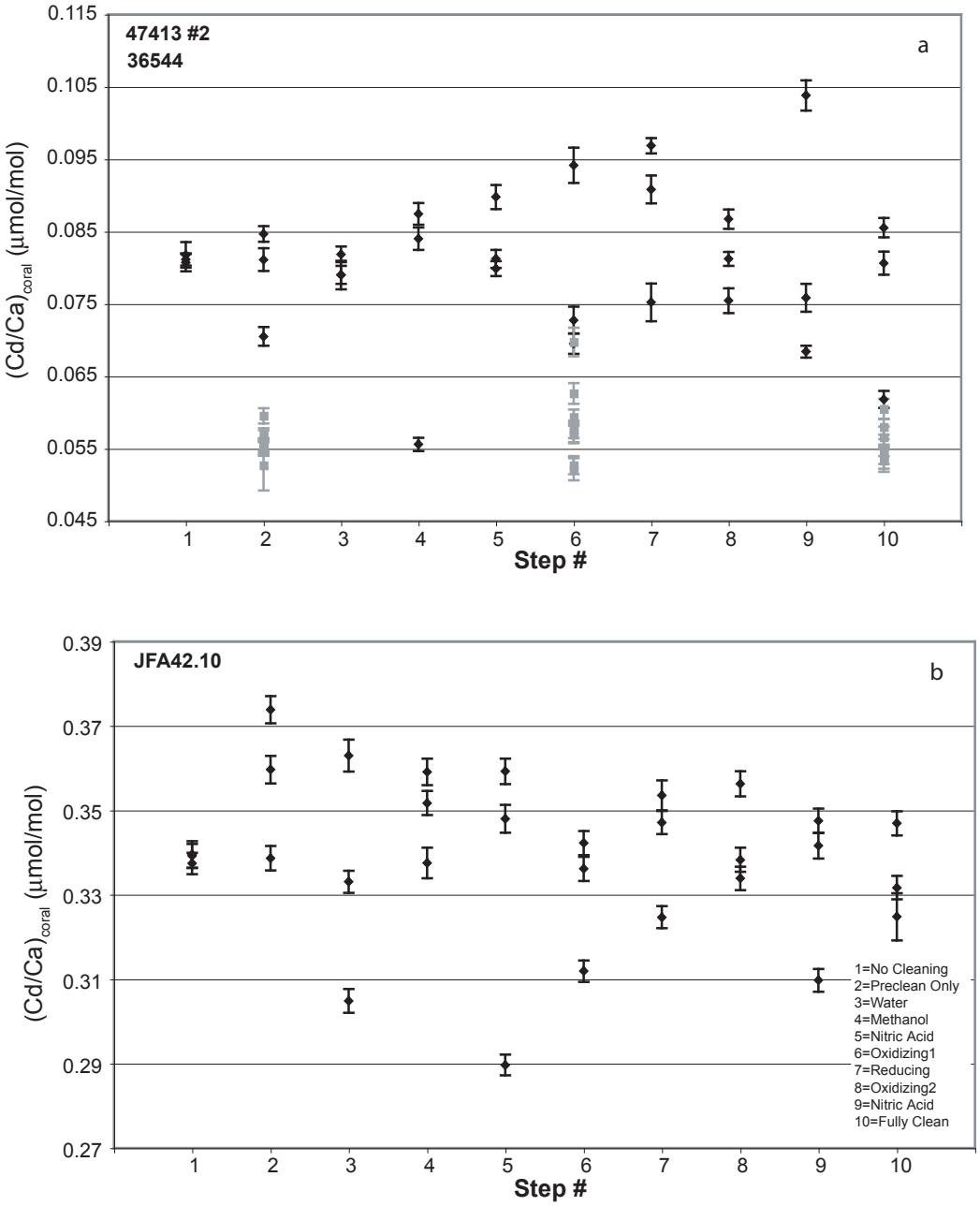

Figure 4.7. Stepped cleaning results from modern *D. dianthus*. (a) The results for low Cd/Ca corals 47413 (run αο) plotted in black and 36544 (run ακ) plotted in gray. (b) The result from high Cd/Ca coral JFA42.10. The step # (x-axis) refers to the cleaning step listed in the lower right. A detailed description of these steps is contained in the appendix at the end of the chapter. The error bars represent the 2σ analytical error on each measurement. None of these corals show reduced Cd/Ca over the cleaning steps. This is probably because the extraneous Cd was removed with the outer crust of these samples before these samples were subject to this part of the cleaning process. Another possibility is that the cleaning steps are unable to access non-lattice bound Cd within each deep-sea coral piece. The data also suggest that the cleaning process may increase the Cd/Ca variability of the samples.

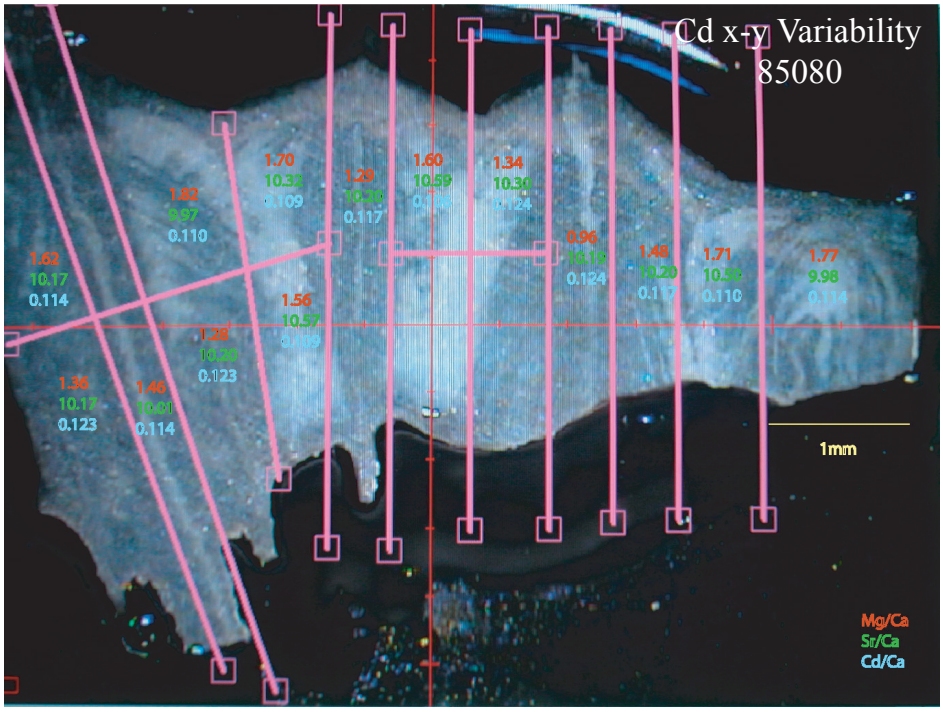

(a)

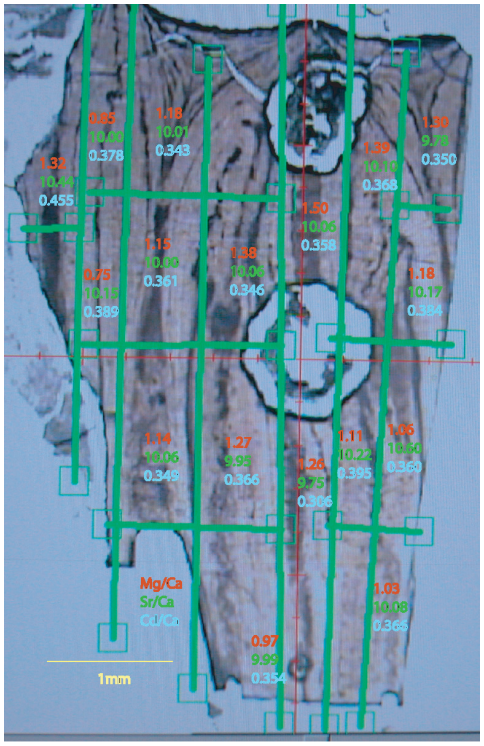

Cd x-y Variability
JFA42.10

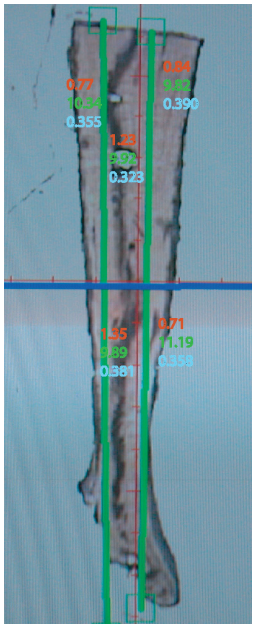

(b)

Figure 4.8. Distribution of Mg/Ca, Sr/Ca, and Cd/Ca in horizontal cross section of *D. dianthus*. (a) Low Cd/Ca coral 85080 under reflected light and (b) high Cd/Ca coral JFA42.10 in transmitted light. These 200mm thick horizontal cross sections were cut along the lines drawn in each image and the resulting pieces cleaned and analyzed for Mg, Ca, Sr, and Cd. Within each section, 3 numbers are listed. These numbers are the Mg/Ca ratio (top/mmol/mol), the Sr/Ca ratio (middle /mmol/mol) and the Cd/Ca ratio (bottom /µmol/mol). Cd/Ca shows no significant correlation with the banding structure of these corals.

correlate with either Mg or Sr (figure 4.9). We then measured Cd/Ca along the trunk of two of the modern deep-sea corals, one from the set of high Cd/Ca corals and the other from the set of low Cd/Ca corals, and we found that Cd/Ca increased to a maximum value toward the top of each coral (table 4.5, figure 4.10). Based on the results from these two corals, we conclude that Cd may be distributed systematically in all *D. dianthus*, with Cd/Ca increasing toward the top of the coral. This trend is especially pronounced in the high Cd/Ca corals and is the origin of the large variability noted in most of these corals. If the cause of the elevated Cd/Ca were attributed to the incomplete cleaning of coral aragonite, this would require a systematic distribution in the non-lattice bound Cd, with more Cd toward the top of the coral. We believe that the likely explanation for the observed trend, however, is that $D_{Cd/Ca}$ in the coral aragonite increased over the lifetime of the coral. In corals with high Cd/Ca, this vital effect is substantial enough to completely overprint the environmental signature.

Investigating the influence of the coral growth process on skeletal Cd/Ca_{coral} is the next step in the development of Cd/Ca_{coral} as a seawater nutrient proxy. With an independent classification scheme, deep-sea coral suitability for Cd/Ca_{water} reconstruction could be determined. A correlation between high-resolution measurements of the coral growth rate and Cd/Ca_{coral} would implicate the process of coral growth as the origin of the observed structure in the Cd/Ca_{coral} record. A Cd/Ca correlation with measurements of chemically similar Zn/Ca would also corroborate coral control over the coral Cd and Zn composition. Duplicating our Cd/Ca results in multiple modern deep-sea corals that grew in the same environment would also be helpful.

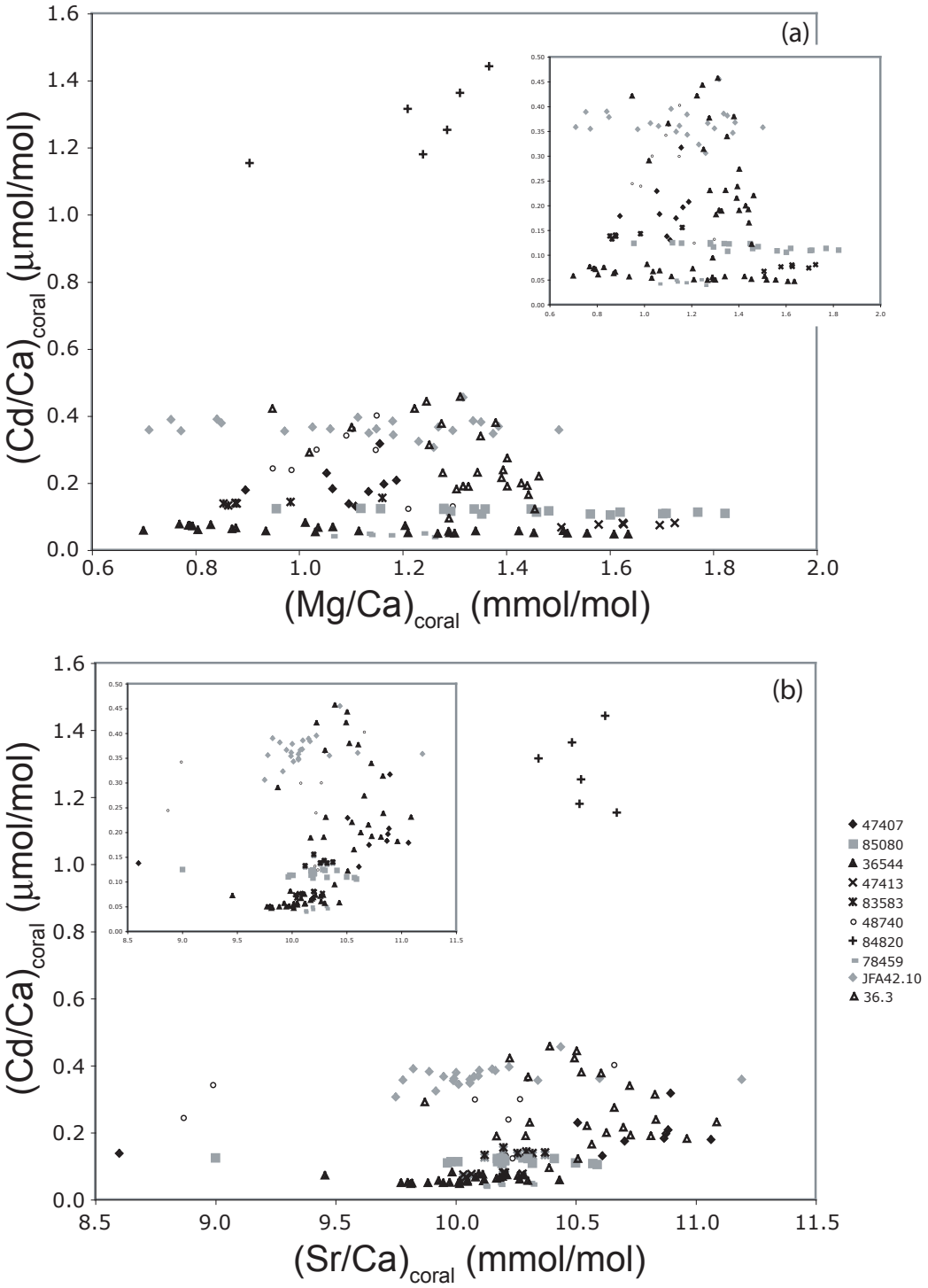

Figure 4.9. Tracer relationships. (a) Most of the corals show no association between Cd/Ca and Mg/Ca. However, the data from high Cd/Ca corals 84820 (+) and 48740 (o) suggest a positive correlation between these tracers. (b) Relationship between Cd/Ca and Sr/Ca shows no correlation between the tracers. In each figure, the nested chart is a zoomed in view of the data. The symbol legend for all plots is shown in the lower right.

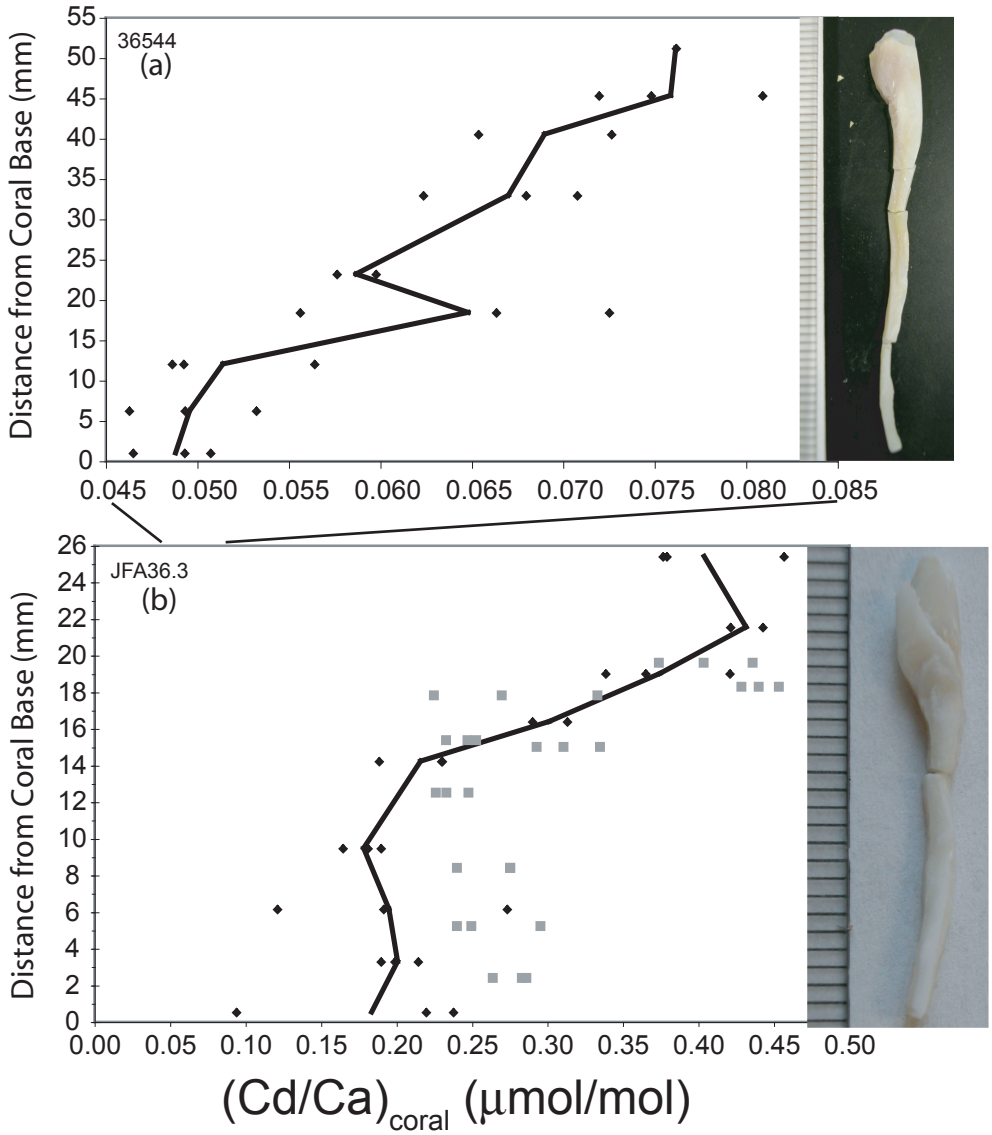

Figure 4.10. Vertical Transects of Cd/Ca in modern deep-sea corals. (a) The top figure is the vertical Cd/Ca record in low Cd/Ca coral 36544. Although the absolute variability is low, there is a trend toward increasing Cd/Ca at the top of the coral. (b) The lower panel shows the record in high Cd/Ca coral JFA36.3. Black diamonds are thecal measurements and gray squares are septal measurements of Cd/Ca in the deep-sea coral.

Coral ID	Run ID	Distance from Coral Base (mm)	$(Cd/Ca)_{coral}$
36544	αω	0.0 - 1.9	0.051
			0.049
			0.047
		5.3 - 7.1	0.046
			0.049
			0.053
		10.5 - 13.5	0.049
			0.056
			0.049
		17.6 - 19.2	0.073
			0.056
			0.066
		21.5 - 24.7	0.060
			0.058
		31.9 - 33.9	0.068
			0.071
			0.062
		39.7 - 41.3	0.065
			0.073
		44.6 - 46.0	0.072
			0.075
			0.081
		50.4 - 52.0	0.076
JFA36.3 thecal	αψ	0 - 1	0.094
			0.220
			0.238
		2.64 - 3.9	0.214
			0.199
			0.190
		5.53 - 6.74	0.273
			0.121
			0.192
		8.32 - 10.58	0.165
			0.190
			0.181
		13.55 - 14.85	0.230
			0.189
			0.230
		15.63 - 17.1	0.290
			0.313
		18.43 - 19.56	0.421
			0.339
			0.365
		20.86 - 22.2	0.421
			0.443
		24.6 - 26.17	0.379
			0.377
			0.457

Table 4.5. Vertical Transect Results

Coral ID	Run ID	Distance from Coral Base (mm)	$(Cd/Ca)_{coral}$
JFA36.3	ββ	1.9 - 2.97	0.283
septal			0.286
			0.263
		4.51 - 6.02	0.295
			0.240
			0.249
		7.19 - 9.68	0.240
			0.275
			0.275
		11.53 - 13.55	0.233
			0.247
			0.226
		14.75 - 16.09	0.253
			0.247
			0.233
		16.09 - 14.00	0.310
			0.293
			0.334
		16.45 - 19.26	0.366
			0.269
			0.333
		18.43 - 20.86	0.403
			0.374
			0.436
		17.1 - 19.56	0.453
			0.440
			0.428
48735.1	βε	3.49 - 5.53	0.243
			0.157
			0.371
		9.83 - 11.13	0.216
			0.287
			0.394
		15.64 - 17.34	0.400
			0.357
			0.532
		21.58 - 23.29	0.472
			0.584
			0.497
		28.23 - 29.53	0.547
			0.101
			0.519
		30.6 - 31.34	0.657
			0.602
			0.608
		33.72 - 36.26	0.671
			0.689
			0.693
		37.31 - 39.53	0.602
			0.627
			0.705
		39.53 - 41.83	0.586
			0.670
			0.630

Table 4.5. Vertical Transect Results (continued)

Another distinguishing feature linking 5 of the 6 high Cd/Ca deep-sea corals is their geographical origin. Five of the high Cd/Ca corals were collected from the eastern North Atlantic and they plot as a cluster in the upper left of figure 4.5. The coral with the highest Cd/Ca_{coral} was collected near the Galapagos Islands, however, so the high Cd/Ca corals cannot be ascribed to one particular geographical region. The Cd/Ca range in the corals from the North Atlantic is very large, even though the corals grew within the last few hundred years when the Cd/Ca of the deep-water was very stable. The most proximate cause of Cd/Ca variability in *D. dianthus* may be a coral vital effect responding to changes in the coral environment (such as food supply, microenvironment, or $[CO_3^{2-}]_{seawater}$).

When we remove the high Cd/Ca North Atlantic and Galapagos samples from the calibration and compare to the foraminifera calibration results, we find that the variability in deep-sea corals is comparable to that of the calcitic and aragonitic foraminifera with no evident depth dependence. We believe that Cd/Ca in these samples may reflect the environmental Cd/Ca signal from the seawater with a $D_{Cd/Ca}$ of 1.3 ± 0.1 for *D. dianthus*.

At the moment, our results imply that at least some deep-sea corals are unsuitable for reconstructions of past $[PO_4^{3-}]$. Using Cd/Ca_{coral} as the sole available indicator of coral suitability, we would partition the samples into three groups. Samples like our North Atlantic and Galapagos samples with Cd/Ca_{coral} greater than about 0.20 would be discounted as samples with an obscured environmental signal. Samples with Cd/Ca_{coral} ranging from 0.10 to 0.20 would be interpreted with caution because they could potentially have significant vital effect complications. Samples with Cd/Ca_{coral} between 0 and 0.10 μmol/mol would be interpreted as being a good record of the average nutrient

concentration of the coral growth site. Interpreting the within-coral Cd/Ca record as a record of Cd/Ca_{water} is a separate issue from the accuracy of individual corals. Both modern samples with vertical Cd/Ca transects show an increase in Cd/Ca over the coral lifespan but grew in water with constant Cd/Ca. Therefore, we interpret this increase as a probable vital effect. Corals that show an increase in Cd/Ca over the vertical growth axis (even if Cd/Ca_{coral} is low) may not necessarily be a record of increasing nutrients.

Our fossil samples from 12.0 and 15.4 ka in the North Atlantic and Cd/Ca_{coral} of 0.15–0.70 and 0.10–0.20, respectively. Both records show an increase in Cd/Ca over the coral lifetime (figure 4.11). With a large Cd/Ca_{coral}, we conclude that the record from 12.0 ka does not reflect an environmental signal. The coral from 15.4 ka has a smaller Cd/Ca that falls in the intermediate range described above and possibly reflects Cd/Ca_{water}. The Cd/Ca_{coral} record within the coral does increase over the coral lifetime at a rate between that of the two modern corals. Therefore, the record within this coral may not be a sign of water mass changes in the past.

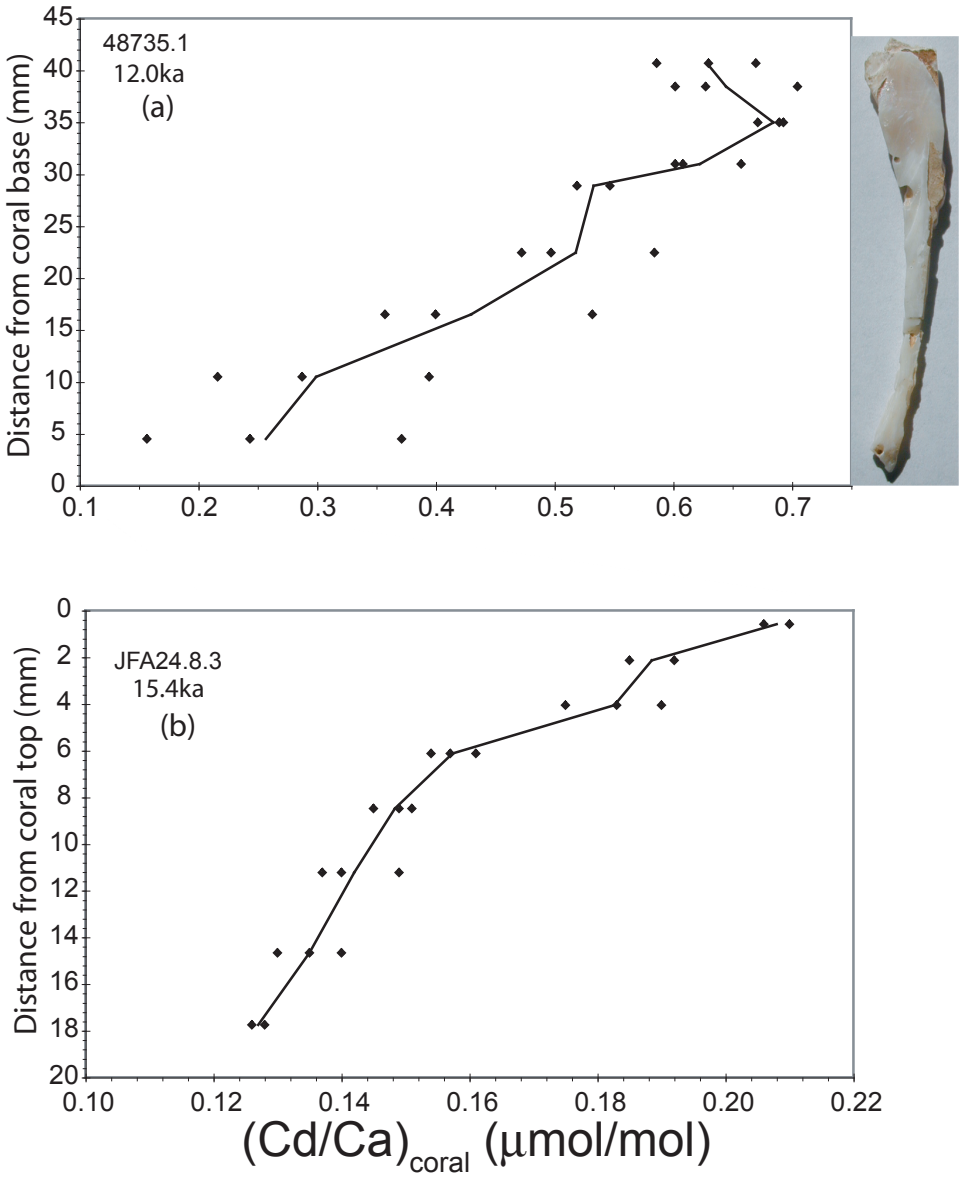

Figure 4.11. Fossil deep-sea coral Cd/Ca results. The upper panel contains the results for the 12.0 ka coral (a) and resembles the results from the high Cd modern corals. Therefore, this coral does not reflect environmental Cd/Ca. The lower panel (b) contains the 15.4 ka fossil coral results from Adkins et al. (1998). This deep-sea coral looks more like the low Cd/Ca corals from the modern calibration, but has a significant increasing trend toward the top of the coral. While this coral probably reflect average ocean Cd/Ca, the increasing trend in the within coral record should be interpreted as an environmental signal with caution because much of the signal could be caused by another mechanism.

Conclusions

Our deep-sea coral Cd/Ca results show that vital effects can obscure the Cd/Ca_{water} signal in deep-sea corals in some cases. We characterize coral vital effects in *D. dianthus* by a high average Cd/Ca_{coral} and large Cd/Ca_{coral} variability within each coral that systematically increases towards the top of the coral. While the systematic trend is present in both high Cd/Ca corals and low Cd/Ca corals, it is most pronounced in the high Cd/Ca corals. When these corals are removed from the calibration data set we see a correlation between Cd/Ca in the coral and Cd/Ca in the seawater that is consistent with a partition coefficient with a value of 1.3 ± 0.1. These results imply that measurements in Cd/Ca in some corals from the past may not be reliable records of seawater Cd/Ca. Therefore, further investigation must be undertaken before Cd/Ca can be considered a reliable proxy for past phosphate concentrations in deep-sea corals.

Bibliography

Adkins, J. F. 1998. Deep-Sea Corals: A New Oceanic Archive, Joint Program in Oceanography/Applied Ocean Science and Engineering, Massachuetts Institure of Technology/Woods Hole Oceanographic Institution, Cambridge.

Adkins, J. F., E. A. Boyle, W. B. Curry, and A. Lutringer. 2003. Stable isotopes in deep-sea corals and a new mechanism for "vital effects." *Geochimica et Cosmochimica Acta* 67 (6):1129-1143.

Adkins, J. F., H. Cheng, E. A. Boyle, E. R. M. Druffel, and R. L. Edwards. 1998. Deep-sea coral evidence for rapid change in ventilation of the deep North Atlantic 15,400 years ago. *Science* 280 (5364):725-728.

Boyle, E. A. 1981. Cadmium, zinc, copper, and barium in foraminifera tests. *Earth and Planetary Science Letters* 53:11-35.

———. 1988. Cadmium: Chemical tracer of deep water paleoceanography. *Paleoceanography* 3:471-489.

———. 1992. Cadmium and d13C paleochemical ocean distributions during the stage 2 glacial maximum. *Annual Review of Earth and Planetary Sciences* 20:245-87.

———. 1995. Limits on benthic foraminiferal chemical analyses as precise measures of environmental properties. *Journal of Foraminiferal Research* 25 (1):4-13.

Boyle, E. A., and L. D. Keigwin. 1985/86. Comparison of Atlantic and Pacific paleochemical records for the last 250,000 years: Changes in deep pcean circulation and chemical inventories. *Earth and Planetary Science Letters* 76:135-150.

Boyle, E. A., L. Lobeyrie, and J.-C. Duplessy. 1995. Calcitic foraminiferal data confirmed by cadmium in aragonitic Hoeglundina: Application to the last glacial maximum in the northern Indian Ocean. *Paleoceanography* 10:881-900.

Boyle, E. A., and Y. Rosenthal. 1996. Chemical hydrography of the South Atlantic during the Last Glacial Maximum: Cd vs d13C. In *The South Atlantic: Past and present circulation*, edited by B. W. Siedler and Webb. Berlin: Springer-Verlag.

Boyle, E. A., F. Sclater, and J. M. Edmond. 1976. On the marine geochemistry of

cadmium. *Nature* 263:42-44.

Delaney, M. L., L. J. Linn, and E. R. M. Druffel. 1993. Seasonal cycles of manganese and cadmium in coral from the Galapogos Islands. *Geochimica et Cosmochimica Acta* 57:347-354.

Elderfield, H., and R. E. M. Rickaby. 2000. Oceanic Cd/P ratio and nutrient utilization in the glacial Southern Ocean. *Nature* 405:305-310.

Frew, R. D., and K. A. Hunter. 1992. Influence of Southern Ocean waters on the cadmium phosphate properties of the global ocean. *Nature* 360:144-146.

Hester, K., and E. A. Boyle. 1982. Water chemistry control of cadmium content in recent benthic foraminifera. *Nature* 298:260-262.

Lea, D. W., and P. A. Martin. 1996. A rapid mass spectrometric method for the simultaneous analysis of barium, cadmium, and strontium in foraminiferal shells. *Geochimica et Cosmochimica Acta* 60 (16):3143-3149.

Linn, L. J., M. L. Delaney, and E. R. M. Druffel. 1990. Trace metals in contemporary and seventeenth-century Galapagos coral: Records of seasonal and annual variations. *Geochimica et Cosmochimica Acta* 54:387-394.

McCorkle, D. C., P. A. Martin, D. W. Lea, and G. P. Klinkhammer. 1995. Evidence for a dissolution effect on benthic foraminiferal shell chemistry: d13C, Cd/Ca, Ba/Ca, and Sr/Ca results from the Ontong Java Plateau. *Paleoceanography* 10 (4):699-714.

Reuer, M. K., E. A. Boyle, and J. E. Cole. 2003. A mid-twentieth century reduction in tropical upwelling inferred from coralline trace element proxies. *Earth and Planetary Science Letters* 210:437-452.

Rickaby, R. E. M., M. J. Greaves, and H. Elderfield. 2000. Cd in planktonic and benthic foraminiferal shells determined by thermal ionisation mass spectrometry. *Geochimica et Cosmochimica Acta* 64 (7):1229-1236.

Rosenthal, Y., P. M. Field, and R. M. Sherrell. 1999. Precise determination of element/calcium ratios in calcareous samples using sector field inductively coupled plasma mass spectrometry. *Analytical Chemistry* 71 (15):3248-3253.

Shen, G. T., and E. A. Boyle. 1988. Determination of lead, cadmium and other trace metals in anually-banded corals. *Chemical Geology* 67:47-62.

Shen, G. T., E. A. Boyle, and D. W. Lea. 1987. Cadmium in corals as a tracer of

historical upwelling and industrial fallout. *Nature* 328:794-796.

APPENDIX A

CLEANING SAMPLES FOR CD/CA

1) Prepare Samples
    a. Label 0.65 mL centrifuge tubes with sample ID–top and side
    b. Weigh samples ~0.5+mg
        i. Tare centrifuge tube and add samples with tweezers (stainless)
2) Precleaning
    a. Water Wash
        i. add ~250 μL mQ-water
        ii. ultrasonicate 20 minutes
        iii. resuspend
        iv. repeat until solution is clear
    b. Oxidizing Solution
        i. add 1 x 250 μL 50:50 mixture of 30% H_2O_2/2M NaOH
        ii. ultrasonicate 20 min
        iii. siphon off solution
        iv. resuspend 3 times with mQ-water
    c. Water Rinse
        i. add ~250 μL mQ-water
        ii. ultrasonicate 2 minutes
        iii. resuspend
    d. Methanol
        i. add 1 x 250 μL CH_3OH
        ii. ultrasonicate 5 minutes
        iii. resuspend 3 times with mQ water
    e. Water Rinse
    f. Bleach
        i. add 1 x 250 μL 50:50 mixture of 30% H_2O_2/1% $HClO_4$
        ii. wait 30–60 s
        iii. resuspend 2–3 times with mQ-water
    g. Water Rinse
    h. Transfer to acid leached polyethylene vials for cleaning
3) Cleaning
    a. Water Rinse–3 times
    b. Methanol Wash
        i. add 1 x 250 μL CH_3OH
        ii. ultrasonicate 2 min
        iii. resuspend 2–3 times with mQ-water
    c. Water Rinse

d. Nitric Acid Wash
    i. add 100 μL 0.2%HNO3
    ii. ultrasonicate 1 minute
    iii. quickly check pH (use 10 μL pipet)
    iv. resuspend 2–3 times with mQ-water
e. Water Rinse
f. Oxidizing Solution
    i. add 1 x 250 μL 50:50 mixture of 30% H_2O_2/0.1M NaOH
    ii. cover rack tightly
    iii. heat for 20 min in boiling water bath, ultrasonicate 5–10 s every 2 min (starting at 0), invert after each ultrasonication
    iv. Rinse 2–3 times with mQ-water
g. Water Rinse–2 times
h. Reducing Solution–ALL IN HOOD
    i. Make up working solution
        1. ~15 mL NH_3/citrate solution
        2. ~15 mL fresh NH4OH
        3. 1 x 1000 μL anhydrous hydrazine
    ii. Add 1 x 250 μL working solution
    iii. Heat for 30 min in boiling water bath, ultrasonicate 5–10 s every 2 min (starting at 0), invert after each ultrasonication
    iv. Resuspend 2–3 times with mQ-water
i. Water Rinse–2 times
j. Oxidizing Solution
k. Water Rinse–2 times
l. Nitric Acid Wash
m. Water Rinse–2 times

4) Transfer and Dissolve
    a. Transfer
        i. Add 1 x 50 μL mQ-water to each tube
        ii. Use 10 μL pipet with cut off pipet tip to transfer sample with a minimum of solution to a new labeled tube
    b. Postcleaning
        i. Add 1 x 100 μL 0.2% HNO_3
        ii. Leave for ~1 min
        iii. Aspirate
        iv. Resuspend 2–3 times with mQ-water
    c. Dissolve
        i. Add 200/250μL 2% HNO_3 and wait for sample to dissolve